

12-2011

Improving the accuracy of radiation pneumonitis dose response models

Yevgeniy Vinogradskiy

Follow this and additional works at: https://digitalcommons.library.tmc.edu/utgsbs_dissertations



Part of the [Medical Sciences Commons](#), and the [Other Physics Commons](#)

Recommended Citation

Vinogradskiy, Yevgeniy, "Improving the accuracy of radiation pneumonitis dose response models" (2011). *The University of Texas MD Anderson Cancer Center UTHealth Graduate School of Biomedical Sciences Dissertations and Theses (Open Access)*. 189.
https://digitalcommons.library.tmc.edu/utgsbs_dissertations/189

This Dissertation (PhD) is brought to you for free and open access by the The University of Texas MD Anderson Cancer Center UTHealth Graduate School of Biomedical Sciences at DigitalCommons@TMC. It has been accepted for inclusion in The University of Texas MD Anderson Cancer Center UTHealth Graduate School of Biomedical Sciences Dissertations and Theses (Open Access) by an authorized administrator of DigitalCommons@TMC. For more information, please contact digitalcommons@library.tmc.edu.

Improving the accuracy of radiation pneumonitis dose response models

A

Dissertation

Presented to the Faculty of
The University of Texas
Health Science Center at Houston
and
The University of Texas
M. D. Anderson Cancer Center
Graduate School of Biomedical Sciences
in Partial Fulfillment
of the Requirements
for the Degree of
Doctor of Philosophy

by

Yevgeney Vinogradskiy, B.S.E., M.S.

Houston, Texas

December 2011

Dedication

I would like to dedicate this work to my parents Luda and Yakov Vinogradskiy

Acknowledgements

I would like to thank my advisor Dr. Mary Martel. She has been a great advisor and an excellent teacher. She has helped guide me through my PhD research and I owe all of my graduate accomplishments to her. I would like to thank Dr. Susan Tucker for teaching me about the modeling and mathematical aspects of dose-response modeling. I would like to thank Dr. Zhongxing Liao for providing excellent clinical input into all of my work. I would like to thank Dr. Followill and Dr. Briere for providing great guidance and input on the direction of my research. I would also like to thank Dr. George Starsckhall and Dr. Stephen Kry for helping form my research proposal in their roles on the advisory committee.

I would like to thank Dr. Guerrero, Dr. Edward Castillo, and Richard Castillo with their help with the ventilation work. I would also like to thank Dr. Ed Jackson and Georgeanne Moore for their help and advice throughout my progression through the Masters and PhD Medical Physics programs.

Thank you to Jimmy Jones, Maria Bellon, Adam Riegel, Adam Chandler, and the rest of my classmates past and present for their support and friendship these last 5 years.

Finally I would like to thank my parents Luda and Yakov Vinogradskiy and my girlfriend Ashly Glasser for their love and support.

Abstract

The prognosis for lung cancer patients remains poor. Five year survival rates have been reported to be 15%. Studies have shown that dose escalation to the tumor can lead to better local control and subsequently better overall survival. However, dose to lung tumor is limited by normal tissue toxicity. The most prevalent thoracic toxicity is radiation pneumonitis. In order to determine a safe dose that can be delivered to the healthy lung, researchers have turned to mathematical models predicting the rate of radiation pneumonitis. However, these models rely on simple metrics based on the dose-volume histogram and are not yet accurate enough to be used for dose escalation trials. The purpose of this work was to improve the fit of predictive risk models for radiation pneumonitis and to show the dosimetric benefit of using the models to guide patient treatment planning.

The study was divided into 3 specific aims. The first two specific aims were focused on improving the fit of the predictive model. In Specific Aim 1 we incorporated information about the spatial location of the lung dose distribution into a predictive model. In Specific Aim 2 we incorporated ventilation-based functional information into a predictive pneumonitis model. In the third specific aim a proof of principle virtual simulation was performed where a model-determined limit was used to scale the prescription dose.

The data showed that for our patient cohort, the fit of the model to the data was not improved by incorporating spatial information. Although we were not able to achieve a significant improvement in model fit using pre-treatment ventilation, we show some promising results indicating that ventilation imaging can provide useful information about

lung function in lung cancer patients. The virtual simulation trial demonstrated that using a personalized lung dose limit derived from a predictive model will result in a different prescription than what was achieved with the clinically used plan; thus demonstrating the utility of a normal tissue toxicity model in personalizing the prescription dose.

Table of contents

Dedication	iii
Acknowledgements	iv
Abstract	v
List of Figures	xi
List of Tables	xvi
Introduction	1
<i>Statement of Problem</i>	1
<i>Current state of radiation therapy in lung cancer</i>	2
<i>Improved outcome shown with dose escalation</i>	3
<i>Dose escalation limited by normal tissue toxicity</i>	4
<i>Use of risk models to predict for radiation pneumonitis</i>	6
<i>Factors affecting the risk of radiation pneumonitis</i>	10
<i>Dose escalation trials using mathematical radiation pneumonitis models</i>	12
<i>Virtual dose escalation trials</i>	13
<i>Patient database</i>	14
<i>Purpose</i>	16
<i>Central hypothesis</i>	17
<i>Specific Aims</i>	17
Specific Aim 1: Spatial Study	18
<i>Introduction</i>	18
<i>GTV Centroid analysis</i>	19
<u>Methods</u>	19

GTV centroid analysis.....	20
Modeling methods.....	21
Analysis of GTV centroids that exclude nodal volume.....	22
<u>Results</u>	23
Qualitative GTV centroid results.....	23
Pneumonitis Rates.....	27
Modeling results.....	31
<u>Discussion</u>	32
<i>3D Dose Spatial Analysis</i>	35
<u>Methods</u>	35
Novel Spatial Analysis.....	35
Lung Division Analysis.....	39
<u>Results</u>	40
<u>Discussion</u>	42
<u>Conclusions</u>	46
Specific Aim 2: Ventilation study	47
<i>Introduction</i>	47
<i>Serial Ventilation Study</i>	53
<u>Methods</u>	53
Patient selection.....	53
Ventilation image processing.....	54
Analysis of ROI data.....	57
<u>Results</u>	58

Ventilation as a function of dose.....	58
Pretreatment ventilation by lobe.....	59
Change in ventilation by lobe over the course of treatment.....	61
<u>Discussion</u>	63
<u>Conclusions</u>	68
<i>Pre-treatment ventilation study</i>	68
<u>Methods</u>	68
<u>Results</u>	71
<u>Discussion</u>	75
<u>Conclusion</u>	81
Specific Aim 3 – Personalized prescription study	82
<i>Introduction</i>	82
<i>Methods</i>	84
<i>Results</i>	95
<i>Discussion</i>	104
<i>Conclusion</i>	110
Conclusions	111
<i>Study uncertainties</i>	111
<i>Conclusions</i>	113
<i>Clinical significance of research</i>	115
<i>Future Work</i>	116
<i>Response to hypothesis</i>	118
References	134

Vita	134
-------------------	-----

List of Figures

Figure 1: A curve showing the negative log-likelihood as a function of TD_{50} . The curve graphically illustrates how 95% confidence intervals are determined and the non symmetric shape of log-likelihood plot.	3
Figure 2: Schematic showing the mapping of GTV centroids from the treatment planning system (A) to the common coordinate system (B). The rectangles surrounding each lung indicate the extreme lung points that were used as boundaries to define the common coordinate system shown in (B). Printed with permission (54).....	3
Figure 3: Coronal view of all GTV centroids (A) displayed according to the presence of severe pneumonitis. The coronal CT slice (B) is shown to indicate the orientation of the GTV centroid plot. Printed with permission (54).	3
Figure 4: Coronal view of all GTV centroids displayed according to tumor stage. Printed with permission (54).	3
Figure 5: Coronal view of GTV centroids displayed according the presence of severe pneumonitis for patients who had stage I and II disease (A) and patients who had stage III and IV disease (B). Printed with permission (54).	3
Figure 6: Coronal view of all GTV centroids displayed according to smoking status. Printed with permission (54).	3
Figure 7: Coronal view of GTV centroids displayed according to the presence of severe pneumonitis when nodal volume is included in the GTV centroid calculation (A) and when nodal volume is excluded in the centroid calculation (B). Printed with permission (54).	3

Figure 8: An example of dose from two coronal planes (intended to represent a 3D dose distribution) mapped from the treatment planning system (A) to the common coordinate system (B). The common coordinate system for each lung is defined by the extreme boundaries of that particular lung. The boundaries for the left and right lung are defined separately. As an example, a rectangle highlights the extreme points of the right lung in the superior, inferior, medial, and lateral orientations (A). The result is a 3D matrix (B) for each lung that contains the dose distribution inside that lung and is defined from 0 to 1 in each orientation. Printed with permission (55).....3

Figure 9: An example slice of a superior-inferior weighting scheme (A), a radial weighting scheme (B), and a ramp function weighting scheme (C). The CT images are included to indicate the orientation of the weighting slices. Printed with permission (55).3

Figure 10: Scatter plots showing a comparison between the total mean lung dose and the superior region mean dose (A), middle region mean dose (B), and inferior region mean dose (C). The severe pneumonitis events are shown as red circles while the non pneumonitis events are displayed as black stars. Printed with permission (55).....3

Figure 11: An example of segmented lung. The sagittal and axial planes are shown. It should be noted that the vasculature within the lung is excluded.....3

Figure 12: An example of a vector map showing the deformation field. The deformation field links lung voxels together from the inhale phase to the exhale phase of the 4DCT dataset.3

Figure 13: An example of a ventilation image overlaid on a coronal CT slice.3

Figure 14: An example of ventilation data and the linear fit for 2 different lobes. The slope of the fit to the lobe 2 data was 3.43, while the slope of the fit to the lobe 1 data was

0.2, which indicated that lobe 2 showed an increase in ventilation over the course of treatment and lobe 1 had little to no change in ventilation over the course of treatment. ...3

Figure 15: The dose distribution (A) and percent ventilation maps (B) for patient 2. The data for this patient provides a representative example of decreased ventilation for the left upper lobe where the tumor caused a central bronchial occlusion.3

Figure 16: Comparison of ventilation between lobes that contained tumors and lobes that did not contain tumors. The difference in average percent ventilation was shown to be statistically significant ($p=0.017$ using a t-test).3

Figure 17: Tumor outline and dose distribution (A) as well as the weekly progression of ventilation images (B) for patient 4. This patient provides a representative example of increasing ventilation in the left upper lobe as the tumor decreases in size.3

Figure 18: Tumor outline and dose distribution (A) as well as the weekly progression of ventilation images (B) for patient 3. This patient provides a representative example of a case where there was no visual evidence of the tumor volume reduction and as a result the ventilation distribution remained unchanged throughout treatment.3

Figure 19: Dose distribution (A), ventilation image (B), and DVH and DFH example for one patient. This patient provides an example where dose was delivered to the non-functional portions of the lung and where the DFH is lower than the DVH. This patient did not develop severe radiation pneumonitis.3

Figure 20: Dose distribution (A), ventilation image (B), and DVH and DFH example for one patient. This patient provides an example where dose was delivered to the functional portions of the lung and where the DFH is greater than the DVH. This patient went on to develop severe radiation pneumonitis.3

- Figure 21: Scatter plot showing the variable change from MLD to ventilation weighted MLD (fMLD). A linear fit to the data is shown as a black line. The pneumonitis rate is 22.4% above the line and 12.8% below the line.....3
- Figure 22: Box plot comparing the ventilation weighted MLD between the pneumonitis and non pneumonitis group. As expected the group that developed pneumonitis had higher ventilation weighted doses than the group that did not develop pneumonitis.....3
- Figure 23: A histogram of the simulation results for the entire population MLD. The histogram confirms that the simulation mean and standard deviation of the normal distribution were 20.58 and 4.55 respectively.....3
- Figure 24: Distribution of genotypes for each SNP. The red bars represent genotypes that were selected as adverse risk factors for radiation pneumonitis and the blue bars represent genotypes that were not a risk factor for developing radiation pneumonitis.....3
- Figure 25: NTCP curves for different combination of genotypes for the 3 SNPs investigated (XRCC, TGFB, VEGF). Knowing each patient's genotype allows for each patient to be placed on one of the curves shown..3
- Figure 26: Three example NTCP plots relating MLD and radiation pneumonitis complication probability. The plot illustrates that for 3 different patients with 3 different genotypes, using a complication probability of 22.6, the MLD limits would be personalized and different for each patient.....3
- Figure 27: An example of how an esophagus DVH is used to calculate the change in dose needed to change the V_{60} to 50%. First the D_{50} is identified, then the ratio of 60 Gy divided by D_{50} is taken as the amount the dose needs to be escalated (or de-escalated in some cases) to achieve a V_{60} of 50%. The theoretical movement of the DVH using a dose

escalation ratio calculated by the method above is shown in green. For this patient example, the dose can be escalated by 600% based on the esophagus. In this patient example, the prescription dose would likely be limited by another normal tissue organ....3

Figure 28: Dose distribution for the patient used in the example calculation.3

Figure 29: A histogram of the difference between the model-generated MLD and the clinically achieved MLD.3

Figure 30: A histogram of the differences between the model-generated prescriptions and the clinically achieved prescriptions.....3

Figure 31: A histogram of the difference between the model-generated prescription dose and the clinically achieved prescription dose for the reduced patient population. Patients were excluded if their clinical dose-volume metrics for the spinal cord, esophagus, or heart exceeded the set limits prior to dose escalating or de-escalating.3

Figure 32: A histogram of the difference in prescriptions according to the presence or absence of severe pneumonitis.3

Figure 33: A histogram of the difference between the model-generated prescription and the clinically achieved prescription displayed according to different complication probabilities.3

Figure 34: Example of a patient that was re-planned such that the model-determined MLD limit could be achieved. Planes of dose distributions are shown for 3D-CRT, IMRT, and protons for one patient.3

List of Tables

Table 1. CTCAE version 3.0 scoring criteria for radiation pneumonitis.....5

Table 2. Pneumonitis rates for each superior-inferior third of the lung.....28

Table 3. Pneumonitis rates for each superior-inferior quartile of the lung.....	28
Table 4. Pneumonitis rates according to quartiles with the two inferior quartiles combined.....	29
Table 5. Pneumonitis rates according divided into thirds for patients grouped according to disease stage.....	30
Table 6. Pneumonitis rates for each superior-inferior third of the lung when nodal volume is excluded from the GTV centroid calculation.....	30
Table 7. Statistical comparison of nominal dose-volume model with modified (to include GTV centroid information) dose volume models according to modeling parameters and corresponding p values. <i>Abbreviations:</i> GTV = gross tumor volume, MLD = mean lung dose; CI = 95% confidence intervals, DMF = dose modification factor; SI = superior- inferior, AP = anterior-posterior, ML = medial-lateral, RL = right-left.....	31
Table 8. Statistical comparison of most accurate current model with most accurate model modified by GTV centroid location. <i>Abbreviations:</i> MLD = mean lung dose; SI = superior-inferior, AP = anterior-posterior, ML = medial-lateral, RL = right-left.....	32
Table 9. A comparison of model parameters and significance values for the various weighting schemes investigated. <i>Abbreviations:</i> CI ₉₅ = 95% confidence intervals, CI ₆₈ = 68% confidence intervals, MLD = mean lung dose; SI = superior-inferior, AP = anterior- posterior, ML = medial-lateral, inf = infinity, RL = right-left.....	40
Table 10. Summary of treatment characteristics.....	54
Table 11. Summary of patient and tumor characteristics.....	54
Table 12. Percent ventilation data for ROIs defined according to V ₂₀	59
Table 13. GTV volume for each patient recorded during pre-treatment and during the	

final week of therapy.....	63
Table 14. Significance values for the various dose-volume and ventilation weighted dose-volume metric investigated. The significance values indicate a difference in the metric between the group that developed severe pneumonitis and the group that did not develop severe pneumonitis.....	74
Table 15. Dose-volume limits used for the virtual simulation study.....	89
Table 16: A single patient example of the procedure used to determine the model-generated prescription. The table shows the patients clinical parameters, the applied dose volume limits, the ratio between the limits and the clinical parameters, and finally the model-generated parameters.....	94
Table 17: The overall clinically achieved prescription, model generated prescription, and changes in prescription for the entire patient population.....	97
Table 18: The overall clinically achieved prescription, model generated prescription, and changes in prescription for the reduced patient population. Patients were excluded if their clinically achieved dose-volume parameters for the spinal cord, esophagus, or heart exceeded the limits set for the study (prior to applying the model-determined MLD limit).....	100
Table 19: Mean and median change in prescription for the 20% complication probability simulation and the 25% complication probability simulation.....	103
Table 20: Data showing the dose limiting organ for the simulation using the 22.6 complication probability.....	103
Table 21: Data showing the dose limiting organ for the simulation using the 20% complication probability and the 25% complication probability.....	104

Table 22: Re-planning example for 2 patients. The 3D-CRT, IMRT and Proton MLDs are shown. The model determined MLD limit is also displayed.....	109
---	-----

Introduction

Statement of Problem

The prognosis for lung cancer remains poor. Out of 1,529,560 new cancer cases in 2010, 240,610 (15.7%) of those were lung cancers. The situation is further exacerbated by the poor prognosis for lung cancer patients. Lung cancer accounts for 29% of all cancer related deaths in men and 26% of all cancer related deaths in women. The 5 year survival rate for lung cancer has been reported to be 15% (1).

Several promising studies have shown that dose escalation to the tumor can lead to better local control and subsequently overall survival for non-small-cell lung cancer (NSCLC) patients (2-5). However, the dose to the tumor is limited by normal tissue radiation toxicity. For NSCLC patients, the most prevalent toxicity is radiation pneumonitis. Radiation pneumonitis occurs roughly in 10-20% of all radiation treatments of NSCLC (6) and usually manifests 1 to 6 months after the completion of radiation therapy. Symptoms of radiation pneumonitis can include cough, fever, shortness of breath, and if left untreated radiation pneumonitis can be lethal.

In order to determine a safe dose that can be delivered to the healthy lung tissue, clinicians and researchers have turned to mathematical models predicting the rate of radiation pneumonitis. The models describe a probability of developing radiation pneumonitis as a function of simple dose-volume metrics derived from the dose volume histogram (DVH). Researchers have also attempted to incorporate patient and clinical factors into predictive risk models (6, 7). However, the data remains inconclusive and inconsistent. As a result, the models and therefore physicians rely mostly on population based dose-volume metrics to design and evaluate thoracic radiation treatment plans.

Better outcomes for lung cancer patients receiving radiation therapy strongly depend on treatment personalization. Treatment personalization can only be made possible by more reliable and accurate radiation pneumonitis dose response models. Therefore, the purpose of this study will be to improve the accuracy of predictive risk models for radiation pneumonitis and to show the dosimetric benefit of using the models to guide patient treatment planning.

Current state of radiation therapy in lung cancer

The survival rates for lung cancer remain poor. There are many reasons for the poor outcome for lung cancer patients. In many instances, physical symptoms may not be present at the time of initial diagnosis. In fact, up to 75% of patients that present with lung cancer have lesions that are unresectable due to the advanced stage of the disease or systematic spread (8). When surgery is not indicated, either because of the advanced stage of the tumor or because the patient is unable to tolerate surgery, a combination of radiation and chemotherapy is used. The exact treatment combination is dependent on the type and clinical staging of the disease. More than 80% of all lung cancers in the United States are NSCLC (1). For early stage NSCLC, surgery is often the treatment of choice with post-operative radiation therapy recommended if there is evidence of microscopic spread. Patients who are unable to tolerate surgery or who present with locally advanced NSCLC (defined as stage IIB-IIIB) are treated with a combination of radiation therapy and concurrent chemotherapy. Overall, approximately 75% of all lung cancer patients in our clinic receive radiation therapy.

Although technological developments have enabled radiation therapy to deliver higher doses to the tumor, the biggest reason for death, for patients receiving radiation

therapy, remains local recurrence of the disease (9-11). Local recurrence can be defined as failure to eradicate the local disease. If the local disease is not controlled, it can subsequently lead to metastatic spread (12). Local control can be as low as 15% for patients who receive standard radiation doses of 66 Gy (13). Studies suggest that an improved local control rate can lead to a significant improvement in overall survival (2).

Improved outcome shown with dose escalation

Currently, the common clinical practice for thoracic radiation therapy is to deliver anywhere from 60-66 Gy to the target in either 1.8 or 2 Gy fractions. Several studies have proposed that one way to increase local control and subsequently overall survival is to escalate the dose to the tumor. As early as 1987, Perez et al (14) performed a study where they randomized patients to four different arms that delivered varying doses of radiation and found that higher doses of radiation were needed to improve tumor control. In another study, Willner et al (15) retrospectively analyzed 135 NSCLC patients who were treated to radiation doses ranging from 30 to 80 Gy. They found that there was a clear dose effect on local control and overall survival. In more recent work, Kong et al. (4) analyzed a dose escalation trial in which NSCLC patients were treated to doses ranging from 63-103 Gy in 2.1 Gy fractions using three-dimensional conformal radiation therapy (3D-CRT). They found that the 5 year control rate was 12%, 35%, and 49%, for patients treated to doses of 63-69, 74-84, and 92-103 Gy, respectively. They concluded that higher doses of radiation were associated with improved outcomes. In another dose escalation trial, Bradley et al. (16) studied 177 patient with inoperable NSCLC. They found that local control rates of 50-78% were achieved with increasing radiation doses. There are currently undergoing multi-institutional studies and protocols to evaluate the possibility

of escalating the dose to the tumor for lung cancer patients (17). Bradley et al (17) report in their initial findings that the maximum tolerated dose was 74 Gy in 2 Gy fractions with three 3D-CRT and concurrent chemotherapy. The 74 Gy dose level was found to be well tolerated by patients and found to have low rates of radiation pneumonitis.

Dose escalation limited by normal tissue toxicity

Although increasing the radiation dose to the target has been shown to improve overall survival; it is impossible to increase the dose to the tumor without increasing the dose to the surrounding healthy tissue. Therefore, the doses that can be delivered to the target are limited by normal tissue toxicities. The two most common toxicities observed in thoracic radiation are acute esophagitis and radiation pneumonitis; with radiation pneumonitis being the more prevalent. Radiation pneumonitis is an acute toxicity that develops within several weeks or months after radiation therapy. Symptoms of radiation pneumonitis include dry cough, low grade fever, shortness of breath, chest pain, and if left untreated radiation pneumonitis can be lethal (7). Treatment for radiation pneumonitis usually consists of steroids, oxygen, or assisted ventilation depending on the severity of the condition.

In order to establish a common classification system, clinicians have tried to establish an objective endpoint that could be used to classify the severity of radiation pneumonitis. One suggestion has been to classify radiation pneumonitis based on dyspnea, which is defined as shortness of breath. The difficulty with dyspnea as an effective end-point is that the condition is non-specific and can be caused by various other medical conditions (such as infection and cardiac arrhythmia) not related to the radiation treatment (6). Most current radiation pneumonitis grading systems rely on

medical intervention. One of the most common scoring systems called the Common Terminology Criteria for Adverse Events (CTCAE) (18) has been proposed by the National Cancer Institute. The scoring system (Table 1) consists of severity grades 1 through 5, ranging from asymptomatic (grade 1) to death due to radiation pneumonitis (grade 5). The most common clinic endpoint used for analysis is grade 3, which is defined as severe symptoms, oxygen indicated, and limited self care in activities of daily living. It should be noted that there are different versions of the CTCAE criteria and several different groups have defined their own criteria for radiation toxicity. The different radiation pneumonitis scoring systems complicate the analysis of data from different groups and institutions. Tucker et al. (19) explored the impact of the scoring system on the relationship between radiation dose and pneumonitis. Their data demonstrated the importance of documenting the criteria for defining radiation pneumonitis.

Grade	Description
1	Asymptomatic; clinical or diagnostic observations only; intervention not indicated
2	Symptomatic; medical intervention indicated; limiting instrumental ADL
3	Severe symptoms; limiting self care ADL; oxygen indicated
4	Life-threatening respiratory compromise; urgent intervention indicated (e.g., tracheotomy or intubation)
5	Death

Table 1: CTCAE version 3.0 scoring criteria for radiation pneumonitis.

The range of symptomatic radiation pneumonitis has been reported to be anywhere from 5 to 50% (6). Some specific examples include a severe pneumonitis rate of 32% in a cohort of 223 patients treated at MD Anderson Cancer Center (20) and a pneumonitis rate of 14% from pooled data reported by Kwa et al. (21). However, it

should be noted that with newer data that includes newer treatment modalities such as IMRT, the pneumonitis rate has been reported to be lower. For example, Sura et al. (22) report a pneumonitis rate of 11% for patients treated with IMRT. Overall, with current radiation therapy methods, the risk of severe radiation pneumonitis is considered to be about 10-20%.

Use of risk models to predict for radiation pneumonitis

In order to try to predict a safe dose that can be given to the lung, researchers and clinicians have turned to predictive mathematical modeling. Mathematical models have been developed to calculate a normal tissue complication probability (NTCP) for radiation pneumonitis. One of the earliest models was developed by Lyman (20). The Lyman model is based on the assumption that the tolerance to radiation dose can be thought of as a normal distribution. Dose dependence can then be described as the integral of the normal distribution which produces a sigmoid curve. Mathematically, the Lyman model can be written as

$$NTCP = \frac{1}{\sqrt{2\pi}} \int_{-\infty}^t e^{-u^2/2} du, \quad \text{Equation 1}$$

where

$$t = \frac{D_{eff} - TD_{50}/V^n}{mTD_{50}/V^n}. \quad \text{Equation 2}$$

D_{eff} is the effective dose, V is the volume, and m , n , and TD_{50} are model fitting parameters. The TD_{50} is the dose corresponding to 50% incidence of the radiation pneumonitis, m is related to the inverse of the slope of the sigmoid curve, and n is the volume parameter. A steeper slope (smaller m) indicates that there is more of a dose

response and that the binary data are separated well, while a smaller slope indicates a flat curve and a smaller dose response. The volume parameter (n) is a characteristic of the tissue and is closer to 1 when an organ is considered to be a “parallel” organ and closer to 0 when the organ is considered to be a “serial” organ. The lung is considered to be a volume organ and therefore most studies suggest that the value of n is closer to 1 (6). The effective dose (D_{eff}) is the dose-volume metric used as the input into the NTCP model. The physical meaning of the effective dose is dependent on the definition used to describe D_{eff} . One common way to calculate the effective dose from the DVH was proposed by Mohan et al (23). The group proposed that the effective dose can be calculated with

$$D_{eff} = \left(\sum_i v_i D_i^{1/n} \right)^n, \quad \text{Equation 3}$$

where i loops over all the dose bins, v is the relative volume, and D is the dose. Equation 3 is meant to reduce the heterogeneous dose distribution into a uniform dose given to a volume. With the n parameter set equal to 1 (as is the case in the lung) the effective dose gets reduced to the mean dose or in the case of lung, the mean lung dose (MLD). Using the DVH reduction scheme proposed by Mohan et al. (23) the expression in Equation 2 can be re-written as

$$t = \frac{MLD - TD_{50}}{mTD_{50}}. \quad \text{Equation 4}$$

The expressions in Equations 1 and 4 are commonly called the Lyman-Kutcher-Burman (LKB) formulation of NTCP (24) which is the most widely used complication probability model in the literature (6). Throughout this work we will use the LKB formulation of NTCP described in Equations 1 and 4.

It is important to note that there are other mathematical models that describe NTCP. One class of models uses other mathematical expressions to described a sigmoid

curve. Examples include the logistic and log-logistic models (25). A study by Seppenwoolde et al. (26) compared different sigmoid models and determined that the MLD formulation of the LKB model was the most accurate predictor of radiation pneumonitis. Another class of models is known as mechanistic models and tries to describe the biological phenomenon of radiation damage. One example of such a model is the “cluster” model proposed by Thames et al. (27). Other mechanistic models have been described that rely on the volume dependence (serial versus parallel) of a tissue (28). Finally, there are models that select several dosimetric features, instead of a single dose-volume metric, to be included in prediction for radiation pneumonitis (28).

The model parameters (for example m and TD_{50}) are fit to a patient dataset using maximum likelihood analysis (29). Maximum likelihood analysis is a method of estimating parameters of a statistical model for binary observations. The likelihood metric can be described by

$$L = \prod_{i=1}^n \Pr(y_i|p), \quad \text{Equation 5}$$

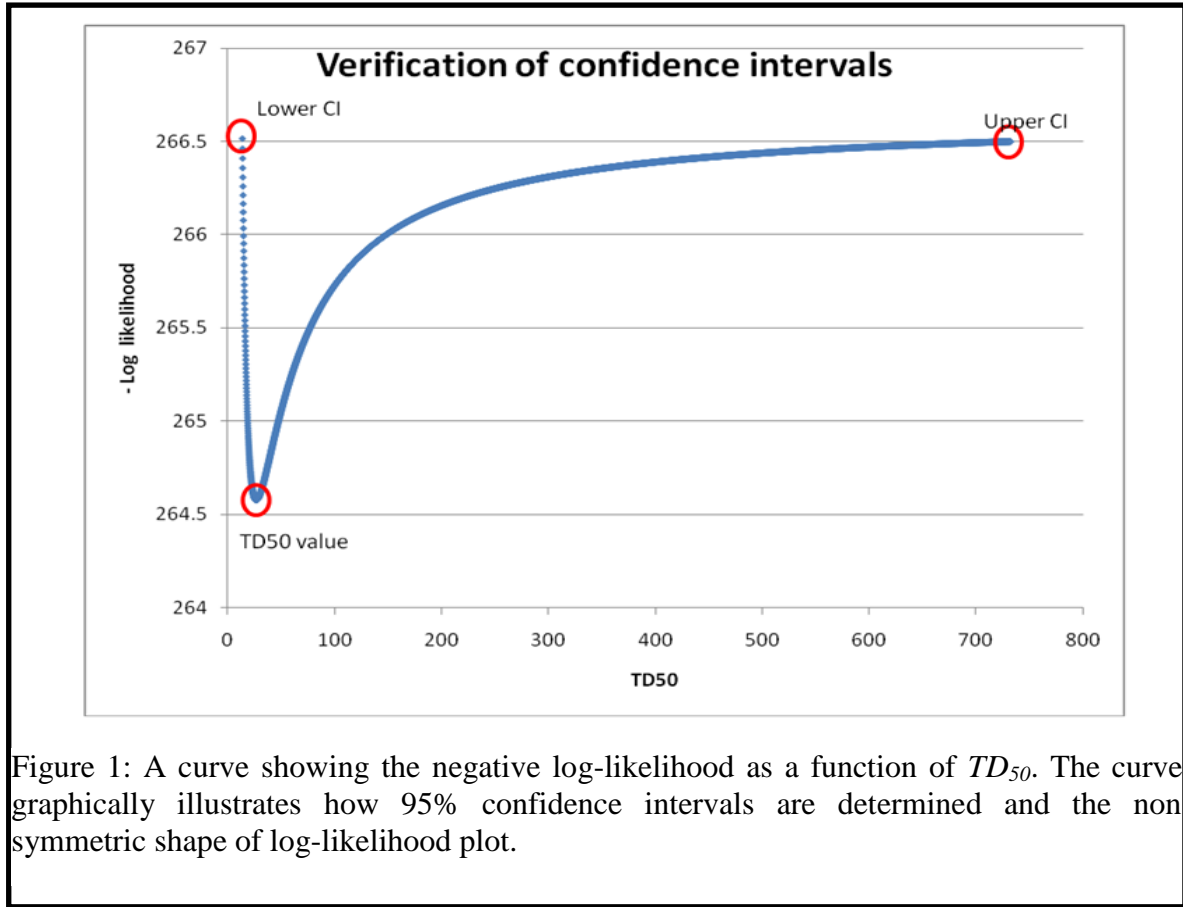
where i is the number of observations, y is the observation, and p is the probability of the observation. In terms of toxicity, i is the number of patients, y is the binary observation of whether or not the patient developed severe pneumonitis (yes or no), and p is equivalent to the NTCP. Substituting and re-arranging terms, the likelihood equation can be written as

$$L = \prod_{i=1}^n NTCP_i^{y_i} (1 - NTCP_i)^{(1-y_i)}. \quad \text{Equation 6}$$

For numerical reasons, the natural logarithm is taken of both sides of Equation 6 and the log-likelihood is computed. Finally, an optimization algorithm can be used to determine the model parameters (for example m and TD_{50}) that maximize the log-likelihood. In

practice, often the negative of the log-likelihood is taken because algorithms may have routines for determining the minimum rather than the maximum.

In order to perform a complete statistical analysis, it is often desirable to obtain 95% confidence limits on the fitting parameters. For a certain fitting parameter, the 95% confidence interval is determined by systematically varying the value of that particular fitting parameter, and optimizing the other parameters to calculate the maximum log-likelihood. The lower and upper 95% confidence intervals are the value of the optimization parameter that equate to a log-likelihood reduction of 1.92. The value of 1.92 is determined by taking half of the chi-squared distribution that equates to a significance level of 0.05. The shape of a log-likelihood curve as a function of one parameter is shown in Figure 1. It should be noted that the shape of the curve is not symmetric.



Factors affecting the risk of radiation pneumonitis

As indicated in Equations 2-4, the two parameters most associated with the probability of developing radiation pneumonitis are dose and volume (6, 20, 30-33). Specifically, researchers have discussed metrics such as MLD and the volume receiving dose greater than a threshold (V_{dose}) value. For example, Wang et al (20) and Martel et al (31) found that patients with a higher MLD had a higher incidence of radiation pneumonitis. Wang et al (20) retrospectively analyzed 223 patients treated with definitive radiation therapy and concurrent chemotherapy. Using univariate analyses, they found that MLD was significantly associated with the risk of developing radiation pneumonitis. Martel et al (31) retrospectively analyzed the DVHs of 64 patients who had their normal lungs irradiated with 3D-CRT. They reported that patients who had radiation pneumonitis

had a greater MLD than patients who did not develop radiation pneumonitis. Other studies, such as those by Yorke et al (34) and Graham et al (30) concluded that the rate of radiation pneumonitis was significantly correlated to V_{20} . Graham et al (30) analyzed the dose volume data for 99 patients treated definitively for NSCLC and reported that V_{20} was significantly associated with the probability of developing radiation pneumonitis. Yorke et al (34) used 78 patients from a Phase I dose escalation study and reported that ipsilateral lung V_{20} was amongst one of the significant variables correlated with radiation pneumonitis. It is important to note that the literature also suggests that within individual datasets the dose-volume parameters are often correlated with one another (6, 20, 34).

In addition to dose-volume parameters, researchers have attempted to identify clinical and patient factors that could help predict for the rate of radiation pneumonitis. Some of the factors include: the use of chemotherapy (35), performance status (36), smoking status (37), genetic information (38), tumor location within the lung (32, 33, 39), and functional status of the lung (40-42). In the lung literature survey, Marks et al (6) report inconclusive results relating the risk of radiation pneumonitis and surgery. Another controversial treatment factor that has been investigated is the use of chemotherapy. Many chemotherapy agents are known to cause pulmonary toxicities and perhaps exacerbate radiation induced lung injury. In fact, from clinical experience, many physicians believe that chemotherapy increases the chance of developing radiation pneumonitis. However, this result has not been proven in the literature. For example, Graham et al (30), in their univariate analyses, did not find the use of chemotherapy to be significantly associated with the risk of developing radiation pneumonitis. Similarly, Robnette et al (36) did not find the use of chemotherapy to be predictive of radiation

pneumonitis. In the same study, Robnette et al (36) did find a correlation between performance status and radiation pneumonitis. Yuan et al (38) reported that certain genotypes were associated with a lower risk of radiation pneumonitis in NSCLC patients. Tumor location within the lung has also been studied as a potential factor associated with radiation pneumonitis. Hope et al (33) found that inferior tumor position was highly correlated with pneumonitis events while Robnette et al (36) did not find a similar pattern. Several studies have suggested that incorporating lung function into predictive models can improve the ability to predict for radiation pneumonitis (42). However, these are largely methodology and proof of concept studies (43). Overall many patient and clinical factors have been investigated in an attempt to improve the predictive power of radiation pneumonitis dose response models; however, the literature remains inconsistent and inconclusive (6, 7).

Dose escalation trials using mathematical radiation pneumonitis models

Several groups have used predictive mathematical models to guide dose escalation trials for NSCLC patients (4, 16, 44-47). The main idea in all of these trials was to use individual patient lung dose volume parameters to guide the tumor dose. The tumor dose was escalated until the lung dose volume constraints were met. For example, Bradley et al (16), set lung V_{20} limits while escalating the tumor dose. They reported that the dose was safely escalated using 3D-CRT to 83.9 Gy for patients with V_{20} values $<25\%$, and to 77.4 Gy for patients with V_{20} values between 25% and 36%. The group reported that elective nodal failure occurred in less than 10% of all patients. Other studies (46, 47) used the MLD to determine achievable tumor dose. Belderbos et al (46) escalated the prescription dose based on MLD. They reported that dose escalation was safe up to 94.5 Gy in 42

fractions in patients with MLD < 13.6 Gy. They also reported that they found higher doses were associated with better overall survival for smaller tumor volumes. Baardwijk et al (48) used a MLD of 19 Gy and a maximum spinal cord dose of 54 Gy to escalate tumor dose. They reported that their prescribed dose was 64.8 ± 11.4 Gy with a severe pneumonitis rate (grade 3 or higher) of 21%. A few studies went a step further (4, 44) and explicitly used NTCP models to determine dose volume constraints that yielded an acceptable complication probability. Kong et al (4) escalated dose based on the LKB NTCP model. Using the model, they binned patients into different bins according to the effective volume V_{eff} . The group defined V_{eff} as the volume of normal lung that would have to be uniformly irradiated to a given reference dose to result in a similar predicted level of radiation pneumonitis (4). Overall the group was able to deliver doses ranging from 63 Gy to 103 Gy in 2.1 Gy fractions. The study reported survival of 4%, 22%, and 28%, for patients receiving 63-69, 74-84, and 92-103 Gy, respectively. Overall, these results were promising and demonstrate that higher radiation doses can improve overall survival. Currently, the practice is to prescribe 60 to 70 Gy to the target for NSCLC patients. All of the dose escalation studies achieved target doses that are higher than those routinely given in the clinic. The local control and overall survival results were also promising. Although these studies represent a step in the right direction, it is important to point out that the models were entirely based on basic dose volume constraints. Incorporating other, non-dosimetric factors into the model could potentially increase the accuracy and utility of the model and enable further stratification of patients.

Virtual dose escalation trials

It is also possible to conduct virtual dose escalation trials where the theoretical gains in tumor dose can be assessed without the risk of harming patients. Baardfwijk et al (49) performed a dose escalation trial for 65 NSCLC patients. The group determined an individual maximal tolerable dose based on dose volume constraints for the lung and spinal cord. They found that an increase of 5.6% tumor control probability (TCP) could be gained by using the maximum tolerable dose determined by lung and spinal cord dose volume constraints. The group progressed the idea of the virtual trial and performed a prospective feasibility study (50). The study reports that the mean delivered dose was 63.0 ± 9.8 Gy with mild acute lung toxicity rates (1 patient experienced grade 3 pneumonitis). Mackay et al (51) performed a virtual study by prescribing patient dose based on cellular radiosensitivity. The group simulated varying patient radiosensitivities based on measured distributions among cancer patients of the surviving fractions of their fibroblasts given a dose of 2 Gy. They determined that their model showed that improvements in tumor control rates may be achievable through individualizing radiotherapy dose prescriptions.

Patient database

One of the largest NSCLC patient databases is collected at MD Anderson Cancer Center and is described in detail by Jin et al (37). The database includes 576 NSCLC patients that were treated with definitive radiation therapy at MD Anderson from 1999-2005. Patients were treated with either 3D-CRT or IMRT. The database contains patients that were treated with and without chemotherapy. Patients were excluded from the study if their total dose was <50.4 Gy (which is considered a palliative dose), if they had doses per fraction that varied over the course of treatment, or had treatment breaks totaling >7

days. The database includes clinical, dosimetric, demographic, chemotherapy, and outcome information. Some specific examples of the recorded information include: dose volume parameters for the lung, tumor stage and histology, smoking status, pulmonary function test (PFT) data, nodal status, and fractionation scheme. Radiation pneumonitis toxicity was scored by a physician on the basis of clinical presentation and radiographic abnormalities according to the National Cancer Institute's CTCAE version 3.0 (18). The clinically significant end point used for the analysis was severe (grades 3-5) radiation pneumonitis. Grade 3 radiation pneumonitis is defined as severe symptoms, interfering with activities of daily living, and oxygen indicated. Grade 4 radiation pneumonitis is defined as life-threatening respiratory compromise and Grade 5 is death due to radiation pneumonitis. This retrospective study was approved by the Institutional Review Board at MD Anderson.

In the initial clinical analysis of the data, using univariate analyses, patient smoking status was the single factor most correlated with radiation pneumonitis. Other factors correlated with a lower rate of radiation pneumonitis include negative nodal status, use of 4-dimensional computed tomography (4DCT) simulation, and treatment with IMRT (37). Jin et al (37) also identified a DVH curve defined by $V_{20} \leq 25\%$, $V_{25} \leq 20\%$, $V_{35} \leq 15\%$, and $V_{50} \leq 10\%$. In multivariate analysis, smoking status retained significance independent of dose-volume factors (37). Non-smokers were found to have the highest risk for radiation pneumonitis while smokers were found to have the lowest risk for toxicity. Tucker et al (52) found that the volume parameter (n) was not significantly different from 1, indicating that MLD can be used to predict for radiation pneumonitis. Tucker et al (52) also presented an NTCP model that included patient

smoking status and follow up time. The follow up time was included to account for patients that are censored by incomplete follow-up for any reason (including death) and takes into consideration patients who would eventually experience toxicity with sufficiently long follow-up. In other analysis of MD Anderson data, Yuan et al (38) found that certain genotypic expression of Single Nucleotide Polymorphisms (SNP) were associated with a lower risk of radiation pneumonitis.

Purpose

Studies have shown that dose escalation can lead to improved tumor control and subsequently better overall survival for NSCLC patients. However, lung dose is limited by normal tissue toxicity; mainly radiation pneumonitis. If we were able to more accurately predict for radiation pneumonitis, we could further personalize radiation treatment by prescribing a target dose that is tailored to the individual's risk of developing radiation toxicity. Currently, prediction models rely on basic indices derived from the DVH and therefore are too simplistic and not yet accurate enough to be used to individualize tumor doses. Therefore, the purpose of this study will be to improve the accuracy of predictive risk models for radiation pneumonitis and to show the dosimetric benefit of using the models to guide patient treatment planning. The first part of the study will aim to improve the accuracy of radiation pneumonitis dose response models by incorporating spatial and functional aspects into the model. The second part of the study will use a dose response model in a virtual dose prescription trial to determine the potential dosimetric benefit of using a model to determine target dose.

Central hypothesis

The fit of radiation pneumonitis dose response models can be significantly improved by incorporating information about the heterogeneous function of the lung.

Specific Aims

1. To incorporate the spatial location of dose within the lung into the modeling of radiation pneumonitis.

Working hypothesis: The accuracy of radiation pneumonitis dose response models can be significantly improved by incorporating information about the spatial location of dose within the lung.

2. To incorporate ventilation-based functional information into the modeling of radiation pneumonitis.

Working hypothesis: The accuracy of radiation pneumonitis dose response models can be significantly improved by incorporating ventilation based functional information.

3. To determine the potential benefit of using radiation pneumonitis modeling to optimize target dose for individual patients.

Working hypothesis: The relative median difference in prescription dose between the model-generated plans and the clinically used plans will be greater than 5 Gy.

Specific Aim 1: Spatial Study

Introduction

Current models describing the risk of developing radiation pneumonitis are based on dosimetric indices derived from the DVH. As an example, the MLD and V_{20} are metrics that are often used to predict for toxicity (30, 31). By definition, the DVH is a reduction of the 3D spatial dose distribution into the 2D domain. A single metric, such as MLD or V_{20} , is an even further simplification of the 2D data. One consequence of the simplification of the 3D data into a single metric is a loss of spatial information. Spatial information is important because several researchers have proposed that lung function is not homogenous and may vary spatially throughout the lung. Specifically, studies have suggested that patients who get radiation therapy to the base of the lung are more likely to develop radiation pneumonitis than patients who get radiation to the apex of the lung (30, 32-34, 39, 43, 53). Liao et al (39) irradiated mouse lung and determined that the base of the lung is more radiosensitive than the apex. In human studies, this data has been echoed by Yorke et al (32), who calculated various dosimetric indices for different portions of the lung. They found that the mean dose to the inferior lung was highly correlated to radiation pneumonitis. Hope et al (33) and Bradley et al (53) analyzed the spatial location of GTV centroids and determined that inferior tumor position was indicative of higher rates of radiation pneumonitis. On the other hand, Robnette et al (36) did not find a relationship between dose to the lower lung and higher radiation pneumonitis rates. Overall, the data are inconclusive. Furthermore, the previously reported methods have limitations. Several authors note that there is a paucity of events in the lower portion of the lung, making the data unstable in the inferior lobes (33, 54). Many studies have made

conclusions using the GTV centroid to analyze the spatial effect. However, using the GTV centroid is not ideal because the GTV centroid acts as a surrogate for the deposited dose and does not take into account factors such as the volume of the GTV or treatment planning tendencies and techniques. Another issue arises when researchers analyze GTV centroid or dose-volume data by dividing the lung into various geometrical regions. The results of analyzing the data by dividing the lung into regions are sensitive to the location of the boundaries that define the lung divisions. A more rigorous approach is needed to study the relationship between the spatial location of the deposited dose and radiation pneumonitis rates. Therefore, the purpose of this study is to develop a novel method to incorporate the spatial effect into radiation pneumonitis dose response models and to apply the method to the MD Anderson clinical NSCLC patient database to determine if there is a correlation between location and pneumonitis rates. Our hypothesis is that incorporating spatial information will statistically improve the fit of the predictive model. The study will be performed in 2 portions. In the first part of the study we will perform the analysis using GTV centroid information (54) and in the second portion we will incorporate the entire 3D dose distribution (55).

GTV Centroid analysis

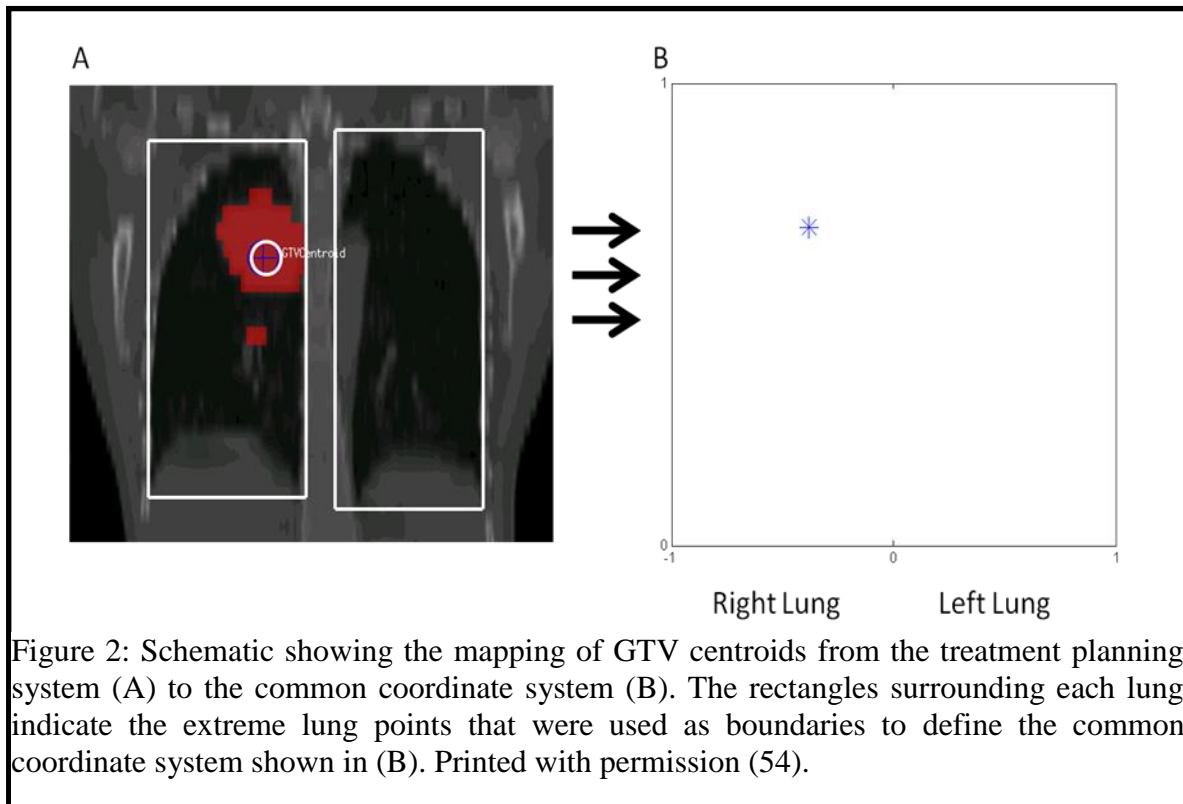
Methods

For this study we used 547 patients from the MD Anderson NSCLC patient database described in the introduction. The methods of the GTV centroid analysis are described in detail by Vinogradskiy et al (54). The first step is to de-archive each patient's treatment plan into the treatment planning system (Pinnacle³, Philips Medical Systems, Milpitas, CA). Because, there are several unused treatment plans for each

patient, the clinically used plan needed to be correctly identified. This was done by cross referencing treatment planning parameters (prescription, number of beams, beam angles, monitor units) with the record and verify system and the patient's paper chart. The rest of this chapter is taken from Vinogradskiy et al (54).

“GTV centroid analysis

The treatment plans for all 547 patients were de-archived into the treatment planning system and the GTV centroid of each patient was mapped onto one common coordinate system similar to the manner described by Hope et al. (33). The boundaries of the coordinate system were defined by the extreme points of each individual patient lung (Figure 2). Once all of the centroids were mapped onto the



common coordinate system, the results were qualitatively analyzed by graphing the data in a coronal orientation. The data were graphed and displayed according to disease stage, smoking status, and the presence of severe pneumonitis. To further analyze the results, we binned the data into equal geometrical regions and used a chi-square test to determine whether there were statistically significant differences between the pneumonitis rates in the various lung regions. In order to further stratify the analysis according to disease stage, pneumonitis rates were calculated for a smaller cohort of patients with stage I and II disease and for another cohort of patients with stage III and IV disease.

Modeling methods

We used the LKB model (24) with the volume parameter (n) set equal to one (52) to calculate NTCP for radiation pneumonitis...The model described in Eq. 4 represents the conventional dose-volume model incorporating MLD and was used as the baseline for statistical comparison with a second model that incorporated GTV centroid location.

To incorporate GTV centroid location into the predictive model we replaced the quantity t (in Eq. 4) with

$$t = \frac{MLD - TD_{50}e^{CL}}{mTD_{50}e^{CL}}, \quad \text{Equation 7}$$

where C is a model-fitting parameter and L is the GTV centroid coordinate. The quantity $\exp(CL)$ can be thought of as a dose modification factor (DMF) on TD_{50} and has been proposed (52, 56) as a way to introduce risk-factors into the NTCP model. Six different orientations were investigated for the GTV centroid coordinate (L in Eq. 7): superior-inferior (SI), right-left (RL), anterior-posterior

(AP), medial-lateral (ML), radial, and SI distance from the mean SI position of all GTV centroids. The radial coordinate was taken as the radial distance from the center point of the medial edge of each lung box. Anatomically, this coordinate is analogous to the radial distance from the center point of the mediastinum. Using maximum likelihood analysis and the likelihood-ratio test, we compared the model that incorporated GTV centroid information and dose-volume information (Eq. 7) to the baseline dose-volume model (Eq. 4) to determine whether adding GTV centroid information significantly improved the fit of the model.

In addition to comparing the GTV centroid location model to the basic dose-volume model, a comparison was made using our best fitting model to date, which currently incorporates dose-volume information, smoking status, and follow-up time (52). Mathematically, smoking status is incorporated into the model by introducing covariate DMFs that account for smoking status (52). The follow-up time accounts for patients that are censored by incomplete follow-up for any reason (including death) and takes into consideration patients who would eventually experience toxicity with sufficiently long follow-up. The likelihood-ratio test was used to compare our current, most accurate model (which incorporated dose-volume, smoking status, and follow-up time) versus the same model with the GTV centroid DMF added in. All statistical work was done with MATLAB software.

Analysis of GTV centroids that exclude nodal volume

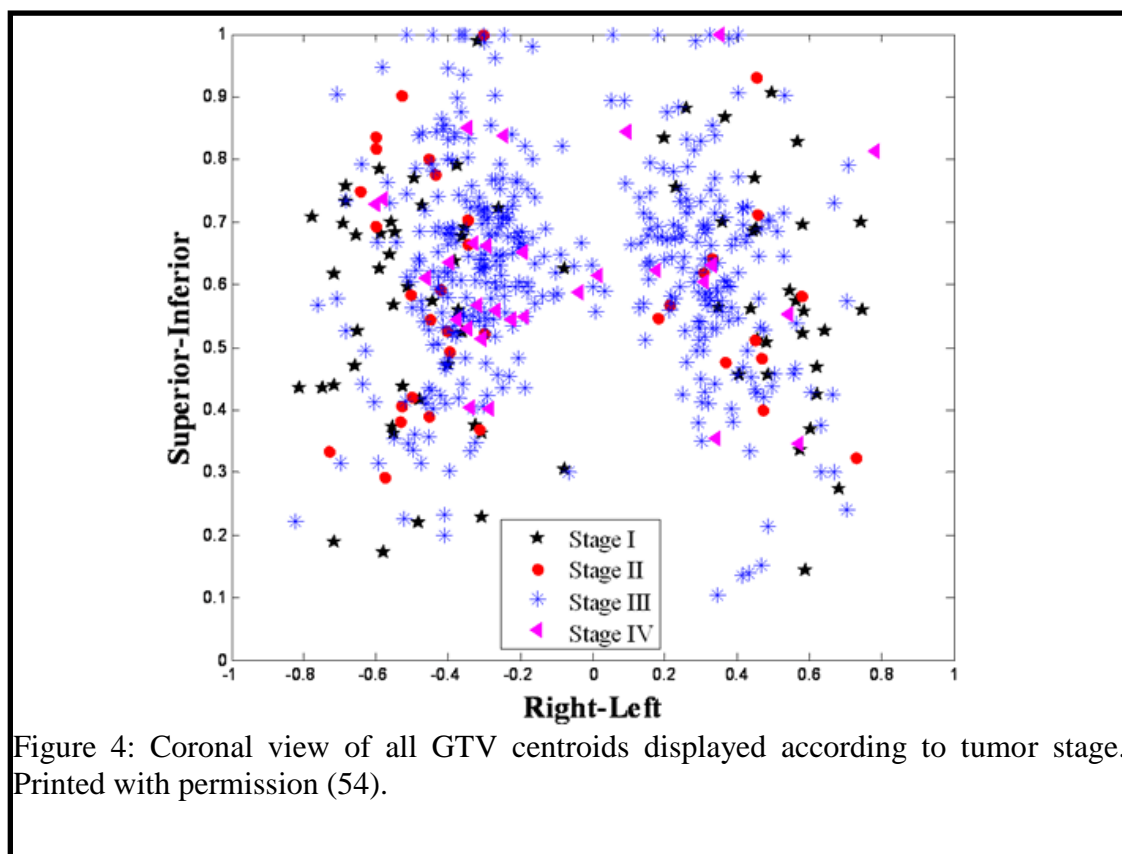
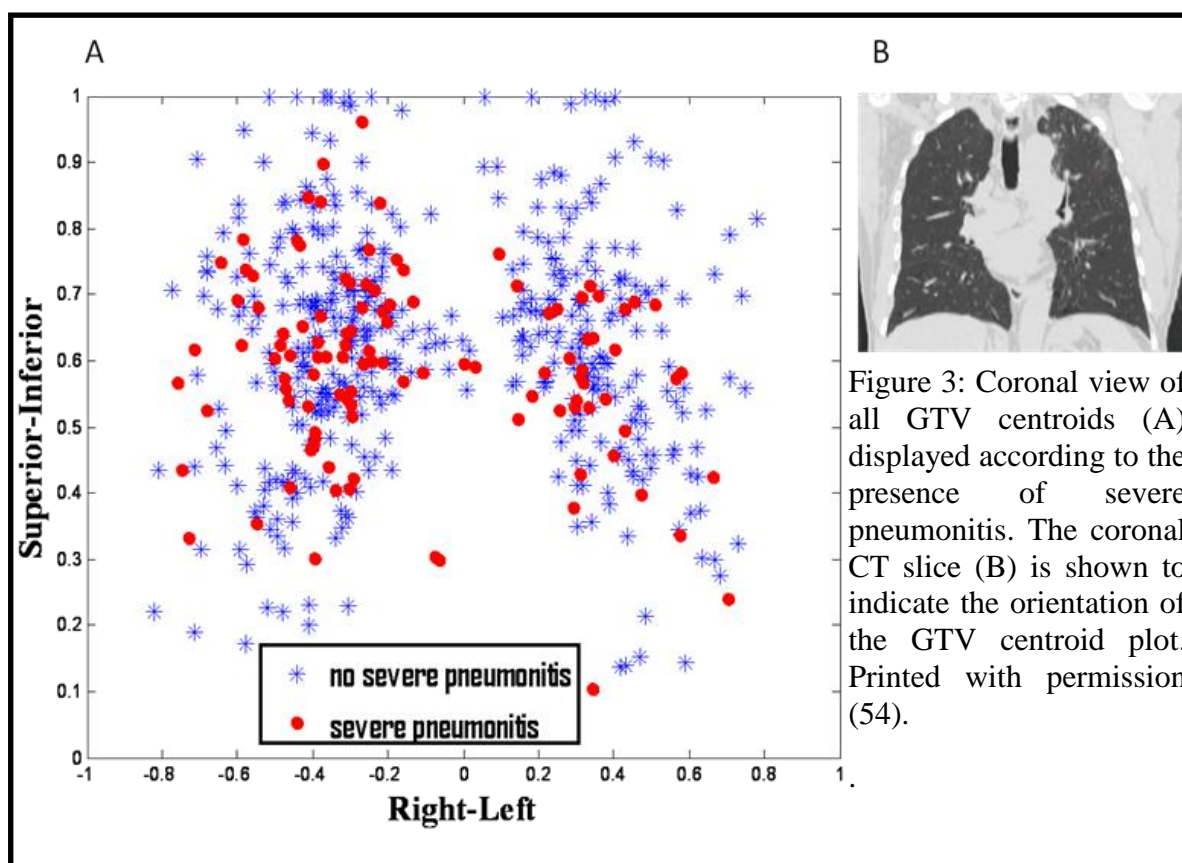
Seventy five percent of the patients in our database had stage III or higher disease, which indicates nodal involvement. The practice in our clinic (and the

method used for this study) is to contour the primary tumor and nodal volume and consider that area the GTV. Therefore, the centroids calculated for this analysis included the primary tumor as well as the nodal volume. The other possibility for performing this type of analysis is to exclude the nodal volume when calculating the centroid of the GTV. There are advantages and disadvantages to both methods. For example, excluding the nodal disease in the centroid calculation has the advantage of better isolating the spatial location of the primary tumor in the lung parenchyma. On the other hand, including the nodal volume provides a GTV centroid that is a better representation of the true location of the deposited dose. In order to determine whether including nodal volume made a difference in our results we re-contoured the GTV of every patient to exclude nodal volume, re-analyzed the data, and compared the results to the results obtained while including the nodal volume in the GTV centroid calculation.

Results

Qualitative GTV centroid results

Of the 547 patients analyzed, 111 (20.3%) experienced severe radiation pneumonitis. Figure 3 shows a coronal view of all GTV centroids. The mean SI position of all tumors was located at 0.62 on a scale of 0 to 1 (0 corresponding to the inferior end and 1 corresponding to the superior end). Graphing of GTV centroid location according to tumor stage (Figure 4) indicated that the GTV centroid of patients with Stage III and IV disease appeared to be



concentrated toward the middle of the grid, which anatomically correlates to the mediastinum, while the GTV centroids of patients with Stage I and II disease were scattered toward the periphery of the lung. The average ML GTV centroid position of patients with stage I and II disease was 0.49 while the average ML GTV centroid position of patients with stage III and IV disease was 0.34 (where 0 is defined as the medial border and 1 is defined as the lateral border). The difference in ML GTV centroid position between the two groups is significantly different ($p < 0.001$ as calculated by the Wilcoxon rank-sum test). The overall spatial pattern of the GTV centroid location for patients with and without pneumonitis appeared to be similar in the cohort of patients with stage I and II disease (Figure 5) and the cohort of patients with stage III and IV disease (Figure 5). In addition, GTV centroids were stratified by patient smoking status (Figure 6). Qualitatively, the GTV centroids of non smokers are notably absent from the superior region of the lung. The average SI GTV centroid position of non smokers is 0.58 (range of 0.23-0.81) while the average SI GTV centroid position for smokers and former smokers is 0.62 (range of 0.10-1.00). However, the difference in SI GTV centroid position between the non smokers and former and current smokers was not significant ($p = 0.172$ as calculated by the Wilcoxon rank-sum test).

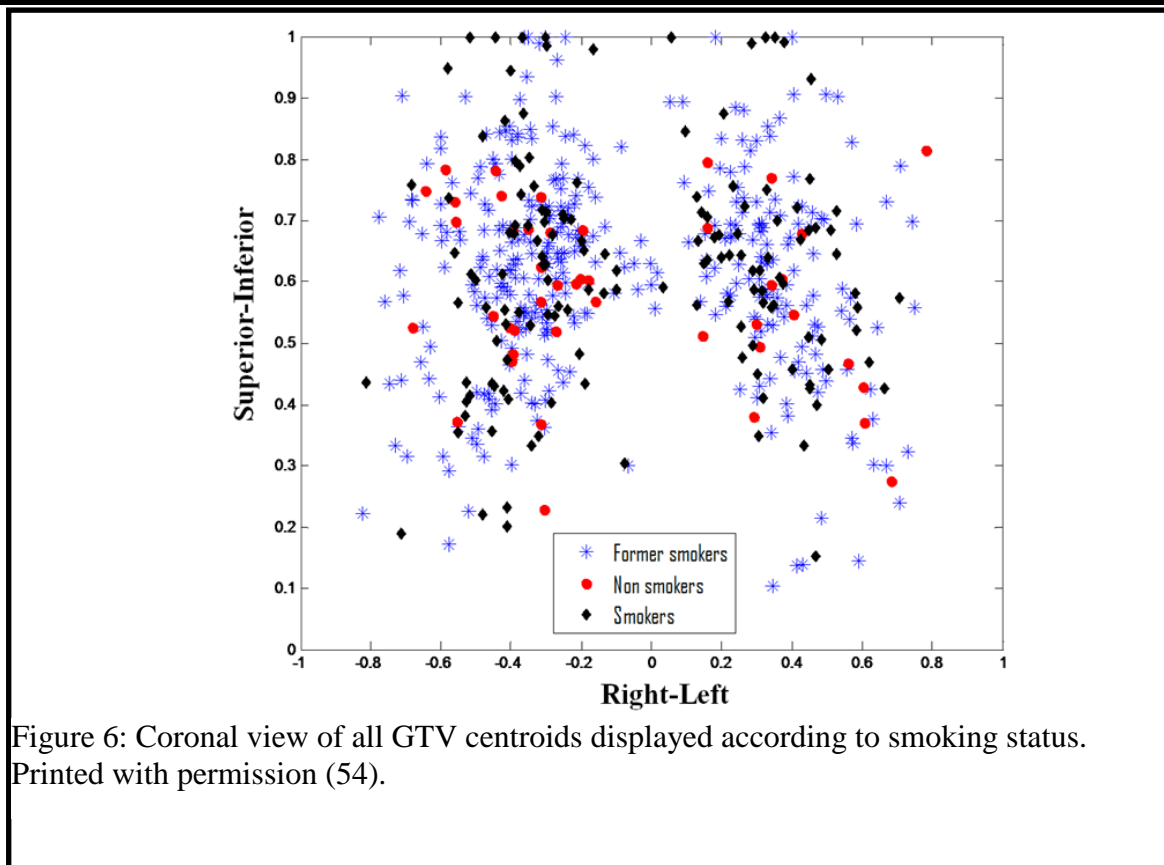
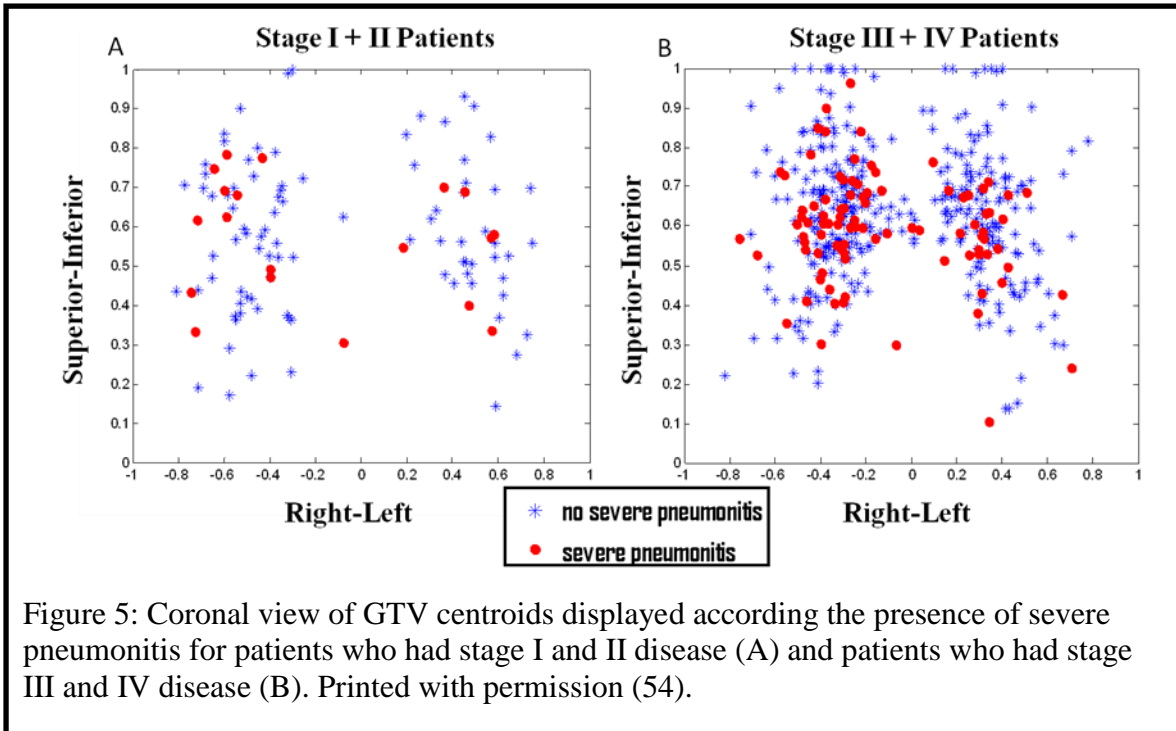


Figure 7 shows a graphical comparison of the GTV centroids that included nodal volume (Figure 7A) and GTV centroids where nodal volume was excluded (Figure 7B). As expected, when nodal volume is excluded, the density of

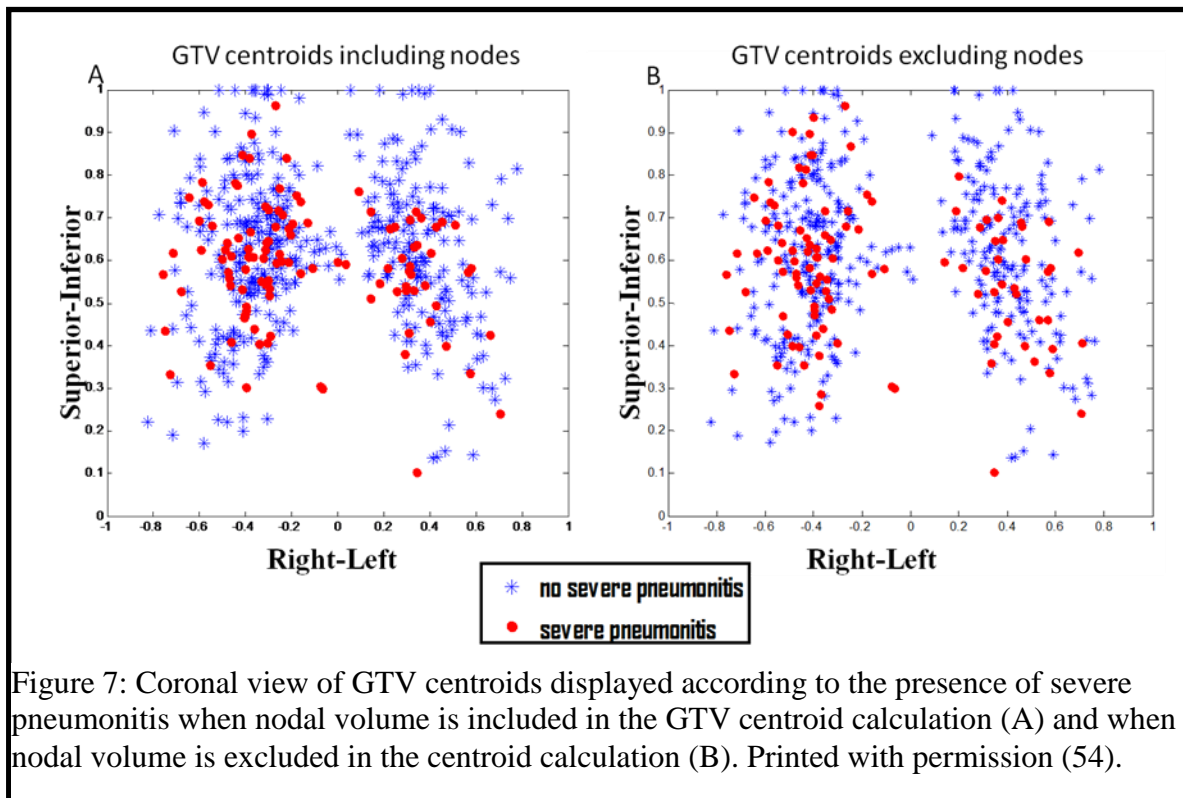


Figure 7: Coronal view of GTV centroids displayed according to the presence of severe pneumonitis when nodal volume is included in the GTV centroid calculation (A) and when nodal volume is excluded in the centroid calculation (B). Printed with permission (54).

the GTV centroids appears to move toward the periphery of the lung away from the mediastinum. However, the severe pneumonitis events appear to have the same spatial distribution whether nodal volume is included or excluded.

Pneumonitis Rates

Our study cohort included 325 right-lung tumors and 222 left-lung tumors. The severe pneumonitis rate was 22.5% (73/325) for the right-lung tumors and 17.1% (38/222) in the left-lung tumors. Table 2 shows the pneumonitis rates when the lungs are divided into equal thirds in the SI orientation. The pneumonitis

rate was lowest in the superior portion of the lung (16%); however, the pneumonitis rates were not significantly different ($p=0.376$ using the chi-square test). Table 3 shows the pneumonitis rates when the lung was divided into equal quartiles.

SI Location (scale 0-1)	Pneumonitis rate
Superior (0.66-1)	0.16 (35/218)
Middle (0.33-0.66)	0.23 (70/301)
Inferior (0-0.33)	0.21 (6/28)

Table 2. Pneumonitis rates for each superior-inferior third of the lung. Printed with permission (54).

SI Location (scale 0-1)	Pneumonitis rate
Superior (0.75-1)	0.11 (11/100)
Upper Middle (0.5-0.75)	0.23 (76/327)
Lower Middle (0.25-05)	0.21 (22/105)
Inferior (0-0.25)	0.13 (2/15)

Table 3. Pneumonitis rates for each superior-inferior quartile of the lung. Printed with permission (54).

The pneumonitis rate was lowest in the upper quartile (11%); again, however, the pneumonitis rates were not significantly different ($p=0.056$). It should also be noted that the most inferior quartile displayed a low pneumonitis rate (13%); however, the number of patients with centroids in this region is small, so the pneumonitis rate is subject to uncertainty (2 pneumonitis events out of 15 total

centroids). Because of the paucity of events in the lower quartile the data for the bottom two quartiles were combined (Table 4). We calculated pneumonitis rates of 11%, 23%, and 20% for the upper quartile, middle quartile, and lower two quartiles, respectively.

SI Location	Pneumonitis rate
Superior (0.75-1)	0.11 (11/100)
Middle (0.5-0.75)	0.23 (76/327)
Inferior (0-0.5)	0.20 (24/120)

Table 4. Pneumonitis rates according to quartiles with the two inferior quartiles combined. Printed with permission (54).

In order to compare our data with prior literature we stratified our data according to lobe. Specifically, we set the upper lobe equal to the upper half of the left lung and upper third of the right lung and the lower and middle lobe aggregate equal to the lower half of the left lung and the lower two-thirds of the right lung. Dividing the data in such a manner yielded pneumonitis rates of 18% for the upper lobes and 24% for the middle and lower lobes. Table 5 shows the pneumonitis rates when the data is further isolated to a smaller cohort of patients with stage I and II disease and another cohort of patients with stage III and IV disease. The pneumonitis rates for stage I and II patients were similar for all 3 regions. The pneumonitis rates were 18%, 17%, and 20% for the superior, middle, and inferior regions respectively. The pneumonitis rate for stage III and IV patients was lower for the superior portion (15%) than for the middle (25%) or the inferior portions (22%).

SI Location (scale 0-1)	Pneumonitis rate for stage I + II patients	Pneumonitis rate for stage III + IV patients
Superior (0.66-1)	0.18 (7/39)	0.15 (28/181)
Middle (0.33-0.66)	0.17 (10/60)	0.25 (62/239)
Inferior (0-0.33)	0.20 (2/10)	0.22 (4/18)

Table 5. Pneumonitis rates divided into thirds for patients grouped according to disease stage. Printed with permission (54).

Table 6 shows the pneumonitis rates when the lung is divided into SI thirds for the GTV centroids that excluded the nodal volume. The pneumonitis rates were 15%, 25%, and 19% for the superior, middle, and inferior portions of the lung respectively. These numbers are similar to what was reported for the GTV centroids that included the nodal volume (Table 2).

SI Location (scale 0-1)	Pneumonitis rate
Superior (0.66-1)	0.15 (32/218)
Middle (0.33-0.66)	0.25 (72/293)
Inferior (0-0.33)	0.19 (7/36)

Table 6. Pneumonitis rates for each superior-inferior third of the lung when nodal volume is excluded from the GTV centroid calculation. Printed with permission (54).

Modeling results

Table 7 shows the modeling parameters, 95% confidence intervals, and significance results. The comparison of the GTV centroid model and the conventional dose-volume model did not yield a statistically significant difference in model fit for the various orientations in GTV centroid spatial location that were investigated (all p values greater than 0.146). It should also be noted that when modeling parameters listed in Table 6 were recalculated for the GTV centroids that excluded the nodal volume, all of the p values remained above 0.05 indicating that including GTV centroid information does not improve the fit of the model to the data. Furthermore, Table 7 illustrates that incorporating GTV centroid information did not increase the predictive power of our current best-fitting model (all p values greater than 0.259).

Model parameters	TD_{50} (CI)	m (CI)	DMF (CI)	p
MLD	33.8 (29.1 43.1)	0.471 (0.37 0.63)	1.000	---
MLD + SI Location	32.4 (24.9 49.9)	0.467 (0.37 0.63)	1.096 (0.55 2.01)	0.766
MLD + AP Location	40.8 (27.4 73.9)	0.469 (0.37 0.63)	0.717 (0.32 1.45)	0.341
MLD + ML Location	34.2 (26.8 49.7)	0.470 (0.37 0.63)	0.967 (0.49 2.01)	0.920
MLD + RL Location	30.9(24.5 42.5)	0.476 (0.37 0.64)	1.246 (0.75 2.50)	0.400
MLD + Radial Location	35.0 (27.2 51.4)	0.469 (0.37 0.63)	0.897 (0.42 2.03)	0.768
MLD + SI distance from mean SI position	31.4 (27.2 39.9)	0.482 (0.38 0.66)	2.185 (0.78 13.97)	0.146

Table 7. Statistical comparison of nominal dose-volume model with modified (to include GTV centroid information) dose volume models according to modeling parameters and corresponding p values. *Abbreviations:* GTV = gross tumor volume, MLD = mean lung dose; CI = 95% confidence intervals, DMF = dose modification factor; SI = superior-inferior, AP = anterior-posterior, ML = medial-lateral, RL = right-left. Printed with permission (54).

Model parameters	p
MLD + Smoking + Time Censored	NA
MLD + Smoking + Time Censored + SI Location	0.802
MLD + Smoking + Time Censored + AP Location	0.301
MLD + Smoking + Time Censored + ML Location	0.893
MLD + Smoking + Time Censored + RL Location	0.259
MLD + Smoking + Time Censored + Radial Location	0.748
MLD + Smoking + + Time Censored + SI distance from SI mean	0.796

Table 8. Statistical comparison of most accurate current model with most accurate model modified by GTV centroid location. *Abbreviations:* MLD = mean lung dose; SI = superior-inferior, AP = anterior-posterior, ML = medial-lateral, RL = right-left. Printed with permission (54).

Discussion

The GTV centroid mapping performed in this study was done in a similar manner to the methods used by Hope et al. (33) and Bradley et al. (16), who divided the lung into quartiles and combined the two most inferior quartiles to account for the paucity of pneumonitis events. Hope et al. (33) reported grade 2 (steroids given for clinically significant pulmonary symptoms) pneumonitis rates of 9%, 25%, 35% for the upper quartile, middle quartile, and lower two quartiles, respectively while Bradley et al. (16) reported 4%, 25%, and 35%, for the upper quartile, middle quartile, and lower two quartiles, respectively. When we divided our data in a similar manner, we calculated pneumonitis rates of 11%, 23%, and 20% for the upper quartile, middle quartile, and lower two quartiles, respectively. The pneumonitis rates from the two studies show good agreement in the upper

two quartiles. However, our results did not show increasing pneumonitis rates toward the inferior of the lung, as indicated in the study by Hope et al. (33) and Bradley et al. (16). It is also possible to compare our data with results presented by Graham et al. (30), who categorized tumor location by lobes and reported pneumonitis rates of 11% for the upper lobe and 29% for the middle and lower lobes. Dividing our data according to lobe yielded pneumonitis rates of 18% for the upper lobes and 24% for the middle and lower lobes. The lower pneumonitis rate in the upper lobe was reproduced; however, the difference in pneumonitis rates between the lobes was not as extreme as that presented by Graham et al. (30). One possible explanation for the discrepancy between the results of our study and those of the studies by Hope et al. (33), Bradley et al. (16) and Graham et al. (30) is the limited incidence of GTV centroids near the inferior region of the lung. Our study and the study by Hope et al. (33) both noted paucity of centroids and events in the inferior portion of the lung, which implies that pneumonitis rates can be erratically driven by the presence or absence of a few events.

The modeling results and the data presented in Figure 7 and Table 6 indicate that there is little difference when comparing GTV centroids that include nodal volume and GTV centroids that exclude nodal volume. Theoretically, there are advantages and disadvantages to using either method; however, our results indicate that the inclusion or exclusion of the nodal volume in the GTV centroid calculation does not influence the relationship between spatial location and pneumonitis rates.

Figure 6 illustrates that GTV centroids located in the superior portion of the lung were associated with smokers and former smokers. The superior portion of the lung also showed the lowest pneumonitis rates (Tables 2-4). Several studies have noted that the risk of developing radiation pneumonitis is influenced by smoking status (37, 52, 57, 58). Our results indicate that smoking status also influences the spatial position of the tumor within the lung. This indication may help explain why lower pneumonitis rates have been observed in the superior region of the lung (32, 33, 53).

Despite our large patient population, we were not able to significantly improve the accuracy of the pneumonitis model by incorporating GTV centroid information. This finding conflicts with other studies, which have reported a correlation between pneumonitis and radiation to the lower lung. One possible explanation is the noted (32, 33) paucity of events in the lower lung. Another potential reason for the discrepancy is that we investigated GTV centroids, while Yorke et al. (32) and Seppenwoolde et al (43) analyzed dose metrics for various regions of the lung.

The methods and data presented in this work builds on prior studies and offers some unique advantages to performing a spatial analysis. This study is done with a large clinical database of 547 patients, which affords it greater statistical power. In addition, the method of including GTV centroid location as a DMF in the predictive model is a rigorous way to analyze the spatial effect because it explicitly aims to separate the dose volume parameter and the spatial parameter. Furthermore, the presented modeling method treats GTV centroid location as a

continuous variable and is therefore not dependant on the location of the lung division (as is the case when dividing the lung into various regions and calculating pneumonitis rates). Finally, the data presented in this work studies the relationship between GTV centroid location and smoking status, disease stage, and whether or not including nodal volume influences spatial results” (54).

3D Dose Spatial Analysis

Methods

The 3D spatial analysis was performed using the same patient database described in the introduction. The study was published by Vinogradskiy et al (55) and is quoted here.

“Novel Spatial Analysis

All patient treatment plans were de-archived into the treatment planning system and the 3D dose distribution of each patient lung was mapped onto one common coordinate system. The boundaries of the coordinate system were defined by the extreme points of each individual patient lung (Figure 8). For each patient, the

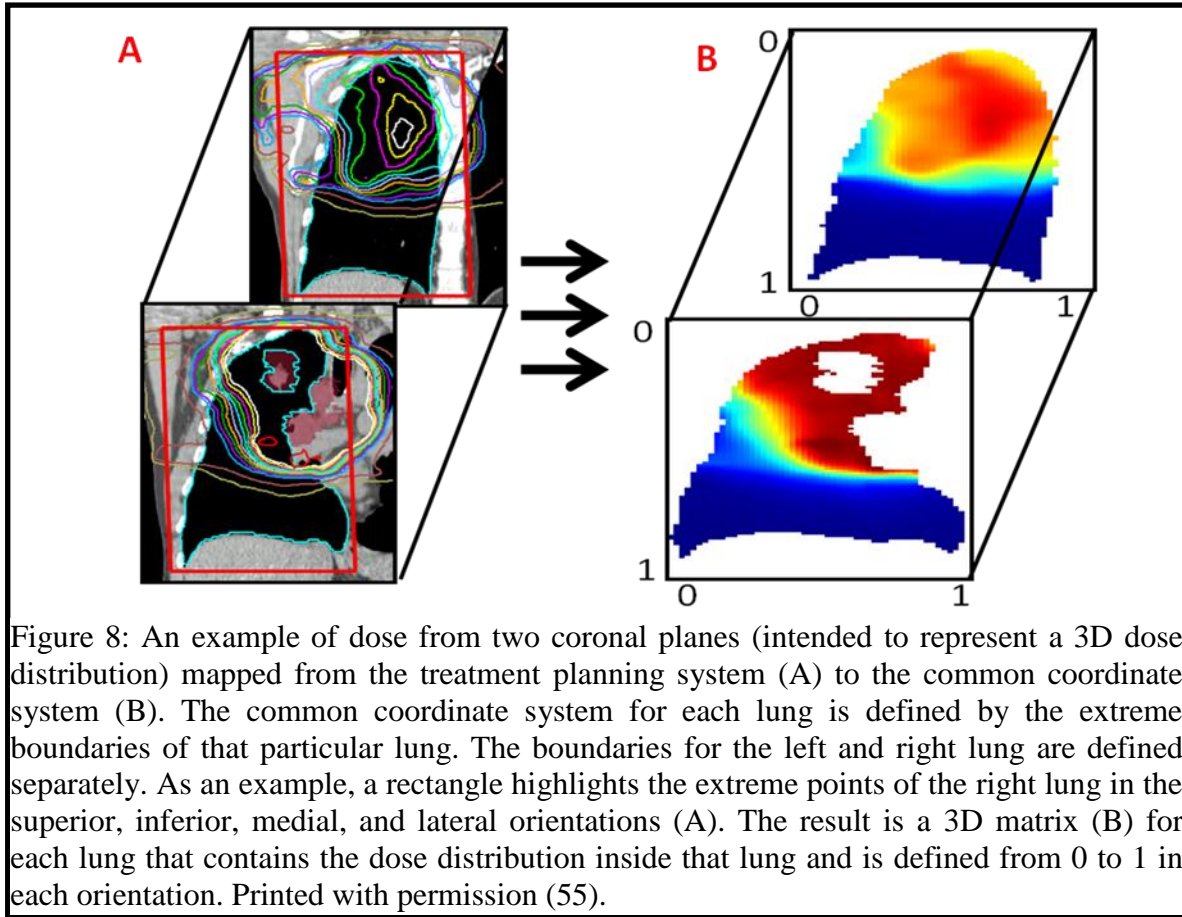


Figure 8: An example of dose from two coronal planes (intended to represent a 3D dose distribution) mapped from the treatment planning system (A) to the common coordinate system (B). The common coordinate system for each lung is defined by the extreme boundaries of that particular lung. The boundaries for the left and right lung are defined separately. As an example, a rectangle highlights the extreme points of the right lung in the superior, inferior, medial, and lateral orientations (A). The result is a 3D matrix (B) for each lung that contains the dose distribution inside that lung and is defined from 0 to 1 in each orientation. Printed with permission (55).

coordinate system for the right and left lungs were determined separately. For example, the extreme medial point of the right lung provided the medial boundary of the right lung coordinate system while the extreme lateral point of the right lung provided the lateral boundary of the right lung coordinate system. The boundaries were defined in the same manner for the anterior-posterior (AP) and superior-inferior (SI) orientations. The end result was a 3D matrix for each lung that contained the dose distribution inside that lung and was defined from 0 to 1 in each orientation. The 3D matrix was a masked image of the dose inside the lung, in other words, each pixel contained a scaled dose value if it was within the lung and 0 if the pixel was outside of the lung contour. This process ensured that each

patient's lung dose distribution was defined from 0 to 1 and was therefore mapped on the same coordinate system. It should be noted that the lung region of interest (ROI) was defined as total lung minus GTV.

Once all dose distributions were mapped onto the common coordinate system the spatial information was incorporated into a predictive radiation pneumonitis model. To be consistent with the literature, we used the LKB formulation (24) to calculate NTCP...To incorporate spatial information into the LKB model, the dose to each voxel was weighted according to its location in the lung. We started with the mathematical definition of *MLD* which can be written as

$$MLD = \sum_i v_i D_i, \quad \text{Equation 8}$$

where v is the volume, D is the dose, and i loops over all the dose bins. Next, we modified the term in Equation 8 to define a spatially weighted effective dose that can be written as

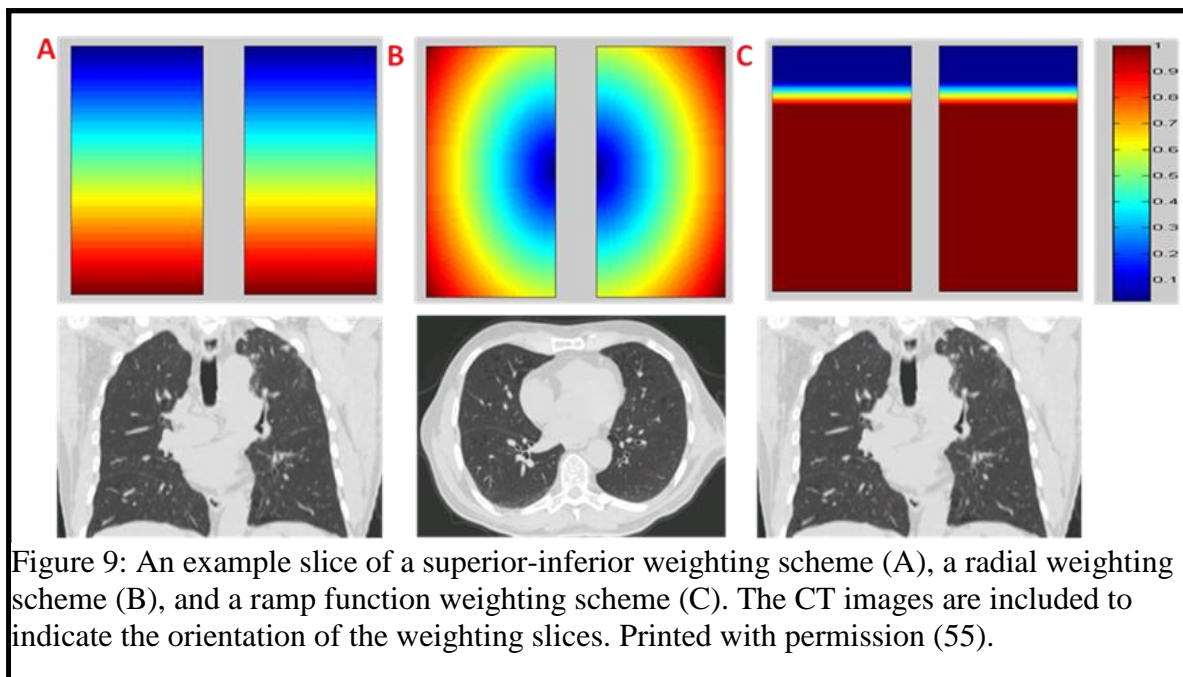
$$D_{eff} = \sum_i v_i D_i (1 + C w_i). \quad \text{Equation 9}$$

Substituting the new effective dose term (Eq 9) and re-writing the parameter t (Eq 4) the new model can be written as

$$t = \frac{(\sum_i v_i D_i + C \sum_i w_i v_i D_i) - TD_{50}}{mTD_{50}}, \quad \text{Equation 10}$$

where C is a model fitting parameter and w is a spatial weighting value that comes from a user-defined spatial weighting matrix. The user-defined spatial weighting matrix is intended to reflect the spatial pattern that is to be investigated. For this work, we investigated spatial weighting matrices that contained linearly scaled values between 0 and 1 according to each of the following orientations: SI, AP, right-left (RL), medial-lateral (ML), and radial. Conceptually, the higher

weighting values imply that a particular region is more radiosensitive than the region described by the lower weighted values. As an example, an SI weighting matrix (Figure 9A) assumes that the dose to the superior lung voxels is less lethal than the dose to the inferior lung voxels while a radial weighting matrix (Figure 9B) assumes the dose to the periphery of the lung is more lethal than the dose closer to the mediastinum.



In addition to linear SI weighting, we investigated a ramp function weighting scheme. The ramp function weighting scheme originated from our previous GTV centroid analysis which found pneumonitis rates of 11%, 23%, and 20% for the superior, middle, and inferior portion of the lung respectively (54). The ramp function weighting scheme (Figure 9C) weighs the superior voxels by 0 and linearly increases the weighting towards 1 for the middle and inferior portions of the lung. The model fitting parameter C allows the relative contribution of the

spatially weighted voxels to change based on the entire population. The sign of the parameter C provides information on whether the optimal fit of the model is along the direction of the weighting scheme chosen (positive C value) or against the direction of the weighting scheme chosen (negative C value). The TD_{50} , m , and C parameters were all fit to our dataset. To test the significance of incorporating spatial information into the LKB model the likelihood ratio test was used. Specifically, the fit of the model that incorporated spatial and dose-volume information (Eq. 10) was compared to the fit of the dose volume model (Eq. 4) to determine whether adding spatial information significantly improved the fit of the model to the data. We present the significance value (p) that demonstrates whether or not there was a statistically significant improvement in the model fit.

Lung Division Analysis

As a byproduct of the lung-mapping method described in the previous section it is trivial to write computer code to divide the lung into various geometrical regions and study the correlation between local dosimetric parameters of each lung region and radiation pneumonitis rates. In order to compare our results with previous work, we divided the lungs according to volume into equal geometrical halves (superior and inferior half) and equal geometrical thirds (superior, middle, and inferior third). A mean dose was calculated for each local region. A multivariate logistic regression analysis with stepwise inclusion of factors was used to determine which local mean dose was independently correlated with radiation pneumonitis. Furthermore, we tested whether the mean

dose to any one particular region was a better predictor of radiation pneumonitis than the overall MLD.

Results

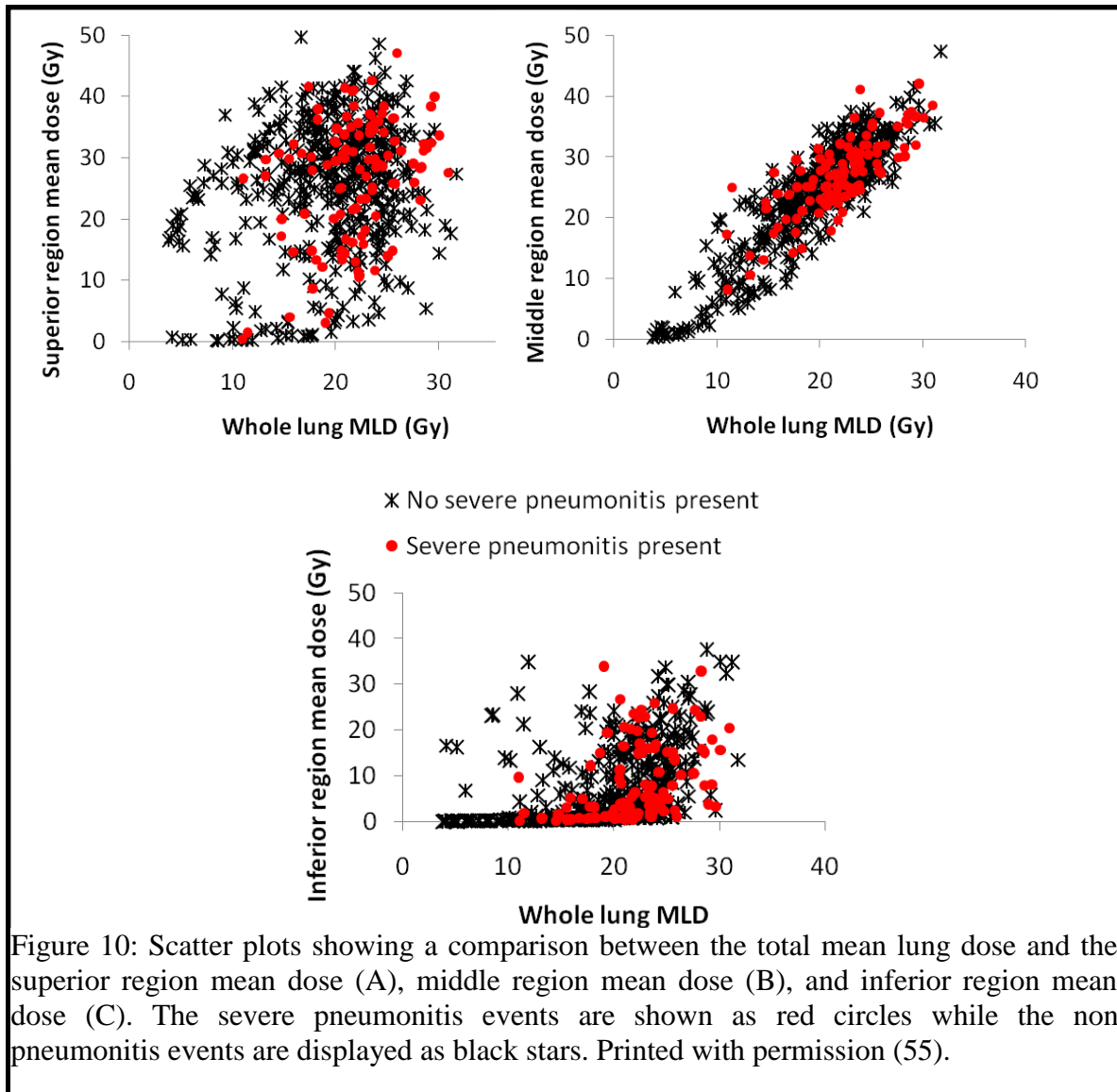
Of the 547 patients analyzed, 111 (20.3%) experienced severe (grade 3 or greater) radiation pneumonitis. Table 9 shows the model fitting parameters, 95% and 68% confidence intervals, and the p values for the various weighting schemes investigated.

Model parameters	Orientation of matrix	$TD50$ (CI_{95}) (CI_{68})	m (CI_{95}) (CI_{68})	C (CI_{95}) (CI_{68})	p
MLD	NA	34.6 (30.1 45.3) (31.9 38.7)	0.488 (0.38 0.67) (0.42 0.57)	NA	NA
MLD + SI Weighting	0 = superior 1 = inferior	29.8 (19.2 99.2) (23.1 44.3)	0.478 (0.37 0.66) (0.41 0.56)	-0.292 (-0.99 3.46) (-0.72 0.54)	0.6468
MLD + AP Weighting	0 = anterior 1 = posterior	27.0 (14.00 732) (18.4 51.3)	0.488 (0.38 0.67) (0.43 0.57)	-0.484 (-1.36 41.5) (-1.05 1.01)	0.6330
MLD + ML Weighting	0 = medial 1 = lateral	37.3 (16.64 inf) (22.7 117.8)	0.489 (0.38 0.67) (0.42 0.57)	0.160 (-1.1103 inf) (-0.7 4.8)	0.9034
MLD + RL Weighting	0 = right 1 = left	32.9 (25.1 51.8) (28.3 39.9)	0.491 (0.38 0.67) (0.42 0.57)	-0.123 (-0.70 0.81) (-0.43 0.26)	0.7189
MLD + Radial Weighting	0 = central 1 = distal	14.1 (10.3 inf) (14.4 56.1)	0.495 (0.37 0.68) (0.42 0.58)	-0.394 (-1.44 inf) (-1.18 1.20)	0.5742
MLD + ramp function Weighting	0 = superior 1 = inferior	21.1 (11.3 inf) (14.5 41.6)	0.470 (0.36 0.65) (0.41 0.55)	-0.418 (-0.74 inf) (-0.63 0.20)	0.4176

Table 9. A comparison of model parameters and significance values for the various weighting schemes investigated. *Abbreviations:* CI_{95} = 95% confidence intervals, CI_{68} = 68% confidence intervals, MLD = mean lung dose; SI = superior-inferior, AP = anterior-posterior, ML = medial-lateral, inf = infinity, RL = right-left. Printed with permission (55).

The comparison of the conventional dose volume model and the spatially weighted dose model did not yield a statistically significant difference in model fit for any of the spatial weighting schemes. These results suggest that taking individual voxel location into account does not significantly improve the fit of the model.

When dividing the lung into two halves, both the mean dose to the superior half and the mean dose to the inferior half were associated with severe pneumonitis. In a stepwise logistic regression analysis, using the mean dose to the superior half, the mean dose to the inferior half, and the overall MLD, the overall MLD was selected at the 0.05 significance level. When dividing the lung in thirds, the mean dose to the middle third was the only dosimetric quantity associated with severe pneumonitis. It is also important to note that the log-likelihood using the overall MLD was greater than the log-likelihood using the middle region mean dose, indicating that the overall MLD was more accurate in predicting radiation pneumonitis than was the mean dose to the middle third. The scatter plot in Figure 10 indicates that when the mean doses to the three regions (inferior, middle, and superior) were compared against the overall MLD, the mean dose to the middle lung region is most correlated with the overall MLD.



Discussion

The presented work proposes a novel method to study the relationship between the spatial location of the deposited 3D lung dose distribution and pneumonitis rates. The method proposed in this study builds on prior work and provides unique advantages to performing a spatial dose analysis. In previous work, there have been two general approaches to studying the relationship

between the spatial effect and pneumonitis rates. These approaches involve dividing the lung into various geometrical regions and studying the dosimetric indices derived from them (34, 43) or studying the GTV centroid locations (30, 33, 53). As noted by Hope *et al.* (33), the GTV centroid acts as a surrogate for the location of the deposited dose and does not take into account GTV volume or treatment planning techniques. In addition, the results of both methods are sensitive to the location of the boundaries that define the lung divisions. The spatial weighting method proposed in this work incorporates the entire 3D dose distribution and treats each orientation as a continuous variable and therefore the results do not depend on how the lung is divided. Furthermore, after all the dose distributions have been mapped onto the common coordinate system, it is then possible to divide the data along any geometrical boundaries without the laborious process of re-contouring and re-calculating dosimetric parameters in the treatment planning system. In this work, we divided the lung into two and three equal-volume superior-inferior regions. However, it would be a matter of a few lines of computer code to divide the dose distributions into any number of divisions along any orientations. Finally, incorporating the spatial dose information into the LKB model and testing for a statistically significant increase in model accuracy allows for a way to mathematically separate spatial location and dose volume effects. We believe this is a more rigorous approach to determining whether the spatial location of the deposited lung dose is correlated with pneumonitis rates.

When dividing our data in a similar manner to Yorke *et al.* (34) (into a superior and inferior region) we found that both regions were significantly

associated with radiation pneumonitis at the 0.05 significance level. While Yorke *et al.* (34) found that only dosimetric indices to the inferior lung region were associated with radiation pneumonitis. Both studies confirmed that dosimetric indices to the entire lung were correlated with pneumonitis. One possible explanation for the disagreement in the results to the superior lung region is the overall location of the deposited dose in the two study populations. When dividing the lung into three regions we found that only the middle region mean dose was associated with radiation pneumonitis and the scatter plot (Figure 10) confirmed that the overall MLD values are most closely resembled in the middle portion of the lung. Most of the patients in our database have clinical stage III or higher disease and the dose to the middle portion of the lung is a product of irradiating the nodes in the mediastinum. Therefore, the best representation of the overall MLD is the mean dose to the middle portion of the lung. It is also important to note that when dividing the lung into regions we found that the best predictor of pneumonitis was the overall MLD and not the mean dose to any one particular region confirming that for our data there is no additional benefit to analyzing different portions of the lung.

The modeling and lung division results indicate that for our patient cohort the spatial location of the deposited lung dose does not influence the risk of radiation pneumonitis. This finding is generally not in agreement with the other studies which indicate a relationship between dose to the inferior lung and pneumonitis rates (30, 33, 34, 53). For example, Hope *et al.* (33) report grade 2 (steroids given) pneumonitis rates of 9% for the upper quartile of the lung, 25%

for the middle quartile, and 35% for the lower two quartiles and Bradley *et al.* (53) cite 4% for the upper quartile, 25% for the middle quartile, and 35% for the lower two quartiles. When we divide our data in a similar manner, we calculated pneumonitis rates of 11%, 23%, and 20% for the upper, middle, and lower two quartiles respectively (54). Comparing our data with the studies performed by Hope *et al.* (33) and Bradley *et al.*, (53) there is good agreement in the upper two quartiles; however, our study does not show decreasing pneumonitis rates towards the inferior of the lung. There are several possible explanations for the differing results. One possible explanation is the difference in methods used to perform the analysis. The studies mentioned above analyzed GTV centroid location while the current study uses the 3D dose distribution. Another possible explanation for the discrepancy is the differing patient populations. As noted earlier, our study contains patients mostly with stage III and higher disease. As a result of irradiating the nodes in the mediastinum most of the dose is concentrated in the middle portion of the lung. Therefore, it is possible that most of the valuable dosimetric information is contained within the middle portion of the lung, overriding any superior-inferior spatial effect. Another possible explanation for the differing results is the lack of information towards the inferior portion of the lung. The Hope *et al.* (33) study and our study (54) both note a lack of centroids towards the inferior lung. The lack of centroids in the inferior lung implies that pneumonitis rates can be erratically driven the presence or absence of a few pneumonitis events.

The novel method was applied to a patient database and it was determined that for our patient cohort the spatial location does not influence the risk of pneumonitis. Because of the number of patients in our study and the rigor of our novel spatial method we believe that the current work adds an important clinical contribution to existing knowledge about the spatial effect in the lung” (55).

There were several limitations to our spatial analysis. We used the LKB MLD model to perform the modeling in this study. We chose this model because it is consistent with what has been cited in the literature (6) and consistent with the methods we previously used to analyze our data (37, 52). In future work, it would be interesting to incorporate spatial information into other mathematical forms of dose response models (26, 27) and test for whether the fit of the model is improved. In addition, as more patient data is collected, it would be informative to perform a 3D spatial analysis for patients grouped by their clinical stage to further isolate the spatial effect.

Conclusions

A novel method using the GTV centroid and the 3D spatial dose distribution was proposed to investigate the relationship between the location of the deposited lung dose and pneumonitis rates. The method provides unique advantages in that it: incorporates the entire 3D dose distribution, treats spatial information as a continuous variable, and aims to mathematically separate spatial and dose volume effects. The novel spatial method was applied to a large 547 NSCLC patient database. The hypothesis of this study is rejected; incorporating spatial information did not improve the fit of the model to the data. Although our results showed lower pneumonitis rates for the superior portion of the lung, we did not find an overall trend of increasing pneumonitis rates toward the inferior

portion of the lung. Furthermore, for our patient cohort, incorporating GTV centroid information or 3D spatial information did not lead to a statistically significant gain in pneumonitis model fit, indicating that for our patient cohort the spatial location of the deposited dose not influence the risk of pneumonitis (54, 55).

Specific Aim 2: Ventilation study

Introduction

For lung cancer patients, lung function may not be homogeneous and may vary throughout the lung. Lung function can be heterogeneous because of the tumor, prior existing lung conditions such as emphysema and chronic obstructive pulmonary disease (COPD), or the inherent heterogeneity of the lung parenchyma. Currently, NTCP models rely on basic dose-volume metrics (such as MLD and V_{20}) and do not take into consideration the heterogeneous lung function. Several researchers have proposed to incorporate imaging to assess lung function and to predict for thoracic toxicity (40-43, 59-62). Most of the studies have investigated either SPECT based perfusion imaging or CT imaging. Nioutsikou et al (42) and Miften et al (41) provide methodology on incorporating SPECT-based functional imaging into predictive modeling. Seppenwoolde et al (43) studied the regional lung differences using perfusion. Ma et al (63) reported a weak correlation between CT-based density changes and PFT results. However, besides CT and SPECT-based perfusion, few imaging modalities have been incorporated into the evaluation of normal tissue toxicity. One potential way to assess lung function is through ventilation. As noted by Vinogradskiy et al (64)...

“An exciting and new form of ventilation imaging has been proposed by Guerrero *et al.* (65). These authors proposed to use 4-dimensional computed tomography

(4DCT) data to calculate ventilation. A 4DCT data set consists of 3-dimensional (3D) CT images resolved into different phases of the breathing cycle (66, 67). Because 4DCT data are routinely acquired for thoracic radiation therapy treatment planning, calculating ventilation maps from 4DCT data does not add any extra dosimetric or monetary cost to the patient. Several groups have investigated different aspects of ventilation imaging (44, 65, 68-71). For example, Yaremko *et al.* (59) discussed the idea of designing treatment plans to avoid highly ventilated areas of the lung, Ding *et al.* (72) studied the changes in lung ventilation after radiation therapy, Castillo *et al.* (73) explored the different ways of calculating ventilation from 4DCT data with corresponding comparative evaluation with clinically acquired SPECT ventilation, and Yamamoto *et al.* (69) investigated 4DCT based ventilation imaging for patients with emphysema” (64).

The detailed methodology of calculating ventilation maps from 4DCT data is described in detail by Vinogradskiy *et al.* (64).

“The first step is to export all of the phases of the 4DCT dataset and appropriately segment both lungs on the exhale and exhale CT datasets. Lung segmentation was performed by delineating lung voxels with CT values from -999 to -250 and by using a three-dimensional morphological growing algorithm (73) to delineate the trachea, main-stem bronchi, and pulmonary vasculature” (64).

An example axial and coronal slice of segmented lung is shown in Figure 11.

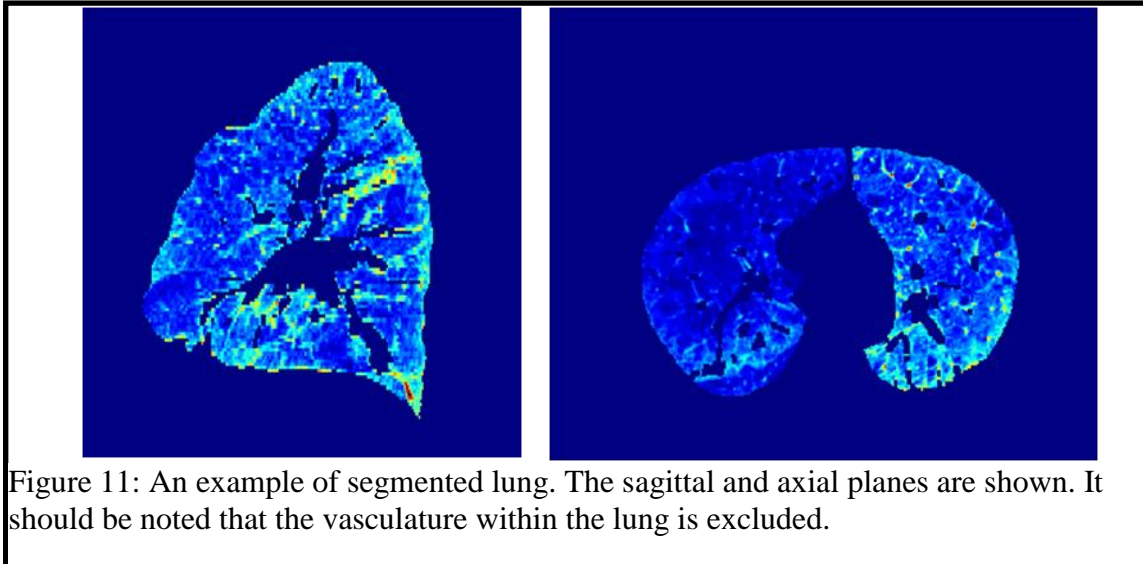


Figure 11: An example of segmented lung. The sagittal and axial planes are shown. It should be noted that the vasculature within the lung is excluded.

The remaining steps of calculating ventilation images are described by Vinogradskiy et al (64).

“Once the lungs were segmented, deformable image registration using trajectory modeling (74) was used to link corresponding lung volume elements together between the inhale and the exhale data sets (Figure 12). It should be noted that 5 phases (half of the breathing cycle) were used for the registration algorithm and the segmentation used for the registration algorithm was more coarse than the procedure used for the ventilation image segmentation. The spatial accuracy of the registration algorithm has been

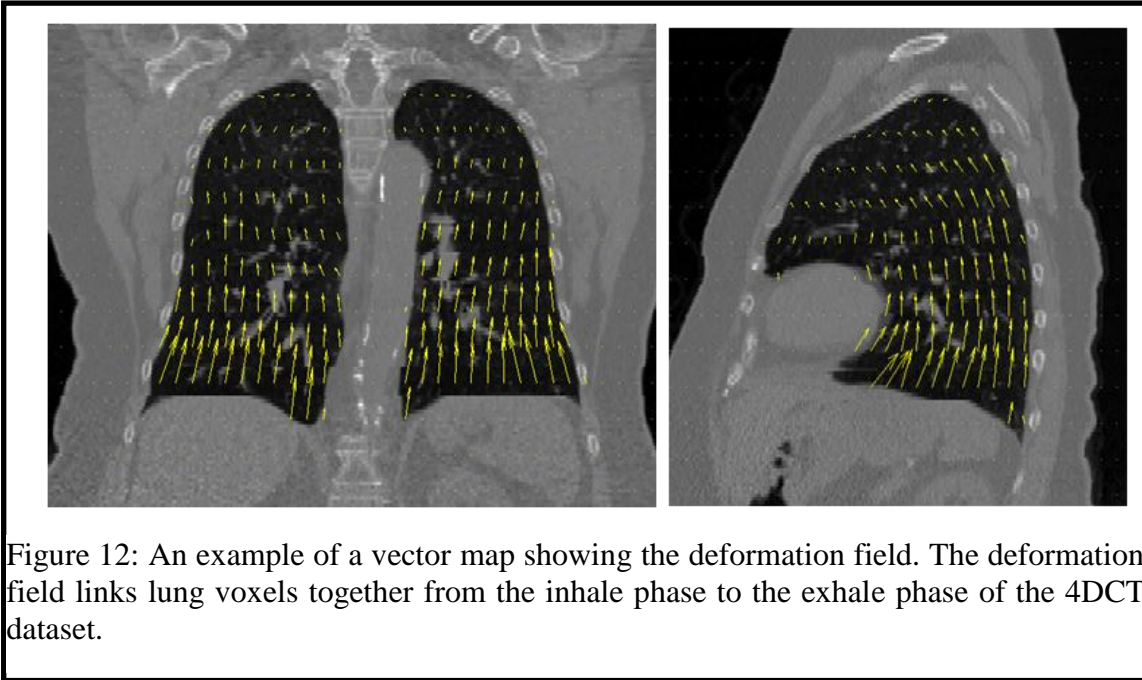


Figure 12: An example of a vector map showing the deformation field. The deformation field links lung voxels together from the inhale phase to the exhale phase of the 4DCT dataset.

reported to be 1.25mm (74). Following spatial registration, corresponding Hounsfield units were input into a density-change-based model. The model can be mathematically written as

$$\frac{V_{in}-V_{ex}}{V_{ex}} = 1000 \frac{HU_{in}-HU_{ex}}{HU_{ex}(1000+HU_{in})}, \text{ Equation 11}$$

where V_{in} and V_{ex} are the inhale and exhale volumes and HU_{in} and HU_{ex} are the inhale and exhale Hounsfield units of the individual lung voxels. The theory behind Equation 11 stems from the assumption that CT voxel content is composed of a linear combination of water-like material with a CT value of 0 and air-like material with a CT value of -1000 (75). Explicit derivation of Equation 11 is provided by Castillo *et al.* (73). The left side of the equation represents the local physiologic specific ventilation and the resulting 3D image displays the ventilation throughout the lung (Figure 13)...

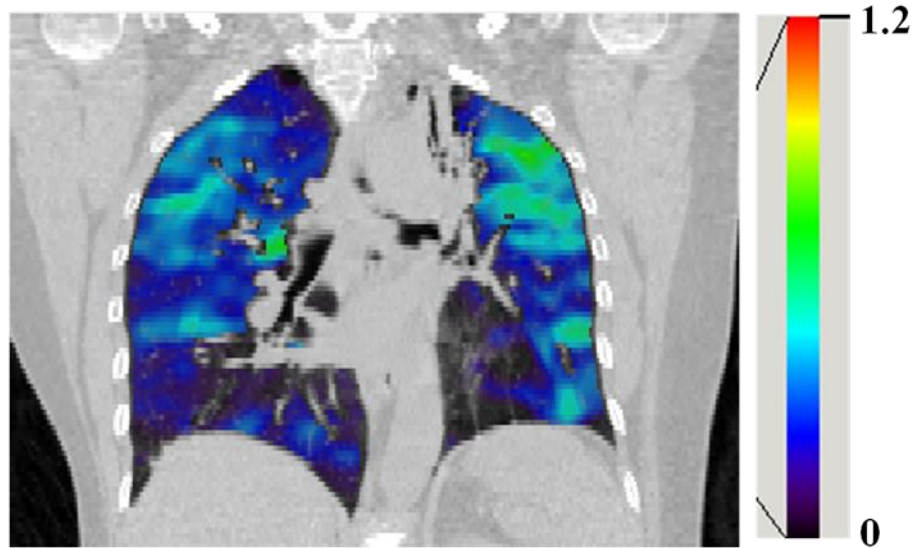


Figure 13: An example of a ventilation image overlaid on a coronal CT slice.

There were several steps taken to address the uncertainties in the ventilation image calculation process. We used 9x9x9 mm voxel averaging to account for noise in the CT image as well as any spatial errors in the deformable image registration algorithm. We visually inspected each ventilation image to check for image artifacts. Whenever relevant, we would re-segment the lungs in an attempt to mitigate the image artifacts. Furthermore, we manually checked each deformation map for any errors and discontinuities and if it would have been necessary we were prepared to rerun the deformation algorithm with different inputs in an attempt to gain a more spatially accurate deformation map. In addition, the ventilation images were assessed for self consistency (73). To assess for self consistency we compared the measured differences in lung volume with the ventilation-calculated differences in lung volume. The measured differences in lung volume were determined by taking the difference between lung volume of corresponding inhale and exhale image pairs. The calculated lung

volume difference was determined by summing the voxel ventilation for the segmented lung.”

It should be noted that other groups have proposed a different method of producing ventilation maps from 4DCT data. These methods calculate the Jacobian of the deformation field (68, 72) to produce ventilation maps. Castillo et al (73) have noted the similarities and differences between the density based method and the Jacobian based method of calculating ventilation images. Their main findings is that the Jacobian based method calculates a change in voxel volume while the density change based method calculates the change in air concentration in a particular voxel.

There is potential for this new and exciting way of calculating ventilation to be incorporated into radiation pneumonitis dose response modeling. Therefore the purpose of this study was to incorporate ventilation based functional information into the modeling of radiation pneumonitis. Our hypothesis was that the accuracy of radiation pneumonitis dose response models can be significantly improved by incorporating ventilation based functional information.

The study will be divided into 2 portions. The first portion will use weekly calculated ventilation images to investigate the mid-treatment changes in lung function that occur throughout the course of radiation therapy. It should be noted that this is strictly not a modeling study but rather an exploratory investigation to assess ventilation change throughout the course of radiation therapy. Specifically, we wanted to quantify the ventilation change as a function of dose and as a function of anatomy. The second part of the study will aim to explicitly incorporate pre-treatment ventilation imaging into the modeling of radiation pneumonitis.

Serial Ventilation Study

Methods

The serial ventilation study is presented from the manuscript published by Vinogradskiy et al (64).

“ Patient selection

All the patients for this study were chosen from a previous protocol that was approved by our Institution’s Review Board. Under the protocol, patients underwent weekly 4DCT scans for the duration of their therapy (76). The protocol was designed to assess weekly lung volume change and weekly lung tumor motion. To be eligible for the study, patients had to have a pathological diagnosis of NSCLC, and their course of radiation therapy had to be scheduled for at least 4 consecutive weeks. During the 4DCT scans, patients were immobilized using a VacLoc immobilization device (Med-Tech, Orange City, IA). The 4DCT images were acquired using cine mode on a multislice helical CT scanner (Discovery PET/CT; GE Healthcare, Waukesha, WI). A physicist was present during each 4DCT scan to make sure the patient’s breathing was not erratic; however, no attempt was made to make breathing equivalent from week to week. We chose 6 patients for our study from this protocol. The patients were chosen retrospectively to represent a wide range of clinical scenarios.

The treatment characteristics of all 6 patients are listed in Table 10 and the patient and tumor characteristics are listed in Table 11. Two of the patients were treated with proton therapy, and 4 patients were treated with IMRT. Two patients experienced severe (grade 3-5) radiation pneumonitis, and 3 patients had prior

lung diseases (such as emphysema and COPD). Each patient had either 7 or 8 4DCT datasets, the first of which was acquired prior to the beginning of treatment.”

Patient	Treatment Modality	Prescription	Mean Lung Dose (Gy)	Presence of severe pneumonitis (time to toxicity)
1	Proton	35 x 2.5 Gy	12.14	Yes (148 days)
2	IMRT	35 x 2 Gy	16.81	no
3	Proton	37 x 2 Gy	14.05	no
4	Proton	37 x 2 Gy	19.27	no
5	Proton	37 x 2 Gy	19.63	Yes (246 days)
6	IMRT	33 x 2 Gy	19.02	no

Table 10. Summary of treatment characteristics.

Patient	Age	Gender	Prior Lung Disease	Tumor location	Tumor Stage	Tumor Histology
1	73	M	COPD, Emphysema	Left lower lobe	IB	Non-differentiated NSCLC
2	67	M	none	Right upper lobe	IIIB	Non-differentiated NSCLC
3	68	M	none	Left upper lobe	IIIB	Squamous cell
4	71	F	none	Left lower lobe	IIIA	Squamous cell
5	77	F	COPD	Left upper lobe	IIIB	Squamous cell
6	72	M	Emphysema	Right lower lobe	IIIA	Squamous cell

Table 11. Summary of patient and tumor characteristics.

The ventilation images were calculated (using the methods previously described) for each week for every patient. The ventilation image processing was done in the manner described by Vinogradskiy et al (64).

“Ventilation image processing

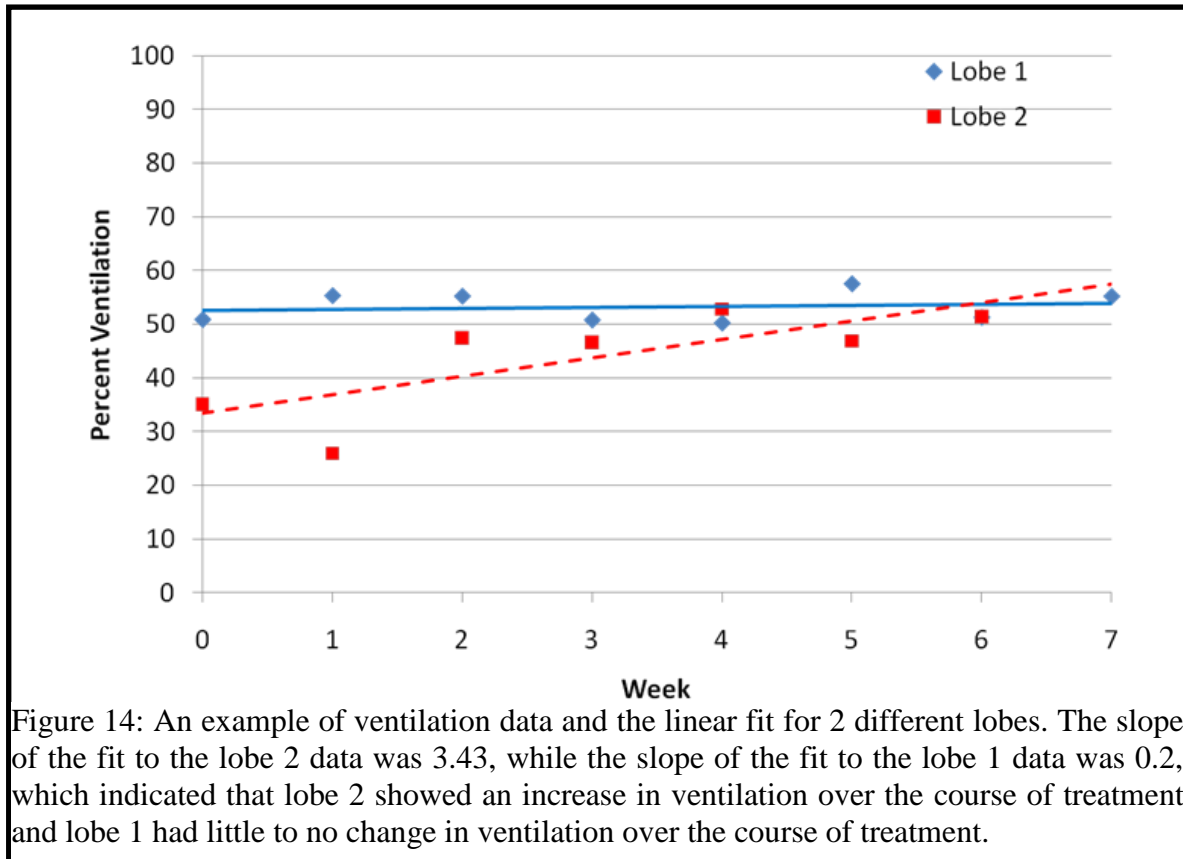
Once all the ventilation images were calculated, the next step was to normalize the data. We normalized the data by converting ventilation images to percentile images (59, 65, 73). Converting ventilation maps to percentile images as a normalization method was advantageous because it was the method least sensitive to the maximum ventilation value on a particular image. In other words, an erroneous hot spot minimally affected the scaling of the rest of the image. The percentile was determined by ordering the ventilation values and for each value calculating the percent that fell below that certain value.

To perform a quantitative analysis, it was necessary to have all the weekly ventilation images defined on the same coordinate system. Because the ventilation image is defined on the exhale CT coordinate system, we could register the exhale CT data sets and then apply the same transformations to the ventilation images. For each patient, we registered the exhale CT data set of each week to week 0 (which we define as the pre-treatment CT data set) using deformable image registration (77). All registrations were visually inspected by overlaying each week's exhale CT data set with the week 0 data set for that particular patient. Once the CT data were registered, the deformable transformations were applied to the ventilation maps.

Having all the ventilation images defined on the same coordinate space enabled us to perform a quantitative analysis. We performed a quantitative analysis by defining ROIs and tracking the ventilation values of those ROIs throughout each week of therapy. We defined ROIs in two ways: according to dose and according to anatomy. For the dose ROIs, we defined the ROI as the

volume that received greater than or equal to 20 Gy (V_{20}). The V_{20} was chosen because it is a common metric used in thoracic treatment planning and evaluation. We defined the anatomical ROIs by contouring the lobes of both the left and right lungs. Once the dose and lobe ROIs were defined we calculated the average percent ventilation for each ROI. The lung mask described was applied to the ventilation images at every time point. Therefore, the tumor volume was masked out for each weekly ventilation image. It should be noted that one patient had a tumor volume that occupied the entire lung lobe during pre-treatment. Therefore, for that particular patient we excluded the week 0 data point. In summary, our data included percent ventilation values for each patient, each week, and each lung lobe as well as percent ventilation values for each patient, each week and each V_{20} region.

To study ventilation change throughout treatment, we made a plot of the average percent ventilation for each ROI as a function of treatment week and performed a linear fit to the data (Figure 14). The slope of the linear fit was the metric used to evaluate ventilation change throughout treatment. A positive slope indicated an increase in ventilation in a particular ROI throughout treatment; a slope of 0 indicated no change in ventilation; and a negative slope indicated a decrease in



ventilation. As an example, Fig. XX shows a lobe that had an increase in ventilation throughout treatment and a lobe that had little to no change in ventilation.

Analysis of ROI data

The V_{20} ROI ventilation and slope data were used to study how ventilation changed throughout treatment as a function of dose. Specifically, we calculated the change in percent ventilation for the V_{20} ROI from pretreatment (week 0) to the final week of treatment. To evaluate the general trend in ventilation change with dose, we used the slope of the linear fit to the V_{20} ROI data.

In addition to dose, the ventilation in the different lobes of the lung was evaluated. Anatomically, ventilation is affected by airway opening or constriction,

and the best way to investigate this physiologic phenomenon using the available data is to organize the data according to lung lobe. First, we evaluated only the pretreatment (week 0) ventilation data. We grouped all the lobes into 2 categories, lobes that contained the GTV and lobes that did not contain GTV, and evaluated the average ventilation for each group. We categorized the lung lobes in this manner because we hypothesized that lobes that contained GTV were more likely to experience airway constriction and ventilation would therefore be significantly lower for those lobes.

Next, the lobe data were evaluated for all the treatment weeks. Particularly, we studied the slope of the linear fit to the lobe ROI data. We grouped all the lobes into 2 categories: lobes that contained GTV volumes that shrank and lobes that either did not contain the GTV or where the GTV did not get smaller. The slopes of the linear fit were statistically compared between the 2 groups of lung lobes using a *t*-test. Our hypothesis was that throughout treatment, the tumor was likely to decrease in volume and cause airway opening for a particular lobe and therefore one would expect the ventilation to increase throughout treatment for that particular lobe.

Results

Ventilation as a function of dose

The ventilation data for the V_{20} ROIs are displayed in Table 12. Ventilation increased in 4 patients and decreased in 2 patients between the final week of radiation therapy and week 0 (defined as pre-treatment). Four patients had a positive slope (slopes of 1.1, 1.4, 1.5, 0.3) of the linear fit to the ventilation

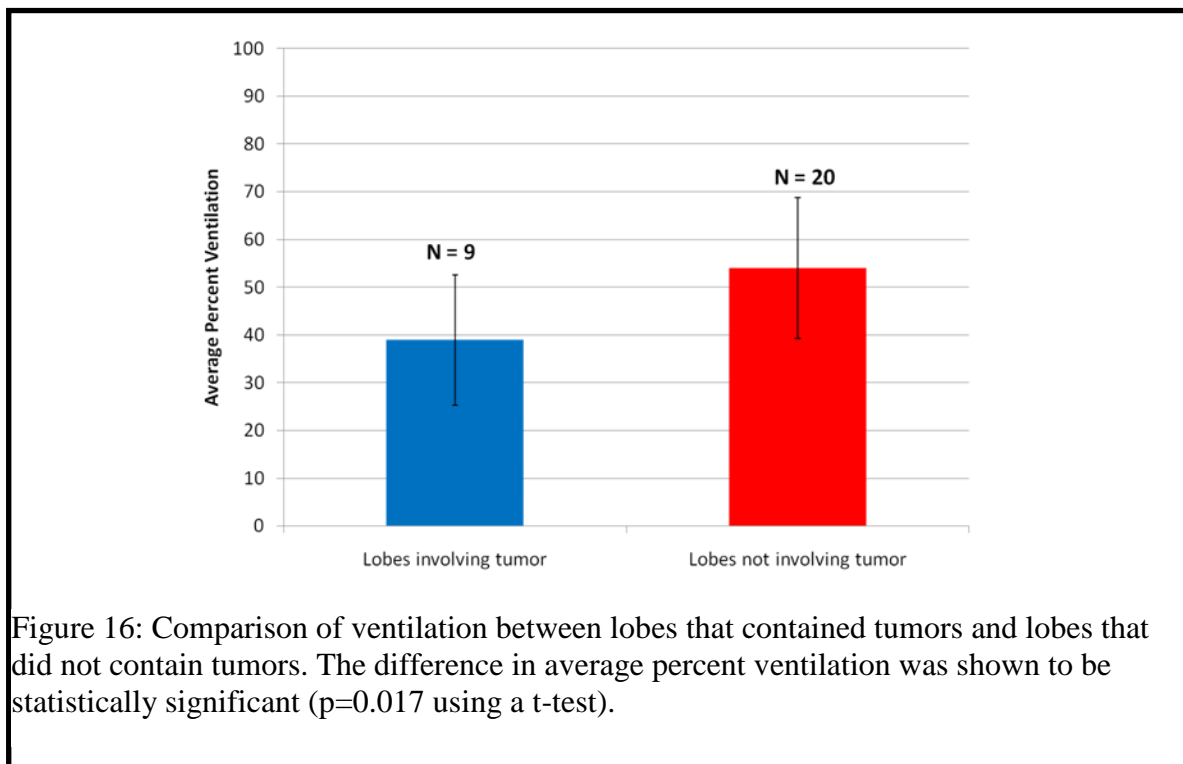
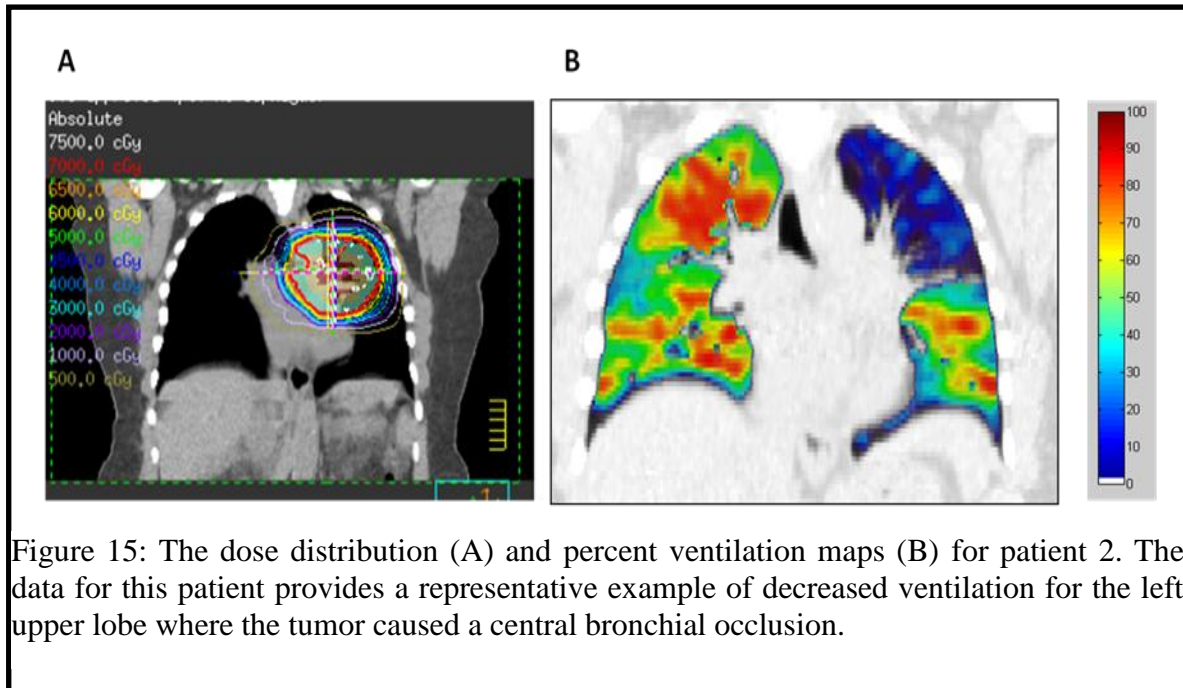
versus week data, indicating an increase in ventilation for the V_{20} region over the course of treatment. Two patients had a negative slope (-0.6, -0.5), indicating decreased ventilation. We found no consistent relationship between dose and ventilation; ventilation increased in some patients over the course of treatment and slightly decreased or did not change in others.

Patient	Week 0 Percent Ventilation for V_{20} ROI (%)	Final Week of therapy Percent Ventilation for V_{20} ROI (%)	Difference in Percent ventilation between the final week and week 0 (%)	Slope of linear fit to Ventilation data (%/Week)
1	56.5	54.1	-2.5	0.3
2	30.1	35.8	5.7	1.1
3	46.9	51.4	4.5	1.4
4	34.7	43.4	8.6	1.5
5	56.8	58.6	1.8	-0.6
6	54.1	53.2	-0.9	-0.5

Table 12. Percent ventilation data for ROIs defined according to V_{20} .

Pretreatment ventilation by lobe

Visually, pretreatment ventilation appeared to be lower in lobes that contained tumor. The decrease in ventilation was particularly evident when the tumor was occluding a central bronchial airway; a representative case is shown in Figure 15. To quantify this phenomenon, the lobes were categorized into 2 groups: lobes that contained tumor and lobes that did not contain tumor. The average pretreatment percent ventilation was $39 \pm 14\%$ (mean \pm standard deviation) for lobes that contained tumor and $54 \pm 15\%$ for the lobes that did not contain tumor (Figure 16). The difference in ventilation between the 2 groups was statistically significant ($p=0.017$ using a t -test).



Change in ventilation by lobe over the course of treatment

Two distinct patterns emerged when we qualitatively analyzed the series of weekly ventilation images for each patient. When tumor volume was visibly reduced, ventilation appeared to increase in the lobe where the tumor volume was reduced. A representative case is shown in Figure 17. When tumor volume was not visibly reduced, the 3D ventilation distribution did not change throughout treatment. A representative case is shown in Figure 18. To assess both trends quantitatively, we grouped the lobes into 2 categories: lobes that contained GTV volumes that shrank and lobes that either did not contain the GTV or where the GTV did not get smaller. The GTV volume reduction for each patient is shown in Table 13. Except for patient 3, all patients experienced a decrease in GTV volume from pre-treatment to the final week of treatment. Therefore, we grouped lobes that contained tumor for patients 1,2,4,5,6 into one group and lobes that did not contain GTV for patients

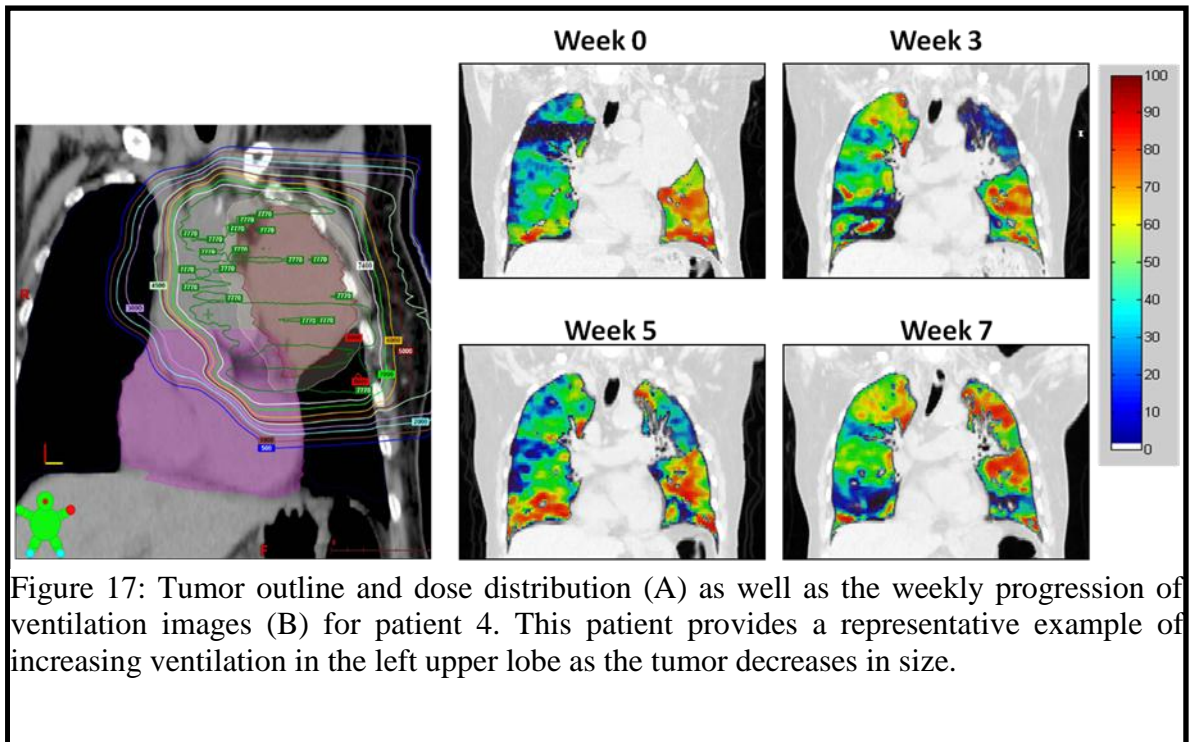


Figure 17: Tumor outline and dose distribution (A) as well as the weekly progression of ventilation images (B) for patient 4. This patient provides a representative example of increasing ventilation in the left upper lobe as the tumor decreases in size.

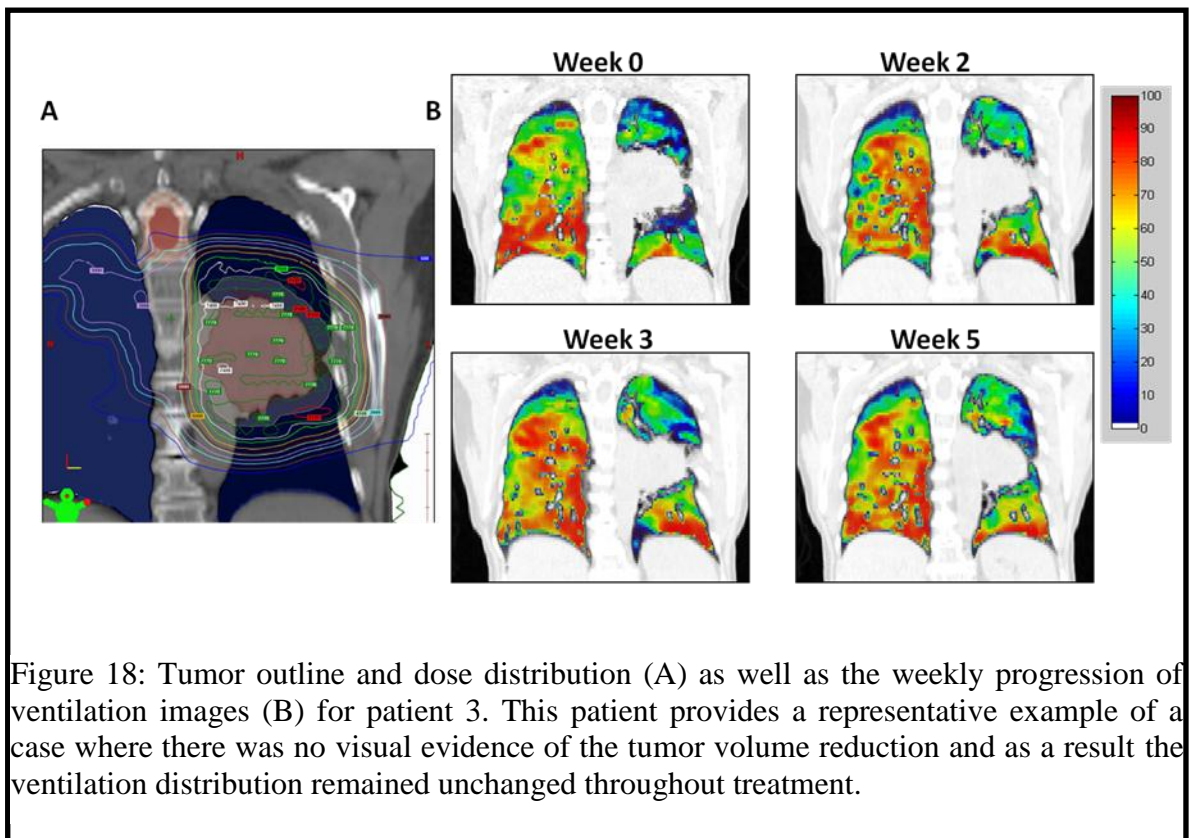


Figure 18: Tumor outline and dose distribution (A) as well as the weekly progression of ventilation images (B) for patient 3. This patient provides a representative example of a case where there was no visual evidence of the tumor volume reduction and as a result the ventilation distribution remained unchanged throughout treatment.

Patient	Week 0 Volume (cc)	Final Week Volume (cc)	Percent difference (%)
1	339.6	148.7	-56.2
2	37.5	21.5	-42.5
3	45.3	45.3	0.1
4	178.8	93.8	-47.6
5	266.1	63.3	-76.2
6	100.6	72.1	-28.3

Table 13. GTV volume for each patient recorded during pre-treatment and during the final week of therapy.

1,2,4,5,6 and all lobes for patient 3 into another group. The slope of the linear fit to the weekly ventilation data was assessed for both groups. The average slope was 1.18 ± 1.49 for the group that contained tumors that shrank and -0.32 ± 1.37 for the group that did not contain tumor (or contained tumors that did not get smaller). The results were statistically different between the 2 groups ($p=0.014$ using a t -test). A slope of 1.18 indicates that ventilation increased throughout treatment, while a slope of -0.32 is taken to mean little to no change in ventilation throughout treatment. The quantitative results confirm the visual observation that ventilation increased as the tumor shrank and remained unchanged when there was no change in the tumor and the surrounding thoracic anatomy.

Discussion

The ventilation results obtained using the dose (V_{20}) ROIs suggest that there is no clear relationship between dose and ventilation function. For some patients, ventilation increased as a function of dose, and for others, ventilation remained unchanged or slightly decreased as a function of dose. These results are in line with the mixed data reported by *Ding et al.* (72), who found decreasing

ventilation for lung regions receiving greater than 24 Gy, and decreasing and increasing ventilation for lung regions receiving less than 24 Gy. It should be noted that our methods of calculating ventilation were slightly different than those used by Ding *et al.* (68, 72). Furthermore, another difference between the studies is that the post radiation therapy 4DCT images from the Ding *et al.* (72) study were not acquired during the last week of radiation therapy, as was done for our study. The biggest factor impacting ventilation is airway obstruction, and in the case of lung cancer, airway obstruction is most influenced by anatomical changes to the tumor. In our study, we believe that the lack of a clear relationship between dose and ventilation was related to the lack of a consistent relationship between dose and changes to the tumor. In some cases, radiation dose caused the tumor to shrink significantly, which led to airway opening and an increase in ventilation; while in other cases, radiation dose had little impact on the tumor size and the surrounding anatomy, causing either a slight decrease or no change in ventilation. Whether or not radiation alone (with no accompanying changes to the tumor) causes a decrease in ventilation is a topic of ongoing research. The dose and lobe results for the 6 patients in our study indicate that when there is no change in the thoracic anatomy, radiation damage to the lung alone does not cause a measureable decrease in ventilation. However, it is possible that the re-ventilation due to airway opening masks the effect of ventilation decrease due to radiation induced lung damage. Furthermore, it is possible that the uncertainties involved in the ventilation image calculation process also mask the dose effects.

When looking at the pretreatment ventilation data, both the representative case (Figure 15) and quantitative (Figure 16) results suggest that lobes that contained tumors had a lower ventilation value and were therefore less functional. This result can be explained physiologically by the fact that the tumor caused a bronchial airway occlusion and the lobe was consequently less ventilated (Figure 15). The airway occlusion appears clearly on the ventilation map but is not as obvious on a conventional CT scan. Since 4DCT scans are acquired as part of routine clinical care, the extra lung function information comes at no extra dosimetric or monetary cost to the patient. A ventilation image that shows obvious ventilation defects (Figure 15) could potentially be used to optimize treatment plan design, as described by Yaremko *et al.* (59). However, further work is needed to verify the ability of 4DCT-based ventilation imaging to identify ventilation defects due to airway occlusion caused by tumors. In the current work, data for 6 patients was analyzed; an ideal study would include more patients and compare defects measured using 4DCT-based ventilation against defects measured using SPECT-based ventilation imaging. Preliminary work by Castillo *et al.* (59, 73) suggests that the highest correlation between 4DCT-based ventilation and SPECT-based ventilation occurs for the lowest percent ventilation values (ventilation defects).

The qualitative (Figure 17 and Figure 18) and quantitative weekly results suggest that 2 distinct phenomena occurred. When tumor volume was reduced and an airway was opened, spatial ventilation was likely to increase; when there was no change in tumor or thoracic anatomy, ventilation was likely to remain the same

or decrease slightly. Ding *et al.* (72) performed a similar analysis looking at the ventilation change for ipsilateral and contralateral lung. They reported a larger increase in ventilation in the ipsilateral lung than the contralateral lung. Seppenwoolde *et al.* (43) also noted re-ventilation (and reperfusion) as a function of the changing tumor anatomy. Our results and those reported by Ding *et al.* (72) and Seppenwoolde *et al.* (43) can be explained by the physiology of ventilation. A ventilation defect is likely to occur if an airway is blocked, and ventilation is likely to improve if the tumor decreases in size and an airway is opened.

We chose to normalize the ventilation images by converting them to percentile maps based on methodology previously used in the literature (59, 65, 73). There are other normalization methods that can be used. For example, the ventilation image could be normalized by dividing by the maximum pixel value in a particular image or by normalizing images for all weeks by a pre-determined ventilation maximum. Seppenwoolde *et al.* (43) normalized SPECT based perfusion images used for a longitudinal study on low dose (< 8Gy) and highly perfused regions of the lung. In the case of weekly 4DCT-based ventilation images we believe converting to a percentile image is ideal because it is the method least sensitive to the maximum ventilation value on any particular image and because each week's ventilation image is normalized to itself. Normalizing each week's ventilation image to itself is advantageous because patients may be breathing with different amplitudes during each treatment week.

There were several limitations to our study. Although much progress has been reported on 4DCT-based ventilation imaging (59, 65, 68-71), the methods

for calculating ventilation are still being perfected. For example, 4DCT-based ventilation calculations are sensitive to image registration spatial errors, and several groups are working on methods to mitigate the effect of the registration uncertainties (72, 74). In addition, the reproducibility of 4DCT-based ventilation imaging has yet to be investigated. The reproducibility of 4DCT-based ventilation imaging is highly dependent on the reproducibility of the 4DCT captured breathing cycle. We hypothesize that global defects investigated in this study would appear consistently in the same region regardless of the captured breathing cycle; however, future work is needed to investigate the reproducibility of 4DCT-based ventilation maps. The process of calculating ventilation images from 4DCT data is still being refined and is not yet fully automated; thus, user input is required throughout the calculation process. In our study, we registered weekly ventilation images by registering the corresponding exhale CT datasets. For patients that showed a reduction in the GTV throughout treatment, the deformable image registration algorithm enlarged the weekly tumor volume in an attempt to match the image to the original pre-treatment tumor volume. The week to week image registration spatial errors may not impact the global ventilation characteristics investigated in our study; however, future work that attempts to perform a pixel by pixel analysis should consider the week to week spatial image registration errors due to tumor volume reduction. Our data set consisted of images taken throughout the course of radiation therapy. However, radiation effects (to normal tissue and tumor) can occur weeks or months after radiation therapy. In future work, we plan to perform a similar analysis on data that

includes 4DCT images acquired several months after the completion of radiation therapy. Finally, in order to completely evaluate lung function it would be preferable to have ventilation as well as perfusion information.

Conclusions

In the current study we present a unique dataset of 4DCT-based ventilation images calculated weekly for 6 lung cancer patients undergoing radiation therapy. For our patient cohort, we did not find a consistent pattern of ventilation change as a function of radiation dose. Furthermore, we determined that pretreatment ventilation was significantly lower for lobes that contained tumors, particularly in cases where the tumor was occluding a central airway. The weekly lobe ventilation data indicated that when tumor volume is reduced the ventilation will increase and when there is no change in the thoracic anatomy, we did not measure a ventilation change. Further developments mitigating the uncertainties and improving the robustness of the calculation method along with more data points will enable us to make stronger and more local conclusions about changes in ventilation for patients undergoing radiation therapy.”

Pre-treatment ventilation study

Methods

The purpose of this study was to incorporate ventilation-based functional information into the modeling of radiation pneumonitis and determine whether incorporating the functional information could improve the fit of our model. Initially, 120 patients from the MD Anderson NSCLC patient database (described in the *Patient Database* section) were selected for this study. These were the patients that contained

data from 4DCT simulation. Upon reviewing the 4DCT images, we decided to exclude 45 patients because of the poor quality of the 4DCT images. The poor quality was due to motion artifacts or because images did not encompass the entire volume of the lung. As a result, we had 4DCT data for 75 patients from our 1999-2005 patient database. In order to increase the number of patients in our study, we selectively chose 17 patients from a database that was being accumulated for 2006. This NSCLC database contained similar information to the 1999-2005 database but contained patients that were treated in 2006 (rather than 1999-2005). We selectively chose patients to include a majority of patients that went on to develop severe (grade 3-5) radiation pneumonitis. The rationale and limitations of selectively choosing patients will be addressed in the discussion section.

For each patient we used the pre-treatment 4DCT data to calculate a pre-treatment ventilation image using the methodology previously described. We normalized the data by converting each ventilation image to a percentile image. Each patient's treatment plan was restored into the treatment planning system providing information about the dose distribution. By definition, the ventilation image is defined on the same coordinate system as the exhale phase (50%) of the 4DCT dataset. The exhale CT phase is defined on the same CT coordinate system as the CT data set (average CT dataset) used to calculate dose. Therefore, the ventilation image and the dose distribution were inherently registered.

For each patient we calculated a DVH and a dose-function histogram (DFH). The DFH was calculated in the manner proposed by Marks et al (61). The first step in computing the DFH was to group the data into dose bins and for each bin add the normalized ventilation values corresponding to that dose bin. The bins were normalized

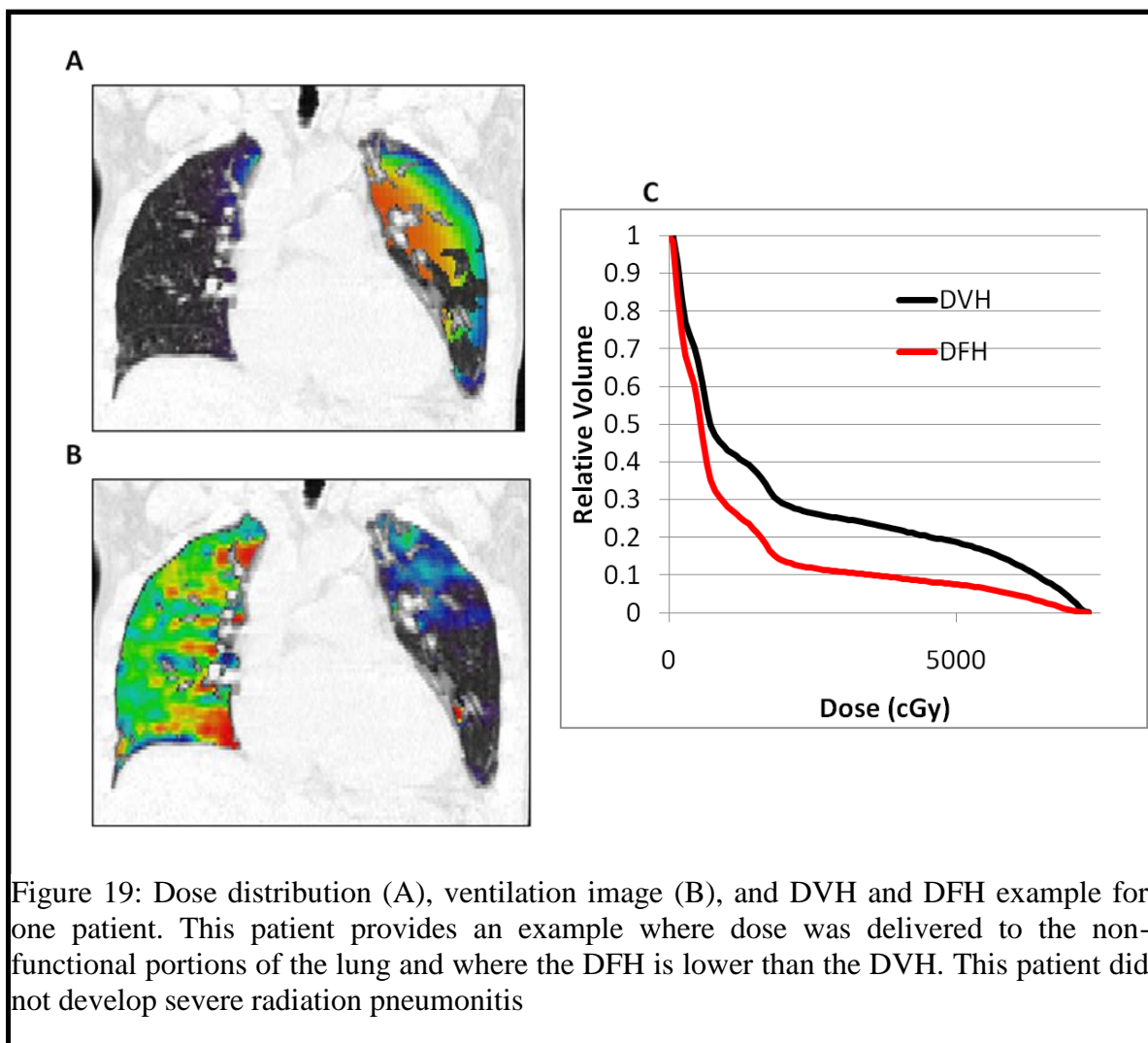
by dividing each bin by the sum of all bins in the histogram. A cumulative DFH was then calculated by summing the fractional ventilation of all the dose bins greater than or equal to the dose of each bin. In addition we calculated a MLD and a functionally weighted mean lung dose (fMLD). The fMLD was calculated by multiplying each dose voxel by the ventilation value of that voxel. Furthermore, we calculated an effective dose (D_{eff}) and the functional effective dose (fD_{eff}) using Equation 3 with the n parameter set equal to 0.5. Although it has been established that the volume parameter (n) is not different from 1 for the lung (6) we decided to investigate different values for n because there has been no precedent set when investigating dose and ventilation relationships in the lung.

We grouped the data into 2 categories: patients who experienced severe (grade 3-5) radiation pneumonitis and patients who did not experience severe pneumonitis (grade 0-2). We compared the MLD, fMLD, D_{eff} , and fD_{eff} , values between the 2 groups using a two-sample t -test and a ranksum test (29). Furthermore, we incorporated the ventilation-based functional information into a predictive risk model. We incorporated the ventilation-based functional information into the model described by Equation 10. The model described in Equation 10 is the same model that was used for the spatial study, except in this instance the weighting values (w_i) were defined by the ventilation image. In other words, the weighting will not be defined by a spatial weighting scheme but rather by a ventilation weighting scheme. Similar to the methodology used for Specific Aim 1, we used the likelihood ratio test to compare the fit of the model that incorporates dose-volume to the fit of the model that incorporates dose-volume and ventilation-based functional information. The likelihood ratio test will determine whether adding in an

additional parameter (ventilation-based functional information) can significantly improve the model fit to the data.

Results

Individual patient examples of a dose distribution, ventilation map, DVH, and DFH are shown in Figure 19 and Figure 20. The example patient shown in Figure 19 had a mean lung dose of 22.9 Gy and did not develop severe radiation pneumonitis. The dose distribution and



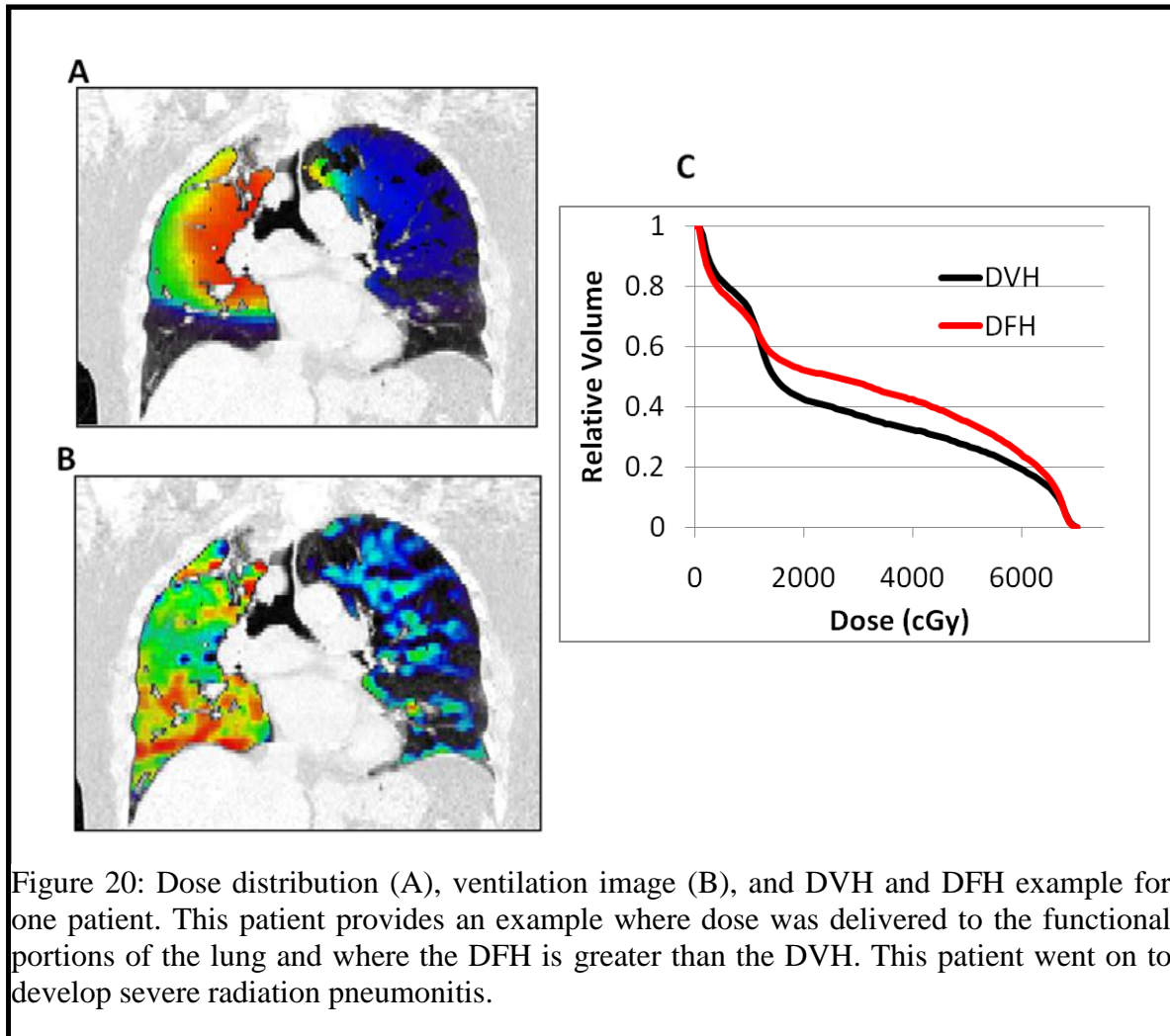
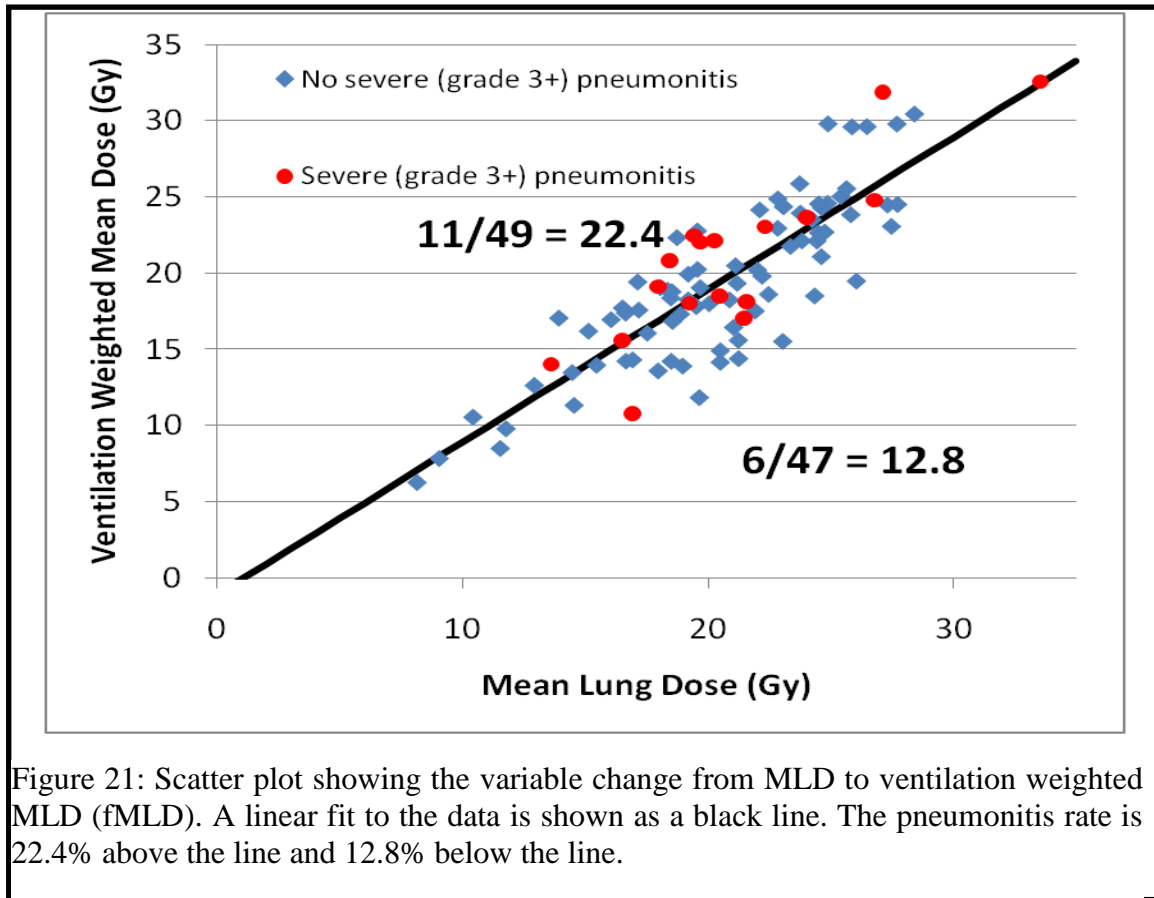


Figure 20: Dose distribution (A), ventilation image (B), and DVH and DFH example for one patient. This patient provides an example where dose was delivered to the functional portions of the lung and where the DFH is greater than the DVH. This patient went on to develop severe radiation pneumonitis.

ventilation image (Figure 19) illustrate that this patient received the majority of dose to the non-functional and non-ventilation portions of the lung. As a result, the DFH appears well below the DVH. By contrast, the example patient shown in Figure 20 received a MLD of 23.2 Gy and did go on to develop severe radiation pneumonitis. The dose distribution and ventilation image indicate that the patient received dose to highly ventilated portions of the lung. As a result, the DFH appears greater than the DVH. Although the MLD and the DVHs of these patients are similar, the difference between the spatial dose and function combination of the 2 patients is highlighted using the DFH.

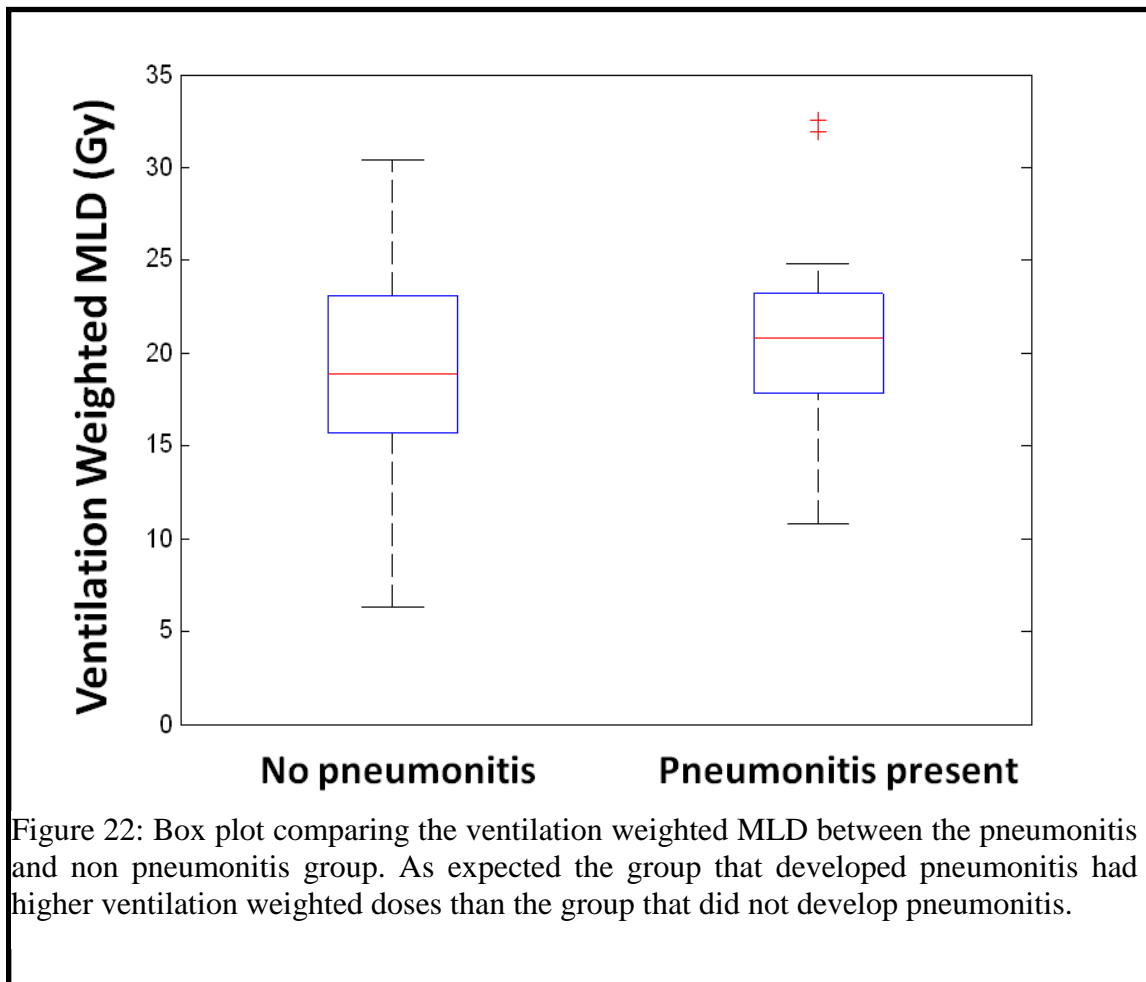
A scatter plot showing the fMLD versus the MLD is shown in Figure 21. This



graph highlights the change of variable in going from the MLD to the fMLD. It is important to note that the scatter plot appears spread out and the data does not lie on a straight line. If the data were to lie on a straight line that would indicate that weighting the dose with the ventilation values would not add any extra information in addition to the MLD. Furthermore, a linear fit to the data is shown in Figure 21. The pneumonitis rate above the line is 22.4% and 12.8% below the line. This indicates that the fMLD helps separate the toxicity data better than the MLD.

The box plot (Figure 22) shows that the fMLD was higher for patients that developed severe radiation pneumonitis. However using a two-sided t test the difference between the 2 groups was not significant ($p = 0.251$). Furthermore, there was no difference between the 2 groups in the MLD, D_{eff} (using $n = 0.5$), and fD_{eff} (using $n = 0.5$),

using either a *t*test or a ranksum test (Table 14). When the model parameters were determined for the dose-volume model (Equation 4) the *m* and TD_{50} values were calculated to be 0.76 and 70.66 respectively. The parameters for the dose-volume and functional model (Equation 10) were calculated to be 1.38×10^6 , 0.61, and



Dose-volume metric	<i>t</i> test	ranksum test
MLD	0.585	1
fMLD	0.251	0.372
$D_{eff}(n=0.5)$	0.350	0.788
$fD_{eff}(n=0.5)$	0.118	0.238

Table 14. Significance values for the various dose-volume and ventilation weighted dose-volume metrics that were investigated. The significance values indicate a difference in the metric between the group that developed severe pneumonitis and the group that did not develop severe pneumonitis.

6.04×10^4 , for the m , TD_{50} , and C values respectively. Using the likelihood ratio test the difference in fits of the two models was not found to be significant ($p = 0.312$).

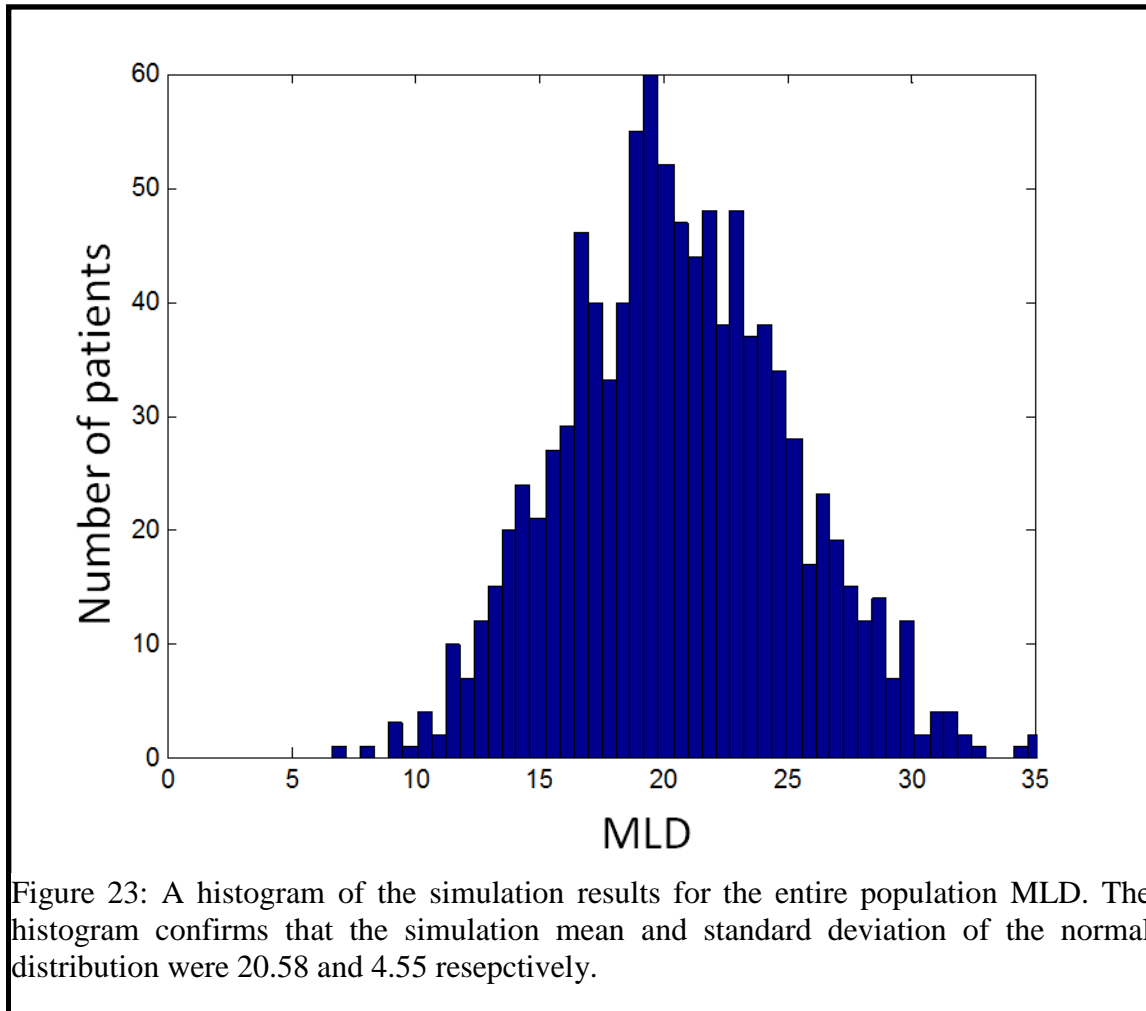
Discussion

We have combined some novel techniques along with the methods proposed by Nioutsikou et al (42) and Miften et al (41) to incorporate ventilation-based functional information into the modeling of radiation pneumonitis. The individual patient examples (Figure 19 and Figure 20), scatter plot (Figure 21), and box plot results are promising. The patient examples illustrate how the combination of dose and function information can lead to a better understanding of the effect of radiation on the normal lung. The scatter plot shows that converting from MLD to a fMLD will separate the data, meaning that the two metrics are not equivalent. Furthermore, using a linear fit, the scatter plot demonstrated graphically that the fMLD is a better predictor of pneumonitis than the MLD. As expected, the box plot indicates that the fMLD is greater for patients that developed severe radiation pneumonitis than for patients that did not develop severe radiation pneumonitis. However, using statistical analysis and maximum likelihood methods the results were not shown to be significant. Based on the promising initial results we believe the statistical results can be improved by incorporating more patients in future work.

The current study contained 96 patients; while this is consistent with the number of patients in similar studies (43, 78, 79), an important question to address is how many patients would be needed to find a statistically significant result. In order to determine how many patients would be needed we performed a sample size simulation. The idea of

the simulation was to simulate data based on existing results, perform the statistical test we were interested in and calculate how many samples are needed for a power ratio of 80%. The power ratio is defined by the ratio of the number of successful samples to the total number of samples. Successful samples could imply statistical significant results at the $p = 0.05$ level or cases where a certain p value is larger than another p value. The first step was to simulate the pneumonitis data. Out of the entire patient population we decided to simulate a 50% pneumonitis rate. While 50% is not representative of a true pneumonitis rate, an assumption is made that we are able to selectively pick our data. Then for the pneumonitis and non-pneumonitis groups we simulated MLD and fMLD. The MLD and fMLD were generated for the pneumonitis and non-pneumonitis group using a normal distribution and mean and standard deviation values calculated from our existing data. For example, the simulation of the MLD was simulated with a mean of 20.58 and a standard deviation of 4.55 (Figure 23). Once all of the MLD and fMLD values were simulated we performed a t test comparing the MLD amongst the pneumonitis and non pneumonitis group and a t test comparing the fMLD among the pneumonitis and non pneumonitis group. We calculated the power as the number of times the p value for the fMLD t test was smaller than the p value for the MLD t test normalized by the total number of simulation. In order to reach 80% power, 680 simulations were needed. It is also possible to perform a power calculation using regression analysis with a probit link. When we performed a regression analysis with the MLD and fMLD, 610 simulations were needed for a power of 80%. It should be noted that the regression analysis is not the ideal test to use because the pneumonitis events are being artificially selected. However, it is promising that both statistics needed around 650 patients for a

power ratio of 80%. Although there are assumptions made in the simulation that could affect the sample size calculation, the exercise underlines that a much larger sample size would be needed to prove statistical significance.



Because 4DCT-based ventilation imaging is a new method of calculating lung function, most of the literature has focused on the methodology to calculate ventilation and as a result there are no papers relating ventilation-based functional information to radiation pneumonitis. Yaremko et al (59) demonstrate that it is possible to reduce highly ventilated portions of the lung using IMRT; however, this is mostly a methodology paper and does not relate ventilation to clinical symptoms. Because of readily available data,

most of the literature has focused on incorporating SPECT-based perfusion imaging into the prediction of thoracic radiation toxicity. Several studies have tried to correlate SPECT-based perfusion changes with pulmonary function test (PFT) data. Studies by Fan et al (78) and Ma et al (63) found significant results in correlating perfusion changes with PFT changes; however, the studies noted modest correlation coefficients (0.18 – 0.30). Lind et al (79) incorporated dosimetric and perfusion information and used receiver operating characteristic (ROC) analysis to evaluate the predictive abilities of each metric. They report that the models that incorporated dose and perfusion were best correlated with pneumonitis; however, they report an area under the ROC curve in the range of 0.61-0.72. These values are not an indicator of a strong relationship between dose and perfusion with radiation pneumonitis. Seppenwoolde et al (43) report that the overall mean perfusion-weighted lung dose and mean perfusion-weighted regional doses to the posterior, inferior, ipsilateral, and central regions were associated with radiation pneumonitis. They also report that the doses to the entire lung and regional doses (not accounting for perfusion) were correlated with pneumonitis. In this instance, it is difficult to distinguish between correlations caused by dose and correlations caused by dose to functional portions of the lung. Kocak et al (40) developed a model to incorporate dose volume and perfusion into the prediction of pneumonitis and applied their model to an independent data set. They report that their model was not able to accurately segregate patients into high and low risk groups. Our data is in line with the results proposed in the literature. Both our results and those of others (40, 43, 63, 78, 79) provide some promising initial findings; however, the data does not turn out to be statistically significant in most cases. There are several possible explanations. One explanation for the

lack of statistical significance is the number of patients in the studies. Specifically, the number of patients developing radiation pneumonitis is low. With more patients, the number of patients developing radiation pneumonitis would increase and the statistical metrics would improve. Our sample size simulation suggested that around 600 patients would be needed for significant results; however, most of the studies are limited to around 100 patients. Another possible explanation is the lack of biological understanding of the relationship between lung function and symptomatic toxicity. There are several metrics and imaging modalities that have been used to describe lung function. These include: PFT, perfusion, ventilation, diffusion, and inflammation. There is no clear conclusion in the literature that any of the metrics (or any combination of the metrics) can be used to completely describe lung function and lung damage. The current study and many of the studies in the literature investigate the relationship between one metric and symptomatic radiation pneumonitis. It is possible that a combination of the imaging modalities (for example ventilation, diffusion, and perfusion) is needed to completely describe lung function and to demonstrate the relationship between lung function and symptomatic toxicity.

There were several limitations to our study. As stated previously, we believe with more patients the statistics of our study could be improved. However, we do not believe the number of patients in this study was unreasonably low. We analyzed 96 patients for this study, by comparison Lind et al (79) had 166, Fan et al (80) had 96, and Seppenwoolde et al had (43) 106. In order to increase the number of pneumonitis events in our study we manually selected a portion of our data. Because some of the data were manually selected, the pneumonitis rate is not representative of the patient population at

MD Anderson and therefore the modeling parameters cannot be compared with those published in the literature. However, because the likelihood ratio test calculates an improvement in model fit to the data, the significance value stated is valid, despite the manually selected patient population. Furthermore, the *t*-test and ranksum statistics comparing the MLD and fMLD for the pneumonitis and non-pneumonitis group are valid as well, despite the manual selection of the data. All of the uncertainties associated with calculating ventilation images discussed in the *Serial Ventilation study* apply to this section as well. Particularly is worth noting that the ventilation images are sensitive to the particular breathing cycle captured by the 4DCT. We normalized our data by converting the ventilation images to percentile images. We normalized the data in this manner because this was the method previously used in the literature (59, 65, 73) and because it is the method that best mitigates the uncertainties associated with calculating 4DCT-based ventilation. However, there are other possibilities for normalizing the data. For example, it is possible to normalize the data using a universal maximum ventilation value or by using the maximum voxel value in a particular image. The magnitude of the ventilation images is dependent on the shallowness and depth of the breathing cycle captured by the 4DCT. Certain patients may not take as large a breath and therefore their ventilation values would be smaller than those of patients who took a deeper breath. This would be equivalent to administering differing amounts of radionuclide in SPECT exam. Patients may have different magnitude values of their ventilation image that may not necessarily be associated with function but rather the amplitude of the breathing captured by 4DCT. As a result, we believe it is best to normalize the ventilation images to themselves (as opposed to using a population based normalization value). Furthermore, by using the

percentile image we mitigate the effect of the maximum voxel value on the rest of the image, which is important because the maximum voxel ventilation values are often the most prone to the uncertainties associated with calculating 4DCT images. In this study, we attempted to associate ventilation with lung function and symptomatic pulmonary toxicity. As mentioned previously, lung function can be defined by ventilation, perfusion, diffusion, inflammation, and PFT data. Therefore, in future work it would be informative to combine these modalities to better determine lung function and improve the prediction for radiation pneumonitis. In addition, as the patient database grows, it would be informative to correlate lung function (as measured by ventilation) by more specific patient groups according to: age, PFT data, and prior lung disease.

Conclusions

In this study we used pre-treatment 4DCT-based ventilation images to determine lung function and help predict for radiation pneumonitis. The hypothesis of the study is rejected because we were not able to achieve a significant improvement in model fit by incorporating ventilation-based functional information. Although we were not able to achieve a significant improvement in model fit with our 96 patient database, we show some promising results indicating that ventilation imaging can provide useful information about lung function in lung cancer patients. We believe more patients are needed to demonstrate a significant relationship between dose to highly ventilated portions of the lung and symptomatic radiation pneumonitis.

Specific Aim 3 – Personalized prescription study

Introduction

Dose escalation trials have been performed that report promising results for lung cancer patients receiving radiation therapy. Dose escalation trials can broadly be categorized into 2 types of dose escalation schemes: randomized dose escalation and dose escalation using dose-volume metrics. The study by Perez et al (11) provides an example of a randomized dose escalation scheme where patients get randomized to a treatment arm and depending on the treatment arm they receive a certain amount of dose to the tumor. More recent studies have employed dose escalation schemes that are based on dose-volume metrics. For example, Bradley et al (16) escalated doses based on V_{20} while Belderbos et al (46) and Van Baardwijk et al (48) escalated dose based on MLD. The group at the University of Michigan went a step further and used NTCP models to calculate effective volume (V_{eff}) and determine the dose based on V_{eff} (45). It should be noted that although the study explicitly incorporated NTCP modeling into the determination of dose, the NTCP model was based solely on dose-volume metrics.

In addition to dose volume, researchers have attempted to incorporate other patient and clinical factors as predictive factors for severe radiation pneumonitis. As noted earlier, studies have proposed a correlation between radiation pneumonitis and chemotherapy (35), performance status (36), smoking status (37), tumor location within the lung (32, 33, 39), and functional status of the lung (40-42). One of the factors that has been investigated in relationship to radiation pneumonitis has been genetic information in the form of SNPs (38). SNPs are a type of biomarker and are considered to be DNA sequence variations. Recent research interest has been focused on identifying SNPs

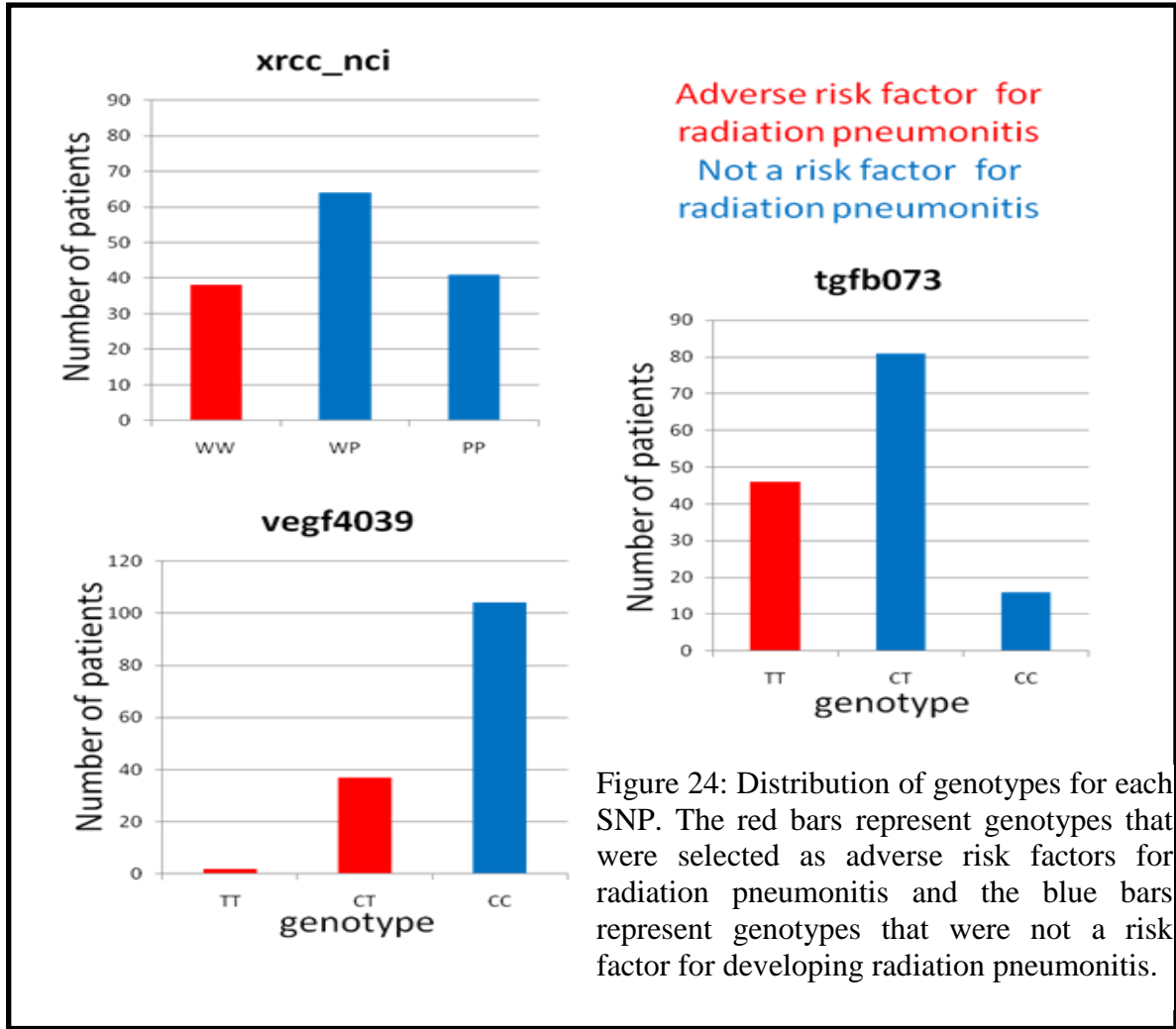
associated with different inflammatory cytokines (signaling proteins). Yuan et al (38) showed that the CT/CC genotypes of the cytokine transforming growth factor *BI* (*TGFB1*) gene were associated with a lower risk of radiation pneumonitis. In a similar study, Anscher et al (81) evaluated 73 patients that were treated with definitive radiotherapy and determined that *TGFB1* appeared to be a useful means to identify patients at low risk for developing radiation pneumonitis. It should be noted however that the data is not consistent. For example, the results reported by De Jaeger et al (82) did not confirm that increased levels of *TGFB1* were a risk factor for developing pneumonitis. Other SNPs have also been investigated. Fogarty et al (83) studied the SNP MC1R and found that it was associated with unexpectedly high severe acute reactions to radiation therapy. In a recent study (84), our group incorporated SNPs as biomarkers into a predictive LKB NTCP model. We analyzed 143 patients with NSCLC treated definitively with radiation therapy. The study genotyped 15 potentially functional SNPs and found that TGFB073 = TT, XRCC_NIH = WW, and VEGF4039 = CT/TT, were selected as adverse risk factors. In other words, patients with the above mentioned genotypes of the 3 SNPs were at a greater risk for developing radiation pneumonitis.

The next logical step in dose escalation studies is to prescribe dose based on NTCP models. Specifically, using NTCP models that are further individualized because they incorporate additional factors besides dose-volume. By using NTCP models that account for patient and clinical factors, the derived lung dose limit and subsequent target dose prescription can become personalized to the patient, rather than being population based. The concept of personalizing a lung dose limit to individuals is an idea that certain thoracic physicians may do already. For example, when deciding how much dose can

safely be delivered to the lung, physicians may consider the patient's chemotherapy status, surgery status, or PFT scores. However, as additional factors are found to be associated with radiation pneumonitis a more rigorous approach is needed. The concept of personalizing the lung dose limit and the prescription dose are demonstrated in the current study. We perform a virtual dose prescription trial where the prescription is determined using an individualized lung dose-volume constraint that is calculated using a NTCP model. We will use a model that is composed of dose-volume and genetic (SNP) information. Our hypothesis is that the median difference between the model-determined prescription and the clinically achieved prescription will be greater than a clinically significant threshold of 5 Gy.

Methods

The patient database used for this study was taken from our previous work (84). The study published by Liao et al (84) contained 143 patients; however, we were only able to de-archive 141 patients into the treatment planning system. Therefore, 141 patients were used for this simulation. The patients had a diagnosis of NSCLC and were treated with definitive radiation therapy both with and without concurrent chemotherapy. The distributions of genotypes for each SNP are shown in Figure 24. Each genotype was well represented within the patient population except for the TT genotype of the VEGF SNP (which was represented by 3 patients).



The first step was to mathematically describe the model that would be used to determine the personalized lung dose limit. To incorporate dose-volume and SNP information we used the LKB NTCP formulation described in Equations 1 and 7. The TD_{50} and m values that were fit to the data were determined to be 36.6 Gy and 0.381 respectively. The SNP data were incorporated as DMF factors. The total DMF (DMF_T) was defined as

$$DMF_T = DMF_{XRCC} DMF_{TGFB} DMF_{VEGF}, \quad \text{Equation 12}$$

where DMF_{XRCC} , DMF_{TGFB} , and DMF_{VEGF} where the DMFs for the individual SNPs. For patients that had a genotype of WW for the XRCC SNP the $DMF_{XRCC} = 0.681$, for

patients that had a genotype of CT or TT for the VEGF SNP the $DMF_{VEGF} = 0.733$, and for patients that had a TT genotype for the TGFB SNP the $DMF_{TGFB} = 0.783$. If the patients did not have the genotypes described above for the 3 SNPs, then their DMFs were set to 1. These were all parameters that were fit to our patient database in the previous study (84). Each DMF factor can theoretically be thought of as effectively reducing the TD_{50} parameter in Equation 7. As the TD_{50} parameter gets reduced the dose response curve is shifted to the left, and for the same MLD there is a greater risk of pneumonitis, or conversely, a lower MLD is needed for the same risk of pneumonitis. Therefore, each selected genotype moves the curve to the left and can be theoretically thought of as increasing a patient's risk for radiation pneumonitis. The NTCP curves described in Equations 1, 7 and 12 are displayed in Figure 25.

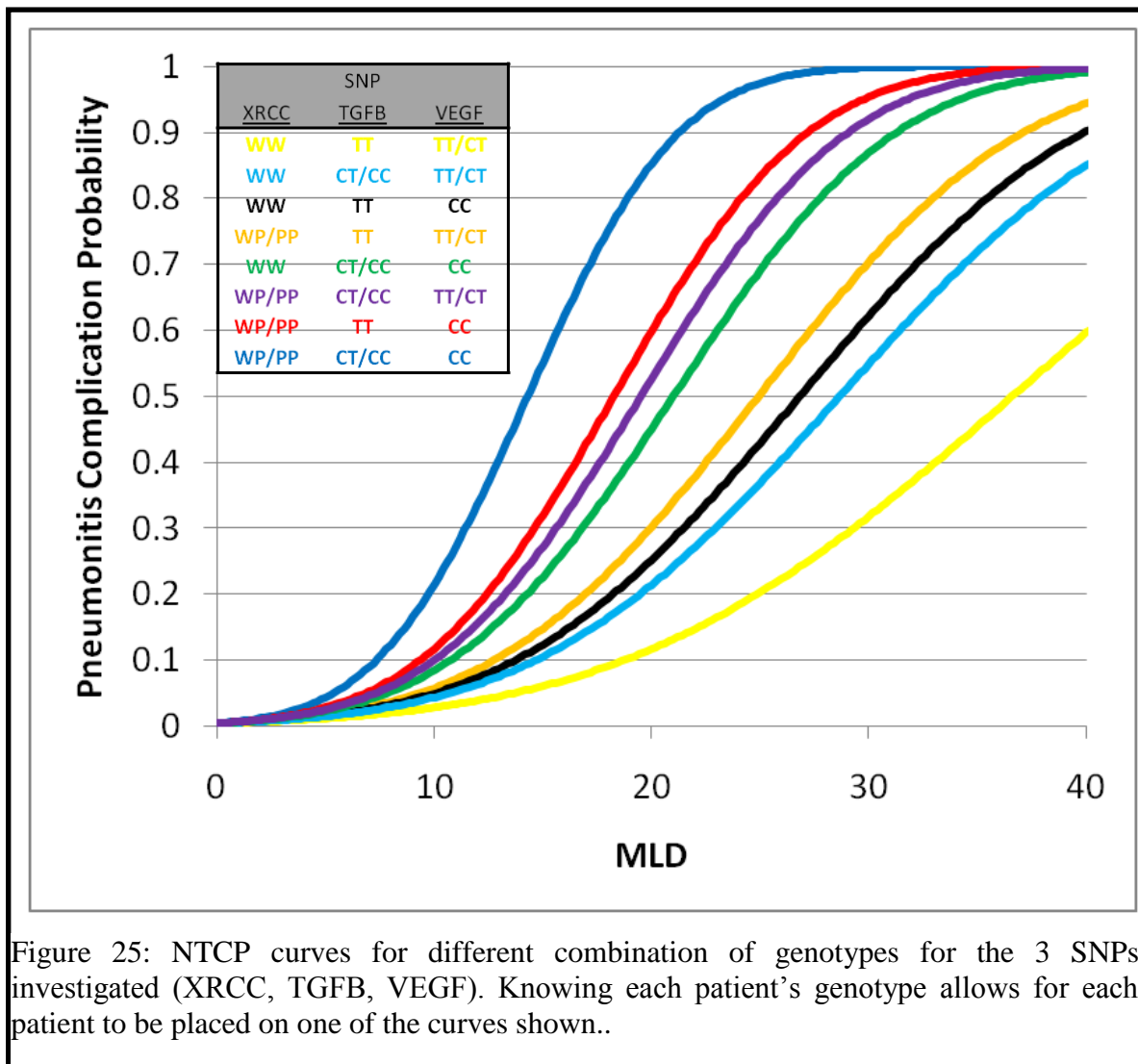
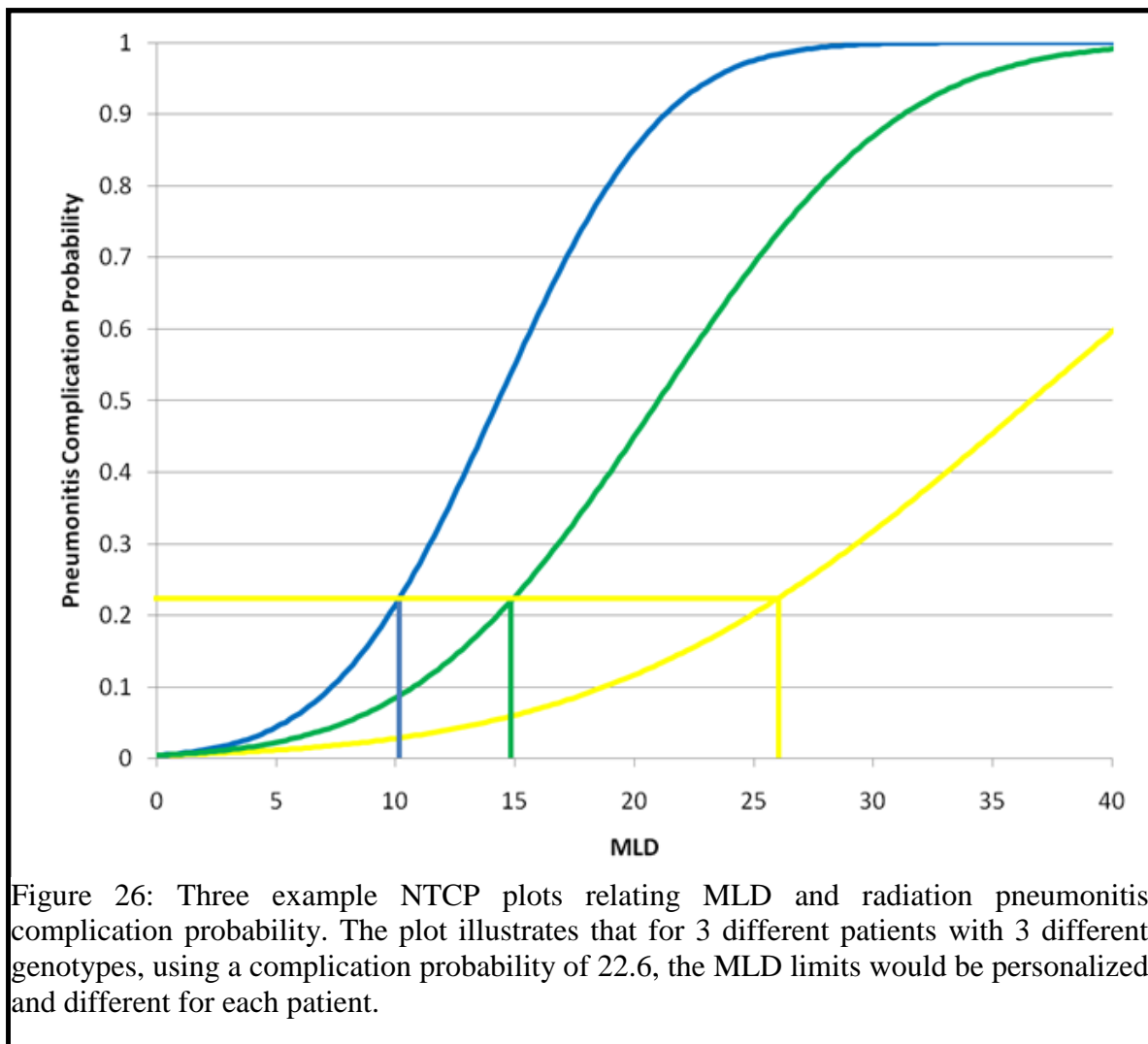


Figure 25: NTCP curves for different combination of genotypes for the 3 SNPs investigated (XRCC, TGFB, VEGF). Knowing each patient's genotype allows for each patient to be placed on one of the curves shown..

There were 8 total curves in the plot because there are 8 different possible combinations of DMF_{XRCC} , DMF_{TGFB} , and DMF_{VEGF} , resulting in 8 different possibilities for the DMF_T . Conceptually, we know the genotype for each patient for the 3 SNPs (XRCC, TGFB, and VEGF) and therefore can determine which one of the 8 curves shown in Figure 25 the patient falls on. The next piece of information needed for the personalized lung dose limit is the acceptable complication probability. In theory, this would be the clinically agreed upon radiation pneumonitis complication probability and would be determined based on a clinical decision balancing tumor control and normal tissue toxicity. For the current

study, we simulated several different scenarios. We simulated a pneumonitis rate of 22.6 % because that was the true complication rate in our dataset. We also simulated complication probabilities of 20% and 25% to study the dependence of the prescription change on the complication probability. Once we know which curve each patient falls on and have an agreed upon complication probability we can determine a personalized dose limit for each patient (Figure 26).



For example, for a complication probability of 22.6% it is possible to have a patient with a SNP genotype that calls for a MLD limit of 10 Gy, 15 Gy, or as much as 26 Gy (Figure

26). The MLD limit is “personalized” because it is based on each individual patient’s genotypical expression of the 3 SNPs. In the current approach, each patient has their own MLD limit (although in this study 8 different MLD limits exist), as opposed to a universal MLD limit that is applied to the entire patient population. In addition to the model derived lung dose limit, we applied treatment planning parameters to the spinal cord, esophagus, and the heart (Table 15). For the spinal cord we used a maximum dose

Organ	Limit
Lung	Model determined
Spinal Cord	$D_{\max} < 50 \text{ Gy}$
Esophagus	$V_{60} < 50\%$
Heart	$V_{50} < 50\%$

Table 15. Dose-volume limits used for the virtual simulation study.

of 50 Gy, for the esophagus we used a V_{60} of 50%, and for the heart we used a V_{50} of 50%. These are in line with the treatment planning parameters used in our clinic.

The DVH and dose-volume parameters for each patient’s clinically used plan were exported. It is important to note that at this point of the study, only the patient’s clinical plan was used. There was no re-planning or re-contouring, and we used the same beam arrangement and design as was used for the clinically delivered plan. We applied the model-determined MLD limit as well as the other treatment planning parameters to the dose-volume parameters exported from the patient’s clinical plan and determined if we could escalate the dose or if the dose needed to be lowered. If all of the clinical parameters fell below the model-determined MLD limit and the other organ limits, then

we could increase the prescription dose. Conversely, if some of the parameters exceeded the model-determined MLD limit or any of the other applied limits, then the prescription dose was lowered. The next step was to determine the quantity by which the dose needed to be escalated or de-escalated. To calculate the dose escalation or de-escalation, we calculated a ratio of the patient's clinical parameters to the set treatment planning limits. It should be noted that while the MLD and the spinal cord max dose can be calculated as a linear scaling, in order to determine a ratio for the volume parameters (used for the esophagus and heart) the DVH needs to be used. For example, to calculate the possible dose escalation or de-escalation due to the esophagus, the ratio of 60 Gy to the D_{50} is taken. A graphical representation of how the ratio of doses was calculated using the DVH is shown in Figure 27.

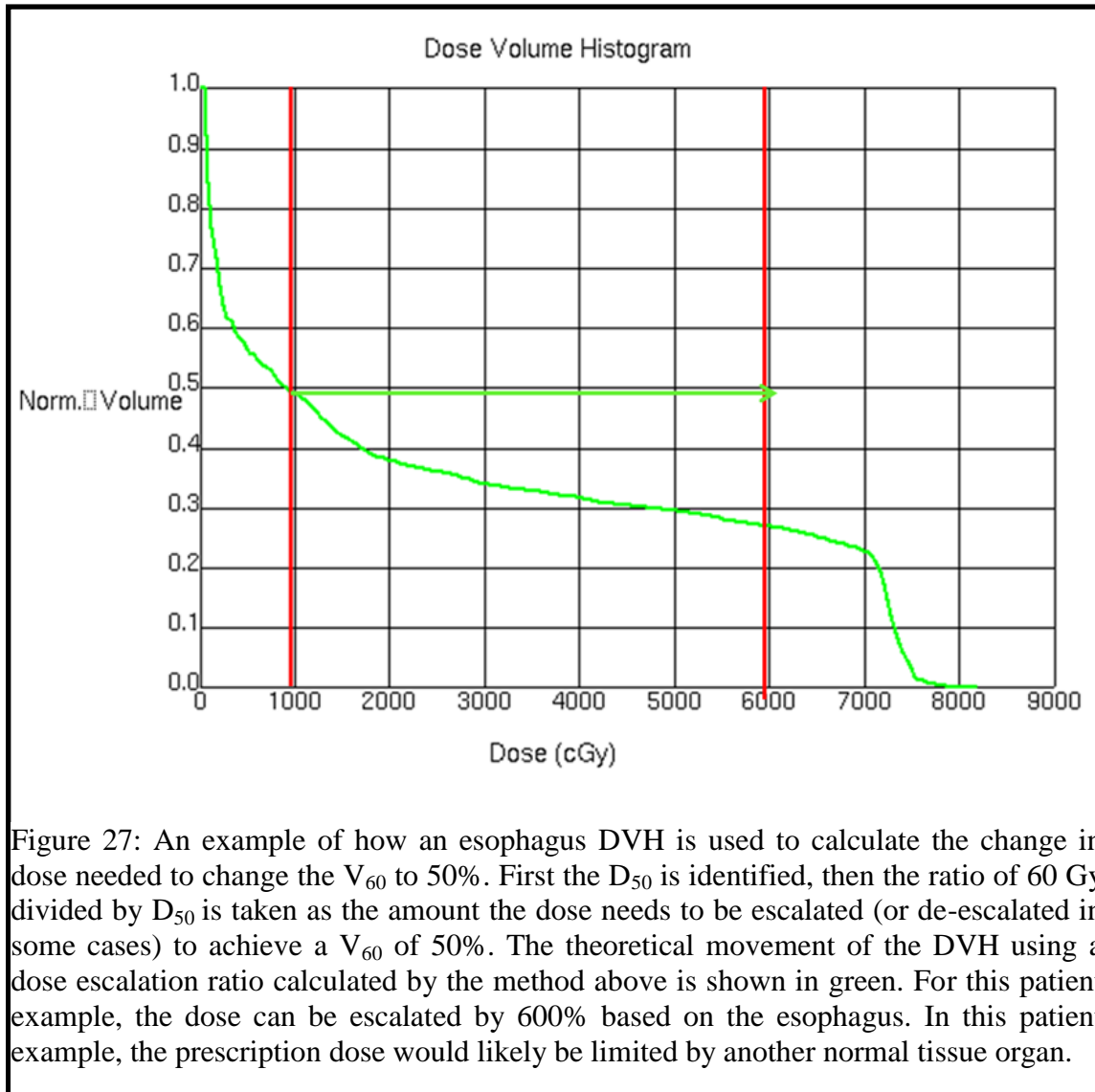
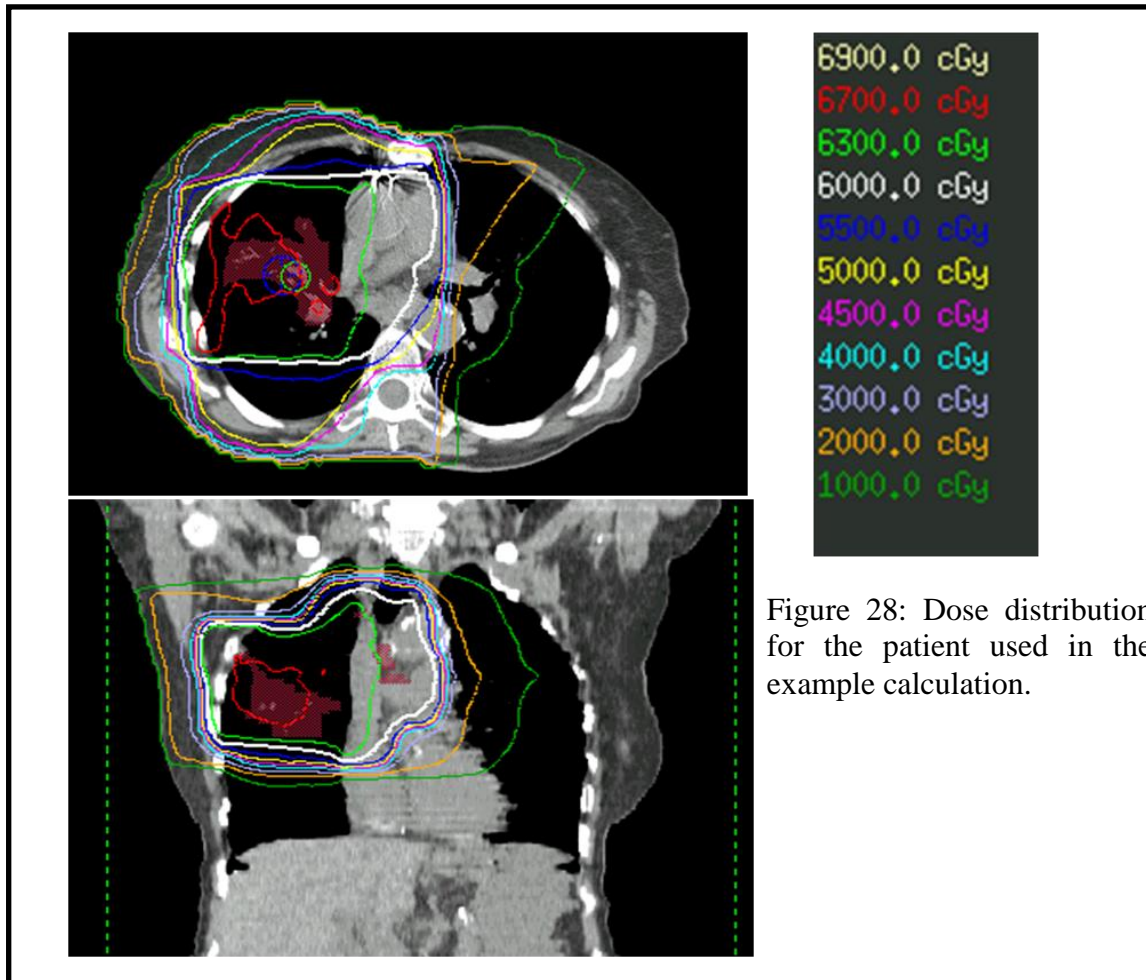


Figure 27: An example of how an esophagus DVH is used to calculate the change in dose needed to change the V_{60} to 50%. First the D_{50} is identified, then the ratio of 60 Gy divided by D_{50} is taken as the amount the dose needs to be escalated (or de-escalated in some cases) to achieve a V_{60} of 50%. The theoretical movement of the DVH using a dose escalation ratio calculated by the method above is shown in green. For this patient example, the dose can be escalated by 600% based on the esophagus. In this patient example, the prescription dose would likely be limited by another normal tissue organ.

Once all the ratios were calculated, for each individual patient, the organ with the minimum ratio was taken as the dose limiting organ. For example, if the dose could be escalated by 6% according to the lung limit and 15% according to the spinal cord limit, then the lung would be the dose-limiting organ and the dose could only be escalated by 6%. Similarly for dose de-escalation, if the dose had to be lowered by -6% according to the lung limit and by -15% according to the spinal cord, then the spinal cord would be the dose limiting organ. Once the dose-limiting organ was determined, the dose escalation or

de-escalation scheme dictated by that organ was applied to the prescription dose as well as the other dose-volume parameters. We then noted the difference in the model-determined prescription dose and the clinically used prescription dose. In other words, if the model-determined prescription was greater than the clinically achieved prescription, then according to the model we should dose escalate for that particular patient, if the model-determined prescription was lower than the clinically used prescription, then according to the model the dose needed to be reduced. In summary, we scaled the prescription dose for each patient according to normal tissue constraints. We used conventional dose-volume constraints for the spinal cord, esophagus, and heart, and a personalized MLD limit determined from a NTCP model. We studied the difference in the model-determined prescription dose and the clinically used prescription dose. The change in prescription was investigated as a function of the selected complication probability. We also noted the differences between the model-determined MLD limit and the clinically used MLD limit. Furthermore, in order to gain an understanding of the dose-limiting organ for the entire patient population, we noted the dose-limiting organ for each individual patient. For 31 of the patients in the study the clinically used dose-volume values for the spinal cord, esophagus, and heart, exceeded the dose-volume limits that we imposed for the study (prior to the model-determined MLD limit being applied). This occurred because the clinician made a decision to exceed dose-volume constraints in favor of better tumor control. To investigate the effect of having these patients in our study, we performed a simulation where the patients that had exceeded dose-volume constraints before the MLD limit was applied were excluded.

It is instructive to go through the personalized dose prescription process for an individual patient example. The patient's dose distribution is shown in Figure 28 and the dose-volume parameters, limits, and ratios are shown in Table 16.



	Prescription (Gy)	MLD (Gy)	Cord max (Gy)	Esophagus V_{60} (%)	Heart V_{50} (%)
Clinical	60	23.6	43.2	37.5	26.1
Limits		24.9	50	50	50
Ratio		1.06	1.16	1.09	4.2
Model- generated parameters	63.6	24.9	45.8	49.7	23.5

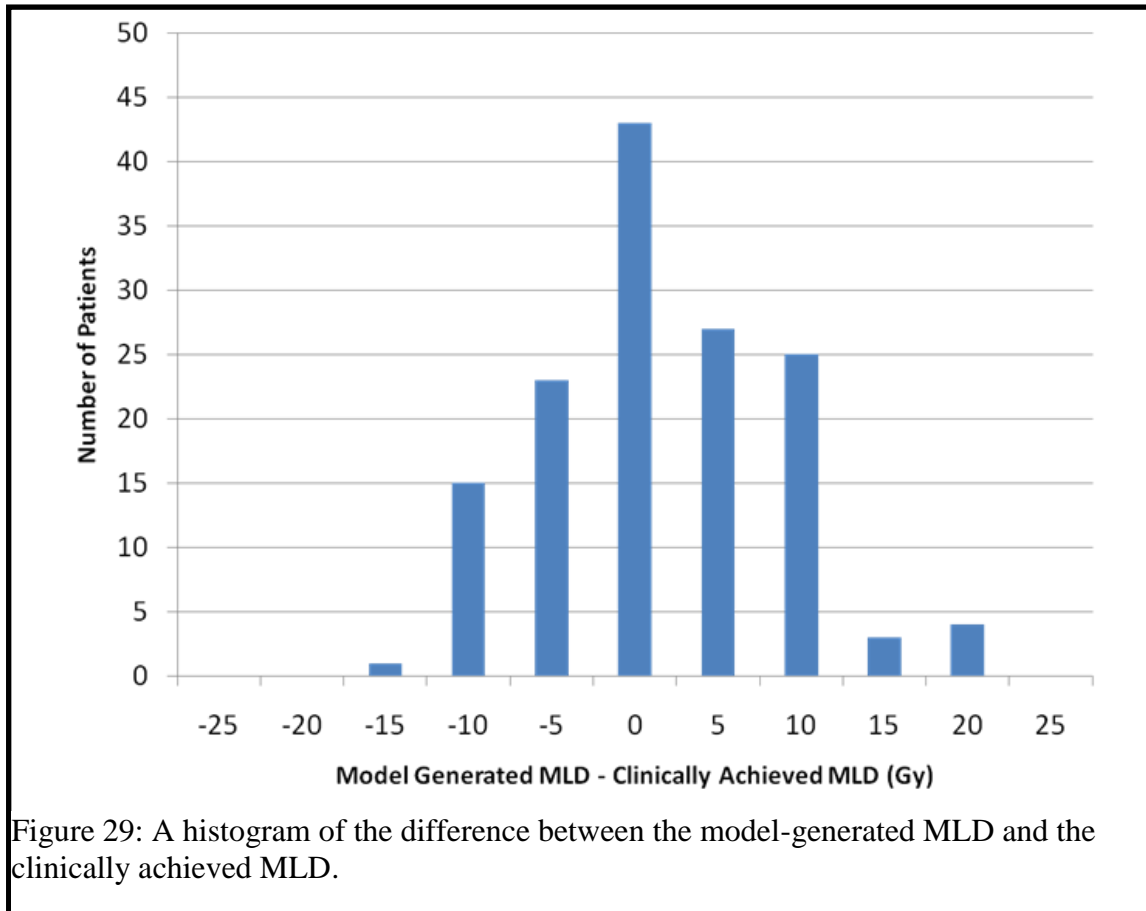
Table 16: A single patient example of the procedure used to determine the model-generated prescription. The table shows the patient's clinical parameters, the applied dose volume limits, the ratio between the limits and the clinical parameters, and finally the model-generated parameters.

This particular patient received 3D-CRT with a prescription dose of 60 Gy. The MLD for the patient was 23.6 Gy, the esophagus V_{60} was 37.5%, and the heart V_{50} was 26.1%. The patient had a genotype of WP for the XRCC SNP, CT for the TGFB SNP, and CC for the VEGF SNP, corresponding to DMFs of $DMF_{XRCC} = 1$, $DMF_{TGFB} = 1$, and $DMF_{VEGF} = 0.733$, for a $DMF_T = 0.733$. Using Equations 1 and 7, along with a $DMF_T = 0.733$ and a complication probability of 20%, the personalized model-determined MLD limit for this patient is 24.9 Gy. The other limits are set as stated above; 50 Gy for the cord max dose, 50% for the esophagus V_{60} and 50% for the heart V_{50} . For this patient, all the dose-volume parameters for the clinically used plan fell below the set limits; therefore, the dose could be escalated. Using a linear relationship, based on the MLD and spinal cord, the dose can be escalated by 6% and 16% respectively. Using the DVH, the dose can be escalated by 9% according to the esophagus and 320% using the heart. The minimum ratio for this patient is 6%; therefore the dose limiting organ will be the lung. The 6% dose escalation scheme is applied to the prescription dose as well as the other dose-

volume parameters. The resulting prescription dose is 63.6 Gy, while the new MLD is 24.9 Gy, the new spinal cord maximum dose is 45.8 Gy, the new esophagus V_{60} is 49.7% and the new heart V_{50} is 23.5%. The metric of interest for this study was the difference between the model generated prescription dose and the clinically achieved prescription dose, which for this patient is calculated to be +3.6 Gy. As expected, the MLD value is maximum, while the other dose-volume parameters don't reach their maximum allowable values.

Results

A histogram of the difference between the model generated MLD and the clinically achieved MLD for all patients is shown in Figure 29. Patients that fell to the left of zero are patients for whom the model predicted a lower dose than what was given clinically. The patients to the right of zero are patients that the model predicted could have received a higher MLD than was given clinically. For example, patients in the 20 Gy bin in Figure 29 are patients that could have theoretically received an increase of 20 Gy to their MLD. As expected, the most frequent occurrence is a small change between the model-generated MLD and the clinically achieved MLD.



A histogram of the difference in the model-generated prescriptions and the clinically achieved prescriptions is shown in Figure 30. The patients to the left of zero are the patients for who the model dictated that the prescription dose is reduced, while the patients to the right of zero are the patients for whom the model predicted that the doses could be escalated. Although there are 35 patients in the 0 Gy bin, the histogram shows that for most patients, there would be a change if the prescription was based on a model.

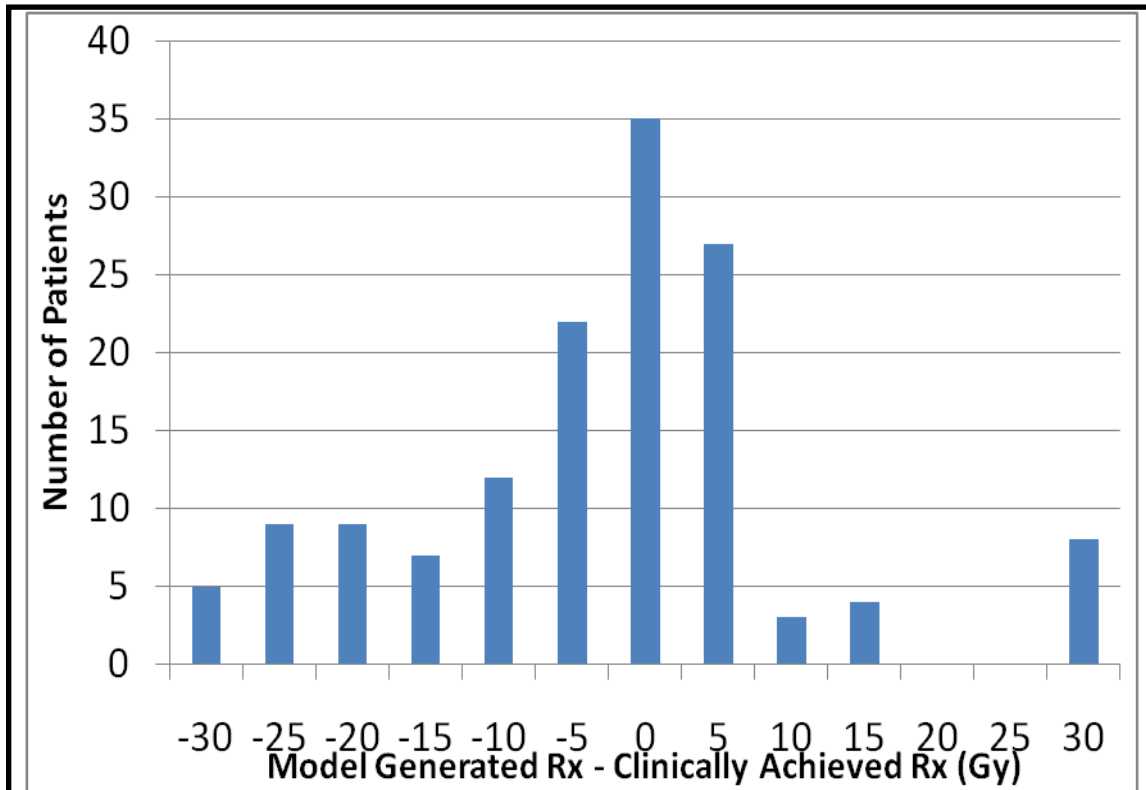


Figure 30: A histogram of the differences between the model-generated prescriptions and the clinically achieved prescriptions.

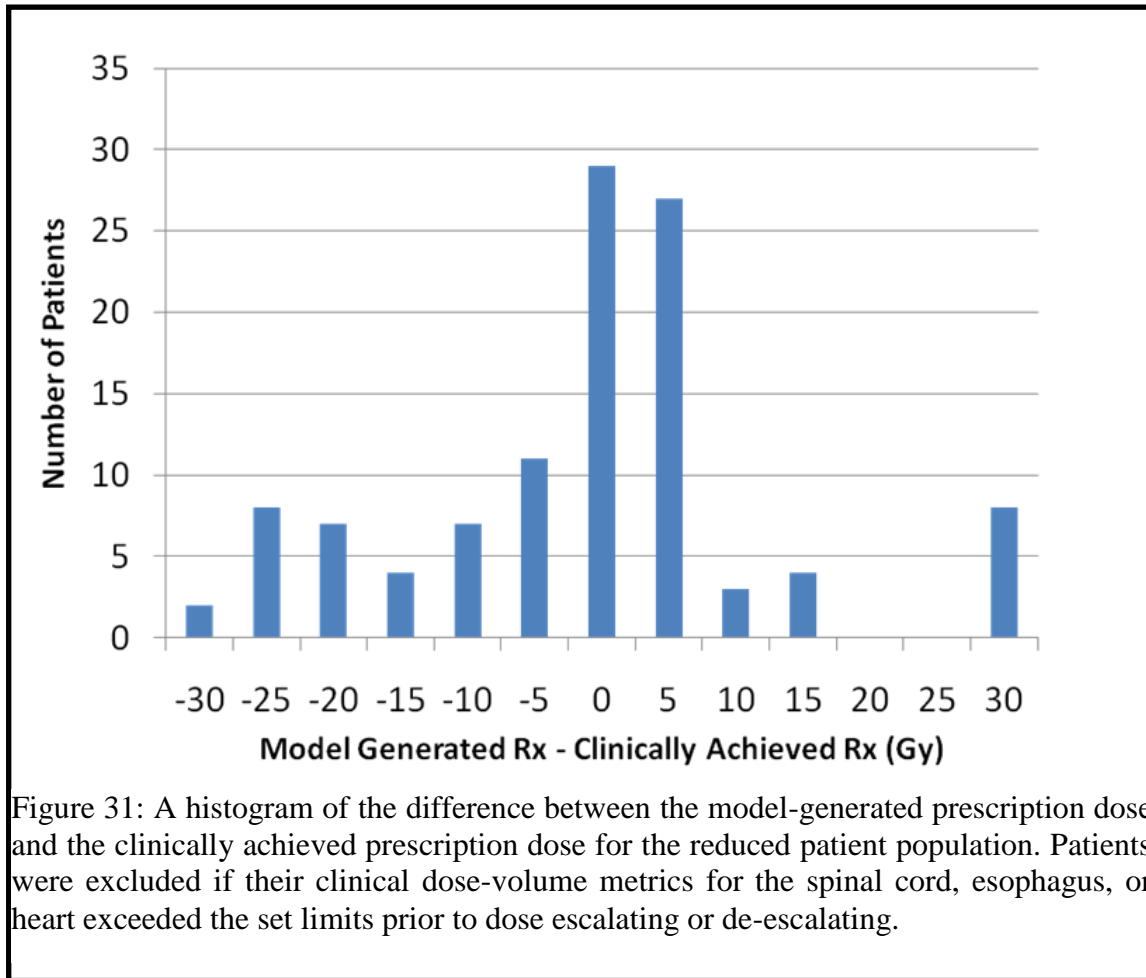
The mean, median, and range of the change in prescription doses are shown in Table 17.

	Clinical Rx (Gy)	Model Rx (Gy)	Model Rx – Clinical Rx (Gy)	Absolute Rx Difference (Gy)
Mean	65.4	62.7	-2.7	10.0
Median	63.0	63.7	-1.7	6.0
Range	60.0-72.0	40.0-100.0	-29.6 – 37.0	0-37.0

Table 17: The overall clinically achieved prescription, model generated prescription, and changes in prescription for the entire patient population.

The average difference between the model generated plans and the clinically used plans was a reduction of -2.7 Gy (with a median value of -1.7 Gy). The range of changes in prescription include a dose reduction of 29.6 Gy and a dose escalation of 30 Gy. In order

to quantify the change in prescription for each patient, regardless of the sign, we calculated the absolute value in the changes in prescription. The mean and the median absolute changes were 10 Gy and 6 Gy respectively, suggesting that for most patients, using the model to generate a prescription dose will result in a change of at least 6 Gy in either direction (dose escalation or de-escalation). The mean and median changes in prescription are both negative (-2.7 and -1.7 respectively from Table 17), implying that overall the model-predicted doses were lower than the clinically achieved doses. This occurred because for 31 patients, the dose-volume parameters for the clinically used plan exceeded the limits that were set for this study (prior to applying the model-determine MLD limit). Excluding these patients, the histogram reveals (Figure 31) that fewer patients appear to the left of zero, or fewer patients for whom the dose needs to be reduced.



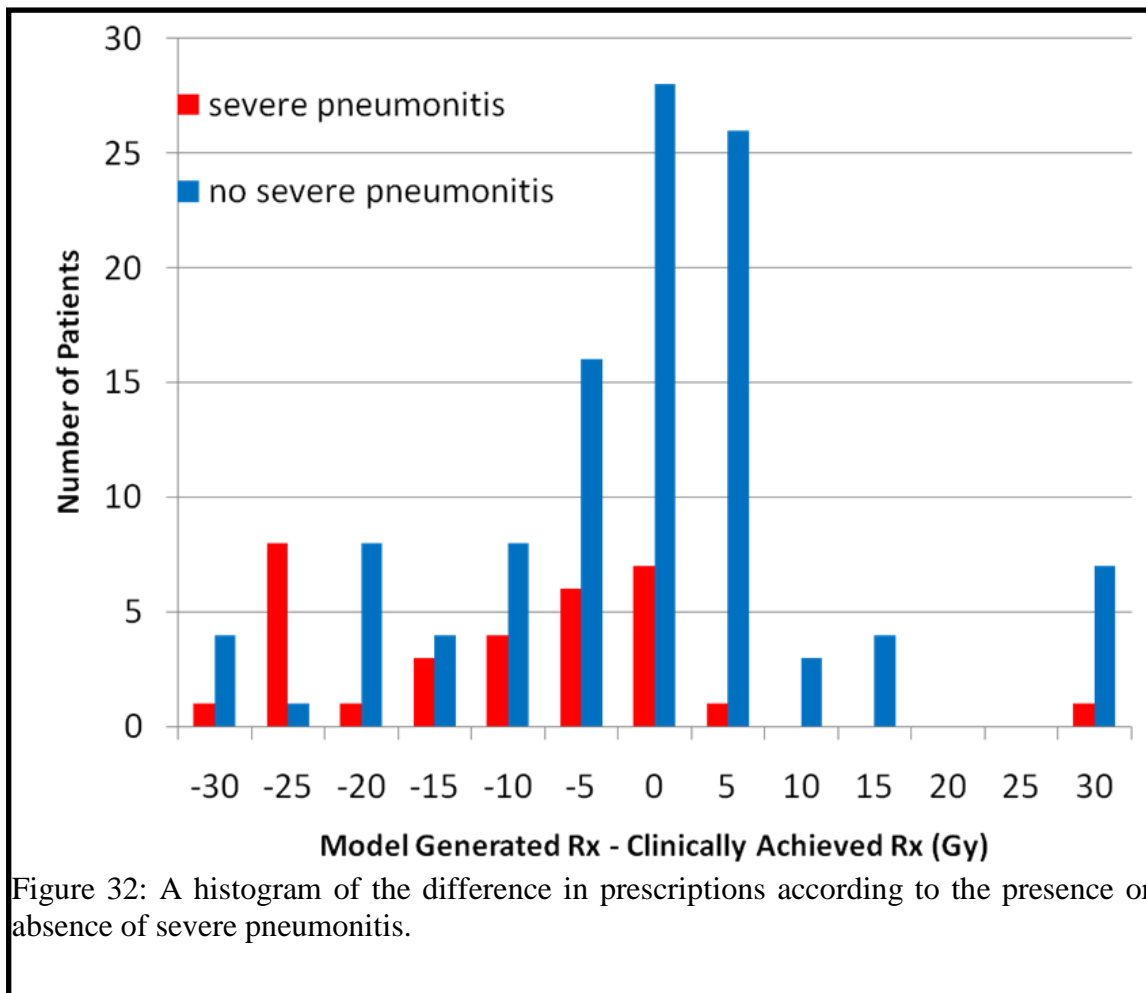
Furthermore, Table 18 shows that the mean and median changes in prescription were -0.7 Gy and 1.4 Gy, respectively, for the reduced patient cohort.

	Clinical Rx (Gy)	Model Rx (Gy)	Model Rx – Clinical Rx (Gy)	Absolute Rx Difference (Gy)
Mean	65.4	65.1	-0.7	10.1
Median	63.0	64.5	1.4	5.8
Range	60.0-72.0	40.0-100.0	-29.6 – 37.0	0-37.0

Table 18: The overall clinically achieved prescription, model generated prescription, and changes in prescription for the reduced patient population. Patients were excluded if their clinically achieved dose-volume parameters for the spinal cord, esophagus, or heart exceeded the limits set for the study (prior to applying the model-determined MLD limit).

These values are closer to zero than the values shown in Table 17. It is also important to point out that when the absolute value of the changes is taken for the reduced patient cohort, the median change for the entire patient population is 5.8 Gy, indicating that for most individual patients using the model will result in a change (dose escalation or de-escalation) of at least 5 Gy.

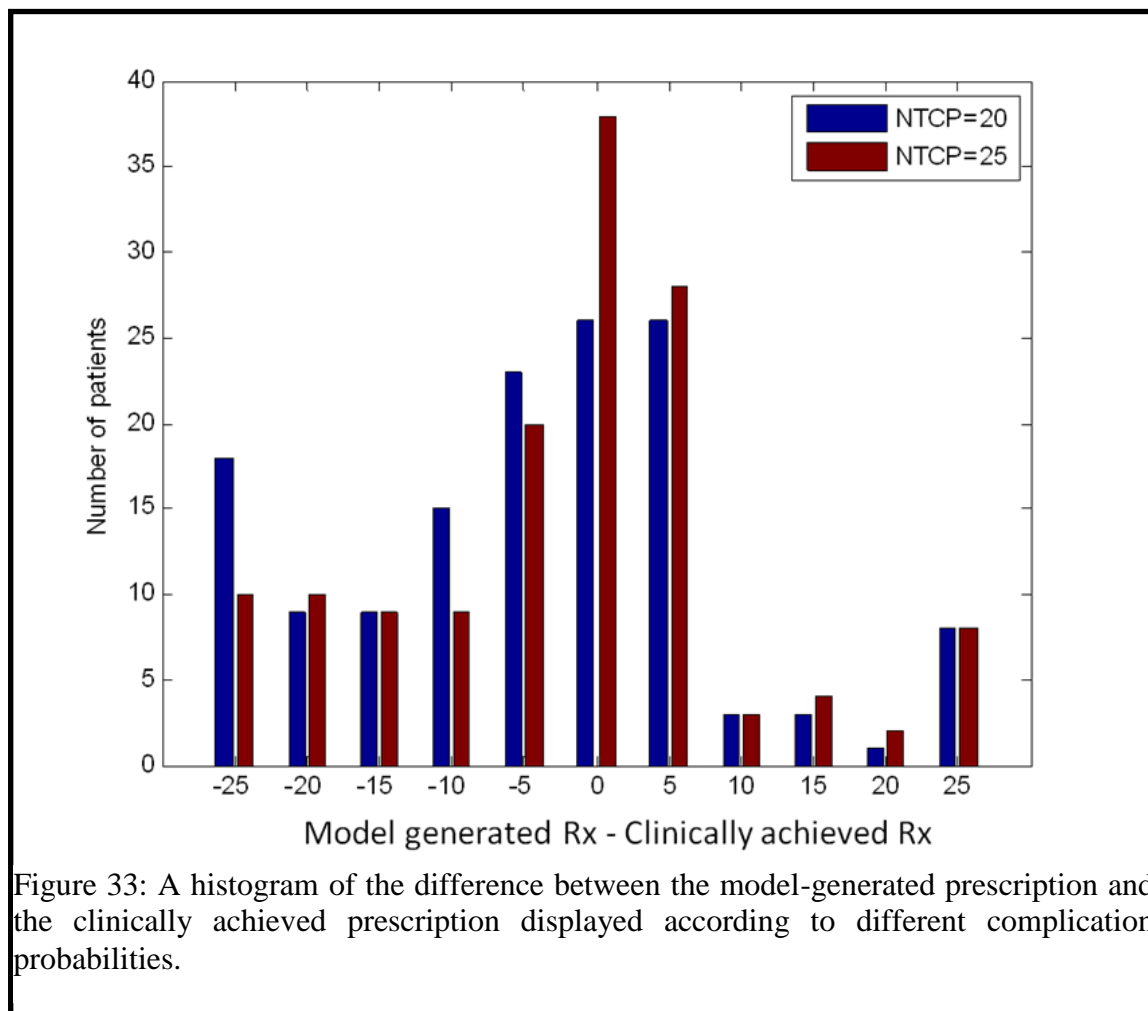
The histogram of the change in prescription according to the presence of pneumonitis is shown in Figure 32.



The patients that developed severe radiation pneumonitis are shown as a separate group in Figure 32. As expected, most of the patients that developed radiation pneumonitis appear to the left of zero, indicating that for those patients the model predicted that the prescription doses needed to be reduced.

The personalized model-determined lung limits (and subsequently prescription values) are highly dependent on the chosen complication probability. We investigated the effect of choosing different complication probabilities on the prescription results. In addition to the nominal complication probability value of 22.6%, we chose to investigate complication probabilities of 20% and 25%. The histogram shown in Figure 33 displays

the change in prescription for the 20% complication probability simulation and the 25% complication probability simulation. As expected, the simulation using the 25% complication probability had fewer patients with a negative change in prescription and more patients with a positive change in prescription than the simulation using the 20% complication probability. These results are quantified in Table 19. The mean and median changes in prescription are higher for the 25% complication probability simulation than for the 20% complication probability simulation. These data suggest that overall, as the complication probability is increased the change in prescription will be skewed towards an increase in dose prescription for each patient.



	Clinical Rx (Gy)	NTCP = 20% Model Rx – Clinical Rx (Gy)	NTCP = 25% Model Rx – Clinical Rx (Gy)
Mean	65.4	-0.3	2.5
Median	63.0	-2.9	0.1

Table 19: Mean and median change in prescription for the 20% complication probability simulation and the 25% complication probability simulation.

The dose limiting organs for the simulation using the 22.6% complication probability are shown in Table 20. As expected, the model-derived lung dose limit was the most frequent dose limiting organ. The lung limit was the limiting factor for 54% of patients, the cord max dose was the limit for 40% of patients, the esophagus was the limit for 4% of patients, and the heart was the limiting organ for 2% of patients.

Dose-volume limit	Number of patients (%)
Model generated lung limit	77 (54%)
Cord	55 (40%)
Esophagus	6 (4%)
Heart	3 (2%)

Table 20: Data showing the dose limiting organ for the simulation using the 22.6% complication probability.

Table 21 shows the dose limiting organ for the simulations using the 20% complication probability and the 25% complication probability. The model generated lung limit was the limiting factor for 59% of patients for the simulation where the complication probability was set at 20% and 50% for the simulation where the complication probability was set at 25%. As the complication probability is allowed to increase and the lung

planning limit is relaxed, the model generated lung parameter becomes a less frequent limiting factor.

Dose-volume limit	NTCP = 20 Number of patients (%)	NTCP = 25 Number of patients (%)
Model generated lung limit	83 (59%)	70 (50%)
Cord	50 (35%)	60 (42%)
Esophagus	5 (4%)	8 (6%)
Heart	3 (2%)	3 (2%)

Table 21: Data showing the dose limiting organ for the simulation using the 20% complication probability and the 25% complication probability.

Discussion

The most significant finding of the virtual simulation is that for individual patients, using a model-generated personalized MLD limit would result in a different prescription than what was used clinically. The histogram of the difference in the MLD underlines that for individual patients the model based on SNPs predicts a different MLD to the patient than was clinically delivered. When the personalized MLD limit is used to determine a model-based prescription, the histogram demonstrates that for individual patients a change will result in the prescription dose. Furthermore, regardless of the complication probability used, the median change in the model-determined prescription and the clinically achieved prescription is over a clinically significant value of 5 Gy (Table 17, 18, 19). If the SNP findings are verified in independent patient cohorts, the prescription changes illustrated in this study would reduce toxicity in certain patients and help push the prescription dose to the maximum tolerable value.

The direction of the change in prescription (dose escalation versus dose de-escalation) is dependent on several factors. First, the direction of the change in prescription is dependent on the sample population used for the modeling study. Using a complication probability of 22.6% the overall change in dose prescription was negative (indicating a dose reduction) for our patient cohort (Table 17). However, when a reduced patient cohort was used that excluded patients for whom initial clinical values exceeded our dose limits, the changes in prescription were around 0, indicating that the positive and negative changes cancelled out (Table 18). The overall change in prescription is also dependent on the exact complication probability that is used. As the complication probability is increased, the lung dose limit is relaxed, and we are able to increase the prescription dose (Figure 33). These results suggest that if using the data in the current study to design a clinical trial, the complication probability and study cohort will have to be taken into account. The allowable complication probability is a clinical decision and must consider the tumor control as well as the normal tissue toxicity. As with any new technology or trial, a logical starting point to use (for the complication probability) is the current existing paradigm in the clinic. Furthermore, each patient population will contain patients whose clinical dose-volume parameters exceed the allowable limits because the physician made a clinical decision to sacrifice normal tissue toxicity for tumor control. We demonstrated the effect of these patients on the overall prescription dose change by running a simulation where they were excluded from our analysis. In a clinical trial, one way to account for these patients is to artificially increase the allowable complication probability.

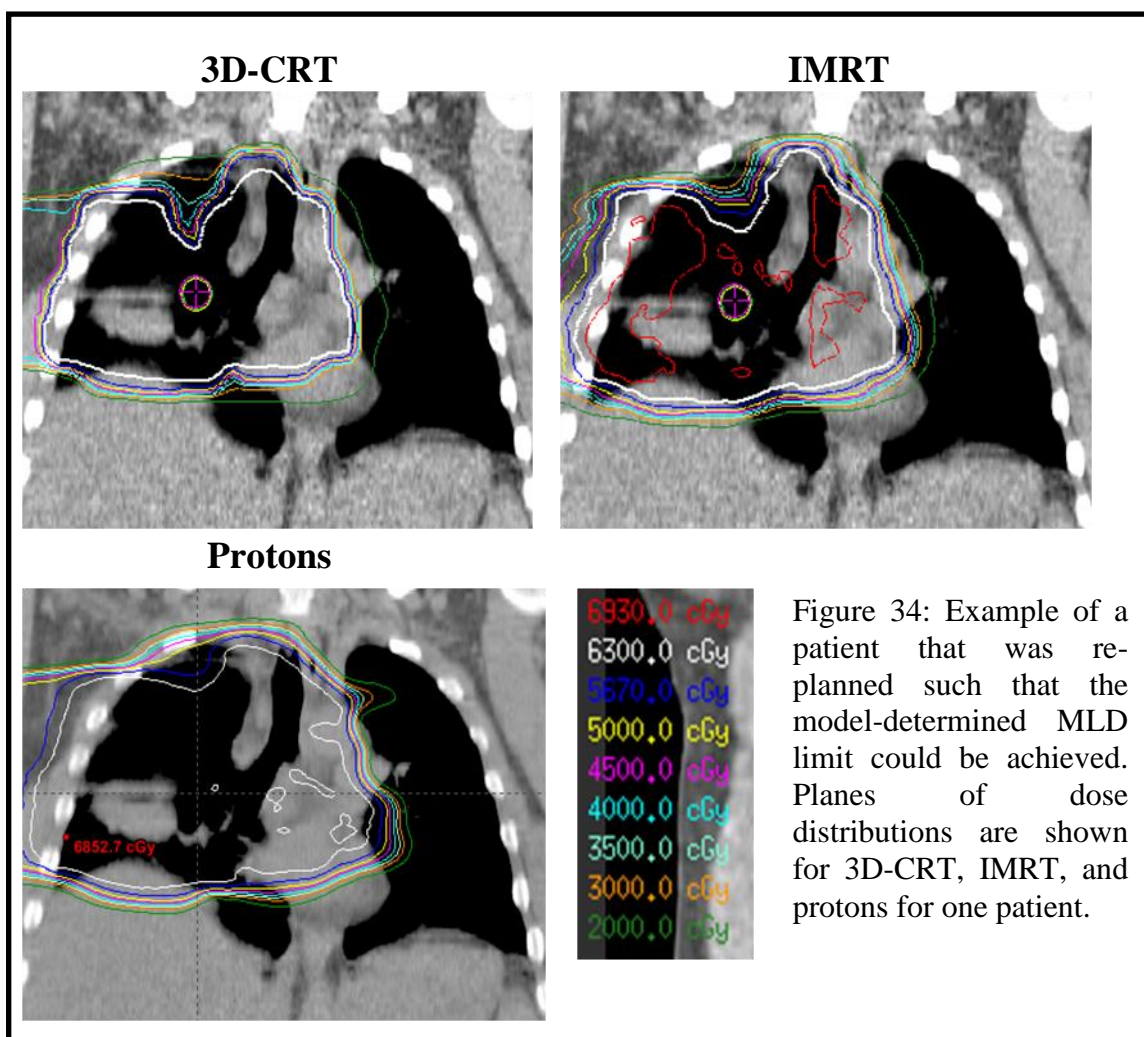
The most frequent dose limiting organ observed was the lung, followed by the spinal cord, esophagus, and the heart (Table 20). These results are in line with what has been observed in the clinic. For thoracic treatment planning, the most frequent dose limiting organ is often the lung, followed by either the spinal cord or the esophagus depending on the location of the tumor. Our results demonstrated that as the allowable lung complication probability is increased the lung limit is relaxed and therefore is a limiting organ for fewer cases.

Van Baardwijk et al (49) performed a simulation study using 65 NSCLC patients where a lung dose limit and a spinal cord limit were used to escalate the doses. Although, the Van Baardwijk et al (49) study did not use genetic biomarkers (SNPs) in their dose prescription scheme, it is pertinent to compare the results of the 2 studies. The Van Baardwijk et al (49) used a nominal starting prescription of 60 Gy, a MLD limit of 19 Gy, and a spinal cord limit of 54 Gy for each patient. They found that on average they could increase the tumor dose by 6.6 Gy using a MLD limit of 19 Gy and a spinal cord limit of 54 Gy. The 6.6 Gy change in target dose is in line with our reported change of around 6 Gy (Table 17). However, it should be noted that we report a median change of 6 Gy (either escalation or de-escalation) in target dose for the entire patient population, while Van Baardwijk et al (49) report an average escalation in target dose of 6.6 Gy. The differences can be attributed to several factors. The population studies used in our simulation and the simulation provided by Van Baardwijk et al (49) are different. The patients in our cohort received prescription doses ranging from 60 to 72 Gy, while all of the patients in the Van Baardwijk et al (49) study started with nominal prescription doses of 60 Gy. Furthermore, Van Baardwijk et al (49) used a population-based MLD limit of

19 Gy while we used individualized MLD limits that are determined from a model that incorporates biomarkers. Furthermore, our patient cohort contained patients for whom the dose-volume metrics for the spinal cord, esophagus, and heart exceeded our set limit prior to any escalation or de-escalation. Despite the differences in study design, both studies illustrate *in silico*, that a change in dose to the target for lung cancer patients can be achieved by prescribing doses that fully utilize the maximum allowable dose values to the normal tissue organs. Our results and those presented by Van Baardwijk et al (49) demonstrate the importance of performing simulation studies. Prior to conducting dose personalization clinical trials, simulation studies are needed to demonstrate the potential gain for the patient.

The current study uses a lung NTCP model to derive a personalized MLD limit that is in turn used to determine a personalized dose prescription for each patient. As modeling methods improve and more data is collected, it is possible that more patient and clinical factors will be found to be associated with the risk of developing radiation pneumonitis. In future work, these additional factors can be incorporated into the model to further personalize the MLD limit and the prescription dose. Furthermore, the concept of using a predictive model to determine a personalized dose limit can be extended to the esophagus, spinal cord, and liver, as data for those organs are accumulated. In this study, a predictive model was used exclusively to scale the prescription dose, in future work it will be possible to use an NTCP model to help with treatment planning. For example, if it is determined by the toxicity model that a patient can withstand a higher MLD, then dose can be taken off another organ (the spinal cord for example) and pushed through the lung. Furthermore, the model can be used to help decide which treatment modality to use for a

patient. If the model-determined MLD limit cannot be achieved with 3D-CRT then the toxicity model can provide further justification to use either IMRT or proton radiation therapy. While the hypothesis that proton treatment plans provide more favorable DVHs than photon treatment plans is still under investigation, for individual patients using a different treatment modality may enable the model determined limit to be achieved. The re-planning step was performed for 2 patients to illustrate the principle. The 2 patients were treated with 3D-CRT and had MLDs of 19.48 and 28.48 Gy. The model-determined limit was 17.81 Gy for the patient that received 19.48 Gy, and 26.16 Gy for the patient that received 28.48 Gy. Under the original assumptions of the simulation the prescription for these 2 patients would be lowered. However, experienced dosimetrists re-planned the patients with IMRT and protons. The 3D-CRT, IMRT, and proton treatment plans for one of patients are shown in Figure 34. Both the IMRT and protons plans results in MLDs below the model-determined limit for both patients (Table 22). The provided example illustrates that for certain patients, the personalized MLD limit may be achieved by re-planning instead of lowering the prescription dose. The model-determined MLD limit can be used in this manner to justify the use of more advanced modalities such as IMRT and proton therapy.



	3D – CRT MLD	IMRT MLD	Proton MLD	MLD Limit
Patient 1	19.48	12.77	8.45	17.81
Patient 2	28.48	24.12	21.74	26.16

Table 22: Re-planning example for 2 patients. The 3D-CRT, IMRT and Proton MLDs are shown. The model determined MLD limit is also displayed.

The work presented in this study is a proof of principle simulation and more work is needed before the proper use of a toxicity model can be determined. The most important work remaining is to verify the SNP results. Because of the large number of

SNPs available for investigation, there is a high probability of finding a significant association between SNPs and pneumonitis. In other words, when a large number of SNPs are investigated, there is a high probability of finding false positives. Therefore, work is underway to validate the SNPs in an independent patient cohort. It should be noted that the SNPs used for the current study were not randomly selected but were chosen because of their association with the inflammation process (38). Finally, it should be noted that this study does not suggest that the proper use of this model is to replace the current clinical paradigm. The model alone cannot be used to make clinical decision about the dose to the tumor. The model does not replace common sense, the clinical judgment of the physician, insurance considerations, or practical considerations. However, we believe that the model can be used as a tool and guide to help physicians make clinical decision. In our clinic, thoracic physicians implicitly (in some cases explicitly) take into account factors such as concurrent chemotherapy, prior surgery, and PFT data when deciding how much lung dose is safe to deliver. With increased data and improved modeling methods more factors may be found to be predictive for toxicity, and a model used in a manner described by the current study can aide physicians in making clinical decisions about how much dose to deliver to the lung.

Conclusion

The current study presents a virtual proof of principle simulation trial where a personalized model-determined lung dose limit was used to change the prescription dose. It was determined that for individual patients the model generated prescription was different than the clinically achieved prescription. The working hypothesis for this study is accepted; the median change for an individual patient was 5.8 Gy. The magnitude and

direction of the change was dependent on the selected complication probability. Furthermore, we found that the model determined lung limit was the most frequent dose limiting organ. As more factors are found to be associated with normal tissue toxicity, a model used in the manner described by the current study can help physicians in determining how much dose can safely be delivered to the tumor and normal tissues.

Conclusions

Study uncertainties

Uncertainties associated with each individual specific aim have been noted in previous sections. For example, the uncertainty associated with calculating ventilation images was investigated in specific aim 1, the uncertainty of using SNPs was noted in specific aim 3, and the uncertainty of using the GTV centroid analysis was discussed in specific aim 1. In addition to uncertainties associated with each specific aim there are several modeling uncertainties that affect all dose-response modeling work. The biggest overall limitation in the dose response modeling field is the toxicity scoring system. The scoring system used for performing a toxicity modeling analysis is subjective. It is subjective to the patient as well as the clinician. For example, one of the criteria for scoring radiation pneumonitis is patient-reported symptoms. This is subjective because certain patients may complain more than others or certain patients may have poor lung conditions prior to beginning treatment and therefore don't report changes in symptoms. Another portion of the radiation pneumonitis scoring criteria is medical intervention. The medical intervention criterion is subjective because some physicians may feel that medical intervention is warranted in certain situations while other physicians may think that no action is necessary. The subjectivity of the scoring system due to both the

clinician and the patient adds uncertainty into the dose-response modeling process because severe (grade 3-5) radiation pneumonitis was the end point for all of our analysis. Another limitation to dose-response modeling is the sparse data that is available. The number of patients developing severe toxicity is low, which is a positive outcome for the patient. However, the low number of events (patients developing radiation pneumonitis) hinders the statistical power of our modeling methods. Finally, in some cases the toxicity reported may not be due to radiation therapy. Patients with NSCLC are often also afflicted with other diseases such as COPD, emphysema, and heart disease. A number of symptoms that may be perceived as being caused by radiation therapy can also be caused by the patient's prior existing conditions. In extreme conditions, even grade 5 toxicity (death) may be difficult to identify because the patient's death may be a result of non-radiation causes (such as tumor progression or pre-existing lung conditions).

The other important factor that adds uncertainty into thoracic dose-response modeling is organ motion. Specifically, intra-fractional organ motion due to breathing and inter-fractional organ motion due to set-up uncertainty can cause a deviation between the intended and delivered dose distributions. Therefore, it is possible that the dose distributions that were used for the dose-response analysis may not be a completely accurate representation of the delivered doses. However, studies suggest that motion causes the largest uncertainty in the dose calculations in heterogeneous dose regions (85) and that motion minimally affects the accuracy of dose calculations to normal tissue when evaluated using the DVH (86). Organ motion also causes uncertainty in the organ contouring process. With the routine clinical use of 4DCT, multiple imaging datasets are

available for contouring of the normal tissue organs. The image set chosen to contour the organs of interest may affect the contour itself.

Conclusions

In specific aim 1 we used our large NSCLC patient database to investigate the relationship between the spatial location of the deposited lung dose and severe radiation pneumonitis. We performed the analysis using the GTV centroid as well as the entire 3D dose distribution. It was determined that for our patient cohort the spatial location of the dose does not influence the risk of radiation pneumonitis.

In specific aim 2 we investigated the utility of 4DCT-based ventilation imaging in assessing lung injury. We first presented a unique dataset of mid-treatment weekly calculated ventilation images. We did not find a consistent pattern of ventilation change as a function of dose. However, we did find that ventilation and ventilation change was a function of anatomy. Specifically, our results showed that pre-treatment ventilation values were lower in lobes that contained the tumor, and if the tumor decreased in size, the lobe was likely to re-inflate and ventilation would increase. Conversely, our results showed that when there was no change in either the tumor or normal tissue anatomy, there was no change in the ventilation distribution. The second portion of specific aim 2 incorporated pre-treatment ventilation images into a dose response model. Although there were some promising results relating pre-treatment function (as measured by ventilation) and severe radiation pneumonitis we were not able to significantly improve the fit of our model using ventilation imaging. We believe more patients may be able to clarify the relationship between dose to highly ventilated portions of the lung and radiation pneumonitis.

In specific aim 3 we performed a proof of principle virtual simulation study where a personalized model-determined lung limit was used to scale the prescription dose. We found that for individual patients, using the personalized model lung dose limit resulted in a different prescription than what was achieved clinically for the patient. The median difference between the model-generated prescription and the clinically achieved prescription was 5.8 Gy. Our simulation results demonstrated the methodology and preliminary data that could eventually be used to design a clinical trial. More work is needed to verify the biomarkers used in our study, add additional factors into the predictive model, and determine the proper use of the toxicity model within the treatment design paradigm.

Clinical significance of research

The spatial study presented in this work adds a significant clinical contribution to existing literature and clinical knowledge. Because of the size of our patient cohort and the rigor of our modeling methods, we believe the current study provides an important addition to the existing knowledge about the relationship between spatial location and radiation pneumonitis. The spatial location within the lung is a pertinent clinical topic because physicians need to know whether it is important to take the spatial location of the tumor within the lung into account when considering how much dose can safely be delivered to the healthy lung. Furthermore, the spatial methods presented in the current work can be extended to other organs and other treatment modalities. For example, it may be of interest whether or not toxicity is dependent on the spatial location of the dose within the esophagus or liver. The methods used in this study can also be extended to thoracic proton therapy.

Although we did not find a statistically significant relationship between ventilation-based functional information and radiation pneumonitis, specific aim 2 provided some promising clinical results. To our knowledge, the serial ventilation study was the first study that has investigated the mid-treatment changes in ventilation. Mid-treatment changes in ventilation may be useful for the clinician to assess. In theory, the physician may take changes in lung function into account when deciding on whether or not to adapt the radiation treatment plan. By incorporating pre-treatment ventilation data into modeling we have provided an important step in using imaging to assess lung function and predict toxicity. There has been a lot of recent interest in using imaging to assess and predict for toxicity (40-43, 59-62). However, the results have been limited by the number of patients enrolled in the studies and by the incomplete understanding and assessment of lung function. In future work, lung function will be assessed by a combination of imaging modalities (ventilation, perfusion, diffusion, and inflammation). The ventilation results presented in this work may provide one of the important pieces necessary to gain a complete understanding of lung function. This work was not only important from a modeling aspect but from a 4DCT-based ventilation aspect as well. There has been a lot of recent interest in 4DCT-based ventilation calculation methodology and using 4DCT-based ventilation imaging to reduce dose to highly ventilated portions of the lung. However, there has been no data to suggest using ventilation imaging in treatment planning will reduce clinical toxicity. This is the first study attempting to relate dose to ventilated portions of the lung and clinical symptoms. Although we did not find a significant result, we show some promising data that can provide the basis for future work relating dose, ventilation, and clinical symptoms.

In the virtual simulation trial, we have provided the methodology that can be used to determine personalized lung dose limits and subsequently personalized prescription doses. As mentioned in specific aim 3, this is something that thoracic physicians may implicitly do already. When deciding how much dose can safely be delivered to the healthy lung, physicians may take into account factors such as surgery status, chemotherapy status, and PFT scores. As more factors are determined to be predictive of radiation pneumonitis, using a model in the manner shown in Specific Aim 3 can be a useful tool and guide for clinicians in determining a personalized lung dose limit and subsequently a personalized prescription. More work is necessary before such a model can be utilized in the clinic; however, the work done in Specific Aim 3 provides the framework in which a model can be used to derive a personalized prescription dose.

Future Work

Future work relating to the specific studies is discussed within each specific aim. For example, as more patients are gathered for the spatial study (specific aim 1) it would be useful to perform the 3D spatial dose analysis for smaller cohorts of patients that are grouped according to disease stage. For the ventilation study (both the serial ventilation study and the pre-treatment ventilation study), more patients are needed. Furthermore, it would be informative to investigate 4DCT-based ventilation images acquired several weeks or months after the completion of therapy, since radiation damage (to the tumor and normal tissue) occurs after the completion of therapy. For the virtual simulation study, the next important step is to verify the SNP data. Another possible continuation of the virtual trial is to include more factors (such as patient smoking status) that may be predictive of radiation pneumonitis into the modeling simulation.

There are a several different ways in which the current research can be extended. One important area is the toxicity scoring system. As mentioned in previous section, the toxicity scoring system for radiation pneumonitis is subjective to the patient as well as the clinician. More work is needed to generate an objective toxicity scoring system. One potential method involves the use of imaging as a surrogate for clinical symptoms. However, since clinical symptoms are the important end point to the clinician, work is needed relating imaging based scoring of radiation pneumonitis and symptom based scoring of radiation pneumonitis.

Imaging can also be used to help identify early changes in lung function that can predict for radiation pneumonitis. In the current study, we investigated ventilation based changes; however, work is needed to get a complete understanding of lung function. In future work, more information about lung function could be gained by combining imaging modalities that assess different aspects of lung function.

It is also possible to extend the current modeling work to other treatment modalities and other treatment sites. For example, the spatial analysis could be extended to patients undergoing proton therapy. The modeling work can be applied to other organs such as the brain, liver, and esophagus. Specifically, it would be informative to apply the spatial work to the liver and esophagus and incorporate functional imaging into predictions methods for the brain and liver.

There is also great potential to incorporate modeling work into hypo-fractionated treatments. Because of their convenience and promising survival rates stereotactic body radiotherapy (SBRT) has been increasing in popularity. However, relatively little is known about thoracic toxicity associated with SBRT (6). More work is needed to relate

basic dose-volume metrics and SBRT toxicity. Once a dose-volume relationship has been established, further work incorporating spatial and functional information can be performed. Another possibility is to apply this work to re-treatments. As survival rates increase radiation re-treatments are becoming more common and as is the case with SBRT, there is relatively little toxicity data for patients undergoing re-treatments. As data is collected, the first step will be to establish a dose-volume relationship and then test for other factors that may be predictive of toxicity.

Response to hypothesis

The purpose of this work was to incorporate spatial and functional information into a predictive model and determine whether the fit of the model to the data could be improved. In a strict sense, the hypothesis is rejected; we were not able to significantly improve the model fit to the data. Specifically, incorporating spatial information and ventilation-based functional information did not significantly improve the fit of the model. Although the hypothesis was rejected the study had some important findings. We did not find a correlation between the spatial location of the dose and radiation pneumonitis. We found that ventilation and ventilation change was a function of the changing thoracic anatomy. We presented some promising (although not statistically significant) results relating pre-treatment ventilation and radiation pneumonitis. Finally, we presented a simulation study where a personalized model-determined lung dose limit was used to change the prescription dose. It was determined that for individual patients the model generated prescription was different than the clinically achieved prescription.

References

1. Jemal A, Siegel R, Xu J, Ward E. Cancer statistics, 2010. *CA Cancer Journal for Clinicians*;60:277-300.
2. Sibley GS, Jamieson TA, Marks LB, Anscher MS, Prosnitz LR. Radiotherapy alone for medically inoperable stage I non-small-cell lung cancer: The duke experience. *International Journal of Radiation Oncology Biology Physics* 1998;40:149-154.
3. Werner-Wasik M, Swann RS, Bradley J, Graham M, Emami B, Purdy J, Sause W. Increasing Tumor Volume is Predictive of Poor Overall and Progression-Free Survival: Secondary Analysis of the Radiation Therapy Oncology Group 93-11 Phase I-II Radiation Dose-Escalation Study in Patients with Inoperable Non-Small-Cell Lung Cancer. *International Journal of Radiation Oncology Biology Physics* 2008;70:385-390.
4. Kong FM, Ten Haken RK, Schipper MJ, Sullivan MA, Chen M, Lopez C, Kalemkerian GP, Hayman JA. High-dose radiation improved local tumor control and overall survival in patients with inoperable/unresectable non-small-cell lung cancer: long-term results of a radiation dose escalation study. *Int. J. Radiat. Oncol. Biol. Phys.* 2005;63:324-333.
5. Machtay M, Swann S, Komaki R, Byhardt R, Paulus R, Sause W, Albain K, Movsas B, Curran WJ. Higher BED is Associated with Improved Local-regional Control and Survival for NSCLC Treated with Chemoradiotherapy: An RTOG Analysis. *International Journal of Radiation Oncology*Biology*Physics* 2005;63:S40-S40.

6. Marks LB, Bentzen SM, Deasy JO, Kong FM, Bradley JD, Vogelius IS, El Naqa I, Hubbs JL, Lebesque JV, Timmerman RD, Martel MK, Jackson A. Radiation Dose-Volume Effects in the Lung. *International Journal of Radiation Oncology Biology Physics*;76:S70-S76.
7. Mehta V. Radiation pneumonitis and pulmonary fibrosis in non-small-cell lung cancer: Pulmonary function, prediction, and prevention. *International Journal of Radiation Oncology Biology Physics* 2005;63:5-24.
8. L.W. Brady HPH, M. Molls. *Advances in Radiation Oncology in Lung Cancer*: Springer-Verlag Berlin Heidelberg; 2005.
9. Perez CA, Stanley K, Grundy G. Impact of irradiation technique and tumor extent in tumor control and survival of patients with unresectable non-oat cell carcinoma of the lung. Report by the Radiation Therapy Oncology Group. *Cancer* 1982;50:1091-1099.
10. Saunders M, Dische S, Barrett A, Harvey A, Gibson D, Parmar M. Continuous hyperfractionated accelerated radiotherapy (CHART) versus conventional radiotherapy in non-small-cell lung cancer: A randomised multicentre trial. *Lancet* 1997;350:161-165.
11. Perez CA, Bauer M, Edelstein S, Gillespie BW, Birch R. Impact of tumor control on survival in carcinoma of the lung treated with irradiation. *Int. J. Radiat. Oncol. Biol. Phys.* 1986;12:539-547.
12. Malissard L, Nguyen TD, Jung GM, Forcard JJ, Castelain B, Tuchais C, Allain YM, Denepoux R, Lagrange JL, Panis X, Rathelot P, Chaplain G, Koechlin M, Rozan R. Localized adenocarcinoma of the lung: A retrospective study of 186

- non-metastatic patients from the French Federation of Cancer Institutes - The Radiotherapy Cooperative Group. *International Journal of Radiation Oncology Biology Physics* 1991;21:369-373.
13. Le Chevalier T, Arriagada R, Quoix E, Ruffie P, Martin M, Douillard JY, Tarayre M, Lacombe-Terrier MJ, Laplanche A. Radiotherapy alone versus combined chemotherapy and radiotherapy in unresectable non-small cell lung carcinoma. *Lung Cancer* 1994;10:S239-S244.
 14. Perez CA, Pajak TF, Rubin P. Long-term observations of the patterns of failure in patients with unresectable non-oat cell carcinoma of the lung treated with definitive radiotherapy. Report by the Radiation Therapy Oncology Group. *Cancer* 1987;59:1874-1881.
 15. Willner J, Baier K, Caragiani E, Tschammler A, Flentje M. Dose, volume, and tumor control prediction in primary radiotherapy of non-small-cell lung cancer. *International Journal of Radiation Oncology Biology Physics* 2002;52:382-389.
 16. Bradley J, Graham MV, Winter K, Purdy JA, Komaki R, Roa WH, Ryu JK, Bosch W, Emami B. Toxicity and outcome results of RTOG 9311: A phase I-II dose-escalation study using three-dimensional conformal radiotherapy in patients with inoperable non-small-cell lung carcinoma. *International Journal of Radiation Oncology Biology Physics* 2005;61:318-328.
 17. Bradley JD, Moughan J, Graham MV, Byhardt R, Govindan R, Fowler J, Purdy JA, Michalski JM, Gore E, Choy H. A Phase I/II Radiation Dose Escalation Study With Concurrent Chemotherapy for Patients With Inoperable Stages I to III Non-

- Small-Cell Lung Cancer: Phase I Results of RTOG 0117. *International Journal of Radiation Oncology Biology Physics* 2010;77:367-372.
18. Trotti A, Colevas AD, Setser A, Rusch V, Jaques D, Budach V, Langer C, Murphy B, Cumberlin R, Coleman CN, Rubin P. CTCAE v3.0: Development of a comprehensive grading system for the adverse effects of cancer treatment. *Semin. Radiat. Oncol.* 2003;13:176-181.
 19. Tucker SL, Jin H, Wei X, Wang S, Martel MK, Komaki R, Liu HH, Mohan R, Chen Y, Cox JD, Liao Z. Impact of Toxicity Grade and Scoring System on the Relationship Between Mean Lung Dose and Risk of Radiation Pneumonitis in a Large Cohort of Patients With Non-Small Cell Lung Cancer. *International Journal of Radiation Oncology Biology Physics*;77:691-698.
 20. Wang S, Liao Z, Wei X, Liu HH, Tucker SL, Hu CS, Mohan R, Cox JD, Komaki R. Analysis of clinical and dosimetric factors associated with treatment-related pneumonitis (TRP) in patients with non-small-cell lung cancer (NSCLC) treated with concurrent chemotherapy and three-dimensional conformal radiotherapy (3D-CRT). *Int. J. Radiat. Oncol. Biol. Phys.* 2006;66:1399-1407.
 21. Kwa SLS, Lebesque JV, Theuws JCM, Marks LB, Munley MT, Bentel G, Oetzel D, Spahn U, Graham MV, Drzymala RE, Purdy JA, Lichter AS, Martel MK, Ten Haken RK. Radiation pneumonitis as a function of mean lung dose: An analysis of pooled data of 540 patients. *International Journal of Radiation Oncology Biology Physics* 1998;42:1-9.
 22. Sura S, Gupta V, Yorke E, Jackson A, Amols H, Rosenzweig KE. Intensity-modulated radiation therapy (IMRT) for inoperable non-small cell lung cancer:

- The Memorial Sloan-Kettering Cancer Center (MSKCC) experience. *Radiother. Oncol.* 2008;87:17-23.
23. Mohan R, Mageras GS, Baldwin B, Brewster LJ, Kutcher GJ, Leibel S, Burman CM, Ling CC, Fuks Z. Clinically relevant optimization of 3-D conformal treatments. *Med. Phys.* 1992;19:933-944.
 24. Kutcher GJ, Burman C. Calculation of complication probability factors for non-uniform normal tissue irradiation: The effective volume method. *International Journal of Radiation Oncology Biology Physics* 1989;16:1623-1630.
 25. Bentzen SM, Tucker SL. Quantifying the position and steepness of radiation dose-response curves. *Int. J. Radiat. Biol.* 1997;71:531-542.
 26. Seppenwoolde Y, Lebesque JV, De Jaeger K, Belderbos JSA, Boersma LJ, Schilstra C, Henning GT, Hayman JA, Martel MK, Ten Haken RK. Comparing different NTCP models that predict the incidence of radiation pneumonitis. *International Journal of Radiation Oncology Biology Physics* 2003;55:724-735.
 27. Thames HD, Zhang M, Tucker SL, Liu HH, Dong L, Mohan R. Cluster models of dose-volume effects. *International Journal of Radiation Oncology Biology Physics* 2004;59:1491-1504.
 28. Marks LB, Yorke ED, Jackson A, Ten Haken RK, Constone LS, Eisbruch A, Bentzen SM, Nam J, Deasy JO. Use of Normal Tissue Complication Probability Models in the Clinic. *International Journal of Radiation Oncology Biology Physics*;76:S10-S19.
 29. Rosner B. Fundamentals of Biostatistics. 6 ed: Thomson Brooks/Cole; 2006.

30. Graham MV, Purdy JA, Emami B, Harms W, Bosch W, Lockett MA, Perez CA. Clinical dose-volume histogram analysis for pneumonitis after 3D treatment for non-small cell lung cancer (NSCLC). *International Journal of Radiation Oncology Biology Physics* 1999;45:323-329.
31. Martel MK, Ten Haken RK, Hazuka MB, Turrisi AT, Fraass BA, Lichter AS. Dose-volume histogram and 3-D treatment planning evaluation of patients with pneumonitis. *Int. J. Radiat. Oncol. Biol. Phys.* 1994;28:575-581.
32. Yorke ED, Jackson A, Rosenzweig KE, Merrick SA, Gabrys D, Venkatraman ES, Burman CM, Leibel SA, Ling CC. Dose-volume factors contributing to the incidence of radiation pneumonitis in non-small-cell lung cancer patients treated with three-dimensional conformal radiation therapy. *Int. J. Radiat. Oncol. Biol. Phys.* 2002;54:329-339.
33. Hope AJ, Lindsay PE, El Naqa I, Alaly JR, Vicic M, Bradley JD, Deasy JO. Modeling radiation pneumonitis risk with clinical, dosimetric, and spatial parameters. *Int. J. Radiat. Oncol. Biol. Phys.* 2006;65:112-124.
34. Yorke ED, Jackson A, Rosenzweig KE, Braban L, Leibel SA, Ling CC. Correlation of dosimetric factors and radiation pneumonitis for non-small-cell lung cancer patients in a recently completed dose escalation study. *International Journal of Radiation Oncology Biology Physics* 2005;63:672-682.
35. Schaake-Koning C, Van den Bogaert W, Dalesio O, Festen J, Hoogenhout J, Van Houtte P, Kirkpatrick A, Koolen M, Maat B, Nijs A, Renaud A, Rodrigus P, Schuster-Uitterhoeve L, Sculier JP, Van Zandwijk N, Bartelink H. Effects of

- concomitant cisplatin and radiotherapy on inoperable non-small- cell lung cancer. *N. Engl. J. Med.* 1992;326:524-530.
36. Robnett TJ, Machtay M, Vines EF, McKenna MG, Algazy KM, McKenna WG. Factors predicting severe radiation pneumonitis in patients receiving definitive chemoradiation for lung cancer. *International Journal of Radiation Oncology Biology Physics* 2000;48:89-94.
 37. Jin H, Tucker SL, Liu HH, Wei X, Yom SS, Wang S, Komaki R, Chen Y, Martel MK, Mohan R, Cox JD, Liao Z. Dose-volume thresholds and smoking status for the risk of treatment-related pneumonitis in inoperable non-small cell lung cancer treated with definitive radiotherapy. *Radiother. Oncol.* 2009;91:427-432.
 38. Yuan X, Liao Z, Liu Z, Wang LE, Tucker SL, Mao L, Wang XS, Martel M, Komaki R, Cox JD, Milas L, Wei Q. Single nucleotide polymorphism at rs1982073:T869C of the TGFbeta 1 gene is associated with the risk of radiation pneumonitis in patients with non-small-cell lung cancer treated with definitive radiotherapy. *Journal of clinical oncology : official journal of the American Society of Clinical Oncology* 2009;27:3370-3378.
 39. Liao ZX, Travis EL, Tucker SL. Damage and morbidity from pneumonitis after irradiation of partial volumes of mouse lung. *International Journal of Radiation Oncology Biology Physics* 1995;32:1359-1370.
 40. Kocak Z, Borst GR, Zeng J, Zhou S, Hollis DR, Zhang J, Evans ES, Folz RJ, Wong T, Kahn D, Belderbos JSA, Lebesque JV, Marks LB. Prospective assessment of dosimetric/physiologic-based models for predicting radiation

- pneumonitis. *International Journal of Radiation Oncology Biology Physics* 2007;67:178-186.
41. Miften MM, Das SK, Su M, Marks LB. Incorporation of functional imaging data in the evaluation of dose distributions using the generalized concept of equivalent uniform dose. *Phys. Med. Biol.* 2004;49:1711-1721.
 42. Nioutsikou E, Partridge M, Bedford JL, Webb S. Prediction of radiation-induced normal tissue complications in radiotherapy using functional image data. *Phys. Med. Biol.* 2005;50:1035-1046.
 43. Seppenwoolde Y, De Jaeger K, Boersma LJ, Belderbos JSA, Lebesque JV. Regional differences in lung radiosensitivity after radiotherapy for non-small-cell lung cancer. *International Journal of Radiation Oncology Biology Physics* 2004;60:748-758.
 44. Rosenzweig KE, Fox JL, Yorke E, Amols H, Jackson A, Rusch V, Kris MG, Ling CC, Leibel SA. Results of a phase I dose-escalation study using three-dimensional conformal radiotherapy in the treatment of inoperable nonsmall cell lung carcinoma. *Cancer* 2005;103:2118-2127.
 45. Kong FM, Hayman JA, Griffith KA, Kalemkerian GP, Arenberg D, Lyons S, Turrisi A, Lichter A, Fraass B, Eisbruch A, Lawrence TS, Ten Haken RK. Final toxicity results of a radiation-dose escalation study in patients with non-small-cell lung cancer (NSCLC): predictors for radiation pneumonitis and fibrosis. *Int. J. Radiat. Oncol. Biol. Phys.* 2006;65:1075-1086.
 46. Belderbos JSA, Heemsbergen WD, De Jaeger K, Baas P, Lebesque JV. Final results of a Phase I/II dose escalation trial in non-small-cell lung cancer using

- three-dimensional conformal radiotherapy. *International Journal of Radiation Oncology Biology Physics* 2006;66:126-134.
47. Adkison JB, Khuntia D, Bentzen SM, Cannon GM, Tome WA, Jaradat H, Walker W, Traynor AM, Weigel T, Mehta MP. Dose escalated, hypofractionated radiotherapy using helical tomotherapy for inoperable non-small cell lung cancer: Preliminary results of a risk-stratified phase I dose escalation study. *Technology in Cancer Research and Treatment* 2008;7:441-447.
 48. Van Baardwijk A, Wanders S, Boersma L, Borger J, Ållers M, Dingemans AMC, Bootsma G, Geraedts W, Pitz C, Lunde R, Lambin P, De Ruyscher D. Mature results of an individualized radiation dose prescription study based on normal tissue constraints in stages I to III non-small-cell lung cancer. *J. Clin. Oncol.*;28:1380-1386.
 49. van Baardwijk A, Bosmans G, Bentzen SM, Boersma L, Dekker A, Wanders R, Wouters BG, Lambin P, De Ruyscher D. Radiation Dose Prescription for Non-Small-Cell Lung Cancer According to Normal Tissue Dose Constraints: An In Silico Clinical Trial. *International Journal of Radiation Oncology Biology Physics* 2008;71:1103-1110.
 50. van Baardwijk A, Bosmans G, Boersma L, Wanders S, Dekker A, Dingemans AMC, Bootsma G, Geraedts W, Pitz C, Simons J, Lambin P, De Ruyscher D. Individualized Radical Radiotherapy of Non-Small-Cell Lung Cancer Based on Normal Tissue Dose Constraints: A Feasibility Study. *International Journal of Radiation Oncology Biology Physics* 2008;71:1394-1401.

51. Mackay RI, Hendry JH. The modelled benefits of individualizing radiotherapy patients' dose using cellular radiosensitivity assays with inherent variability. *Radiother. Oncol.* 1999;50:67-75.
52. Tucker SL, Liu HH, Liao Z, Wei X, Wang S, Jin H, Komaki R, Martel MK, Mohan R. Analysis of radiation pneumonitis risk using a generalized Lyman model. *Int. J. Radiat. Oncol. Biol. Phys.* 2008;72:568-574.
53. Bradley JD, Hope A, El Naqa I, Apte A, Lindsay PE, Bosch W, Matthews J, Sause W, Graham MV, Deasy JO. {A figure is presented}A Nomogram to Predict Radiation Pneumonitis, Derived From a Combined Analysis of RTOG 9311 and Institutional Data. *International Journal of Radiation Oncology Biology Physics* 2007;69:985-992.
54. Vinogradskiy Y, Tucker SL, Liao Z, Martel MK. Investigation of the Relationship Between Gross Tumor Volume Location and Pneumonitis Rates Using a Large Clinical Database of Non-Small-Cell Lung Cancer Patients. *Int. J. Radiat. Oncol. Biol. Phys.*
55. Vinogradskiy Y, Tucker SL, Liao Z, Martel MK. A novel method to incorporate the spatial location of the lung dose distribution into predictive radiation pneumonitis modeling. *Int. J. Radiat. Oncol. Biol. Phys.*
56. Peeters STH, Hoogeman MS, Heemsbergen WD, Hart AAM, Koper PCM, Lebesque JV. Rectal bleeding, fecal incontinence, and high stool frequency after conformal radiotherapy for prostate cancer: Normal tissue complication probability modeling. *International Journal of Radiation Oncology Biology Physics* 2006;66:11-19.

57. Hernando ML, Marks LB, Bentel GC, Zhou SM, Hollis D, Das SK, Fan M, Munley MT, Shafman TD, Anscher MS, Lind PA. Radiation-induced pulmonary toxicity: a dose-volume histogram analysis in 201 patients with lung cancer. *Int. J. Radiat. Oncol. Biol. Phys.* 2001;51:650-659.
58. Kah̃n Z, Csenki M, Varga Z, Szil E, Cserh̃ti A, Balogh A, Gyulai Z, M̃ndi Y, Boda K, Thurz̃³ L. The Risk of Early and Late Lung Sequelae After Conformal Radiotherapy in Breast Cancer Patients. *International Journal of Radiation Oncology Biology Physics* 2007;68:673-681.
59. Yaremko BP, Guerrero TM, Noyola-Martinez J, Guerra R, Lege DG, Nguyen LT, Balter PA, Cox JD, Komaki R. Reduction of normal lung irradiation in locally advanced non-small-cell lung cancer patients, using ventilation images for functional avoidance. *Int. J. Radiat. Oncol. Biol. Phys.* 2007;68:562-571.
60. Zhang J, Ma J, Zhou S, Hubbs JL, Wong TZ, Folz RJ, Evans ES, Jaszczak RJ, Clough R, Marks LB. Radiation-Induced Reductions in Regional Lung Perfusion: 0.1-12 Year Data From a Prospective Clinical Study. *International Journal of Radiation Oncology Biology Physics*;76:425-432.
61. Marks LB, Sherouse GW, Munley MT, Bentel GC, Spencer DP. Incorporation of functional status into dose-volume analysis. *Med. Phys.* 1999;26:196-199.
62. Boersma LJ, Damen EMF, De Boer RW, Muller SH, Valdes Olmos RA, Hoefnagel CA, Roos CM, Van Zandwijk N, Lebesque JV. A new method to determine dose-effect relations for local lung-function changes using correlated SPECT and CT data. *Radiother. Oncol.* 1993;29:110-116.

63. Ma J, Zhang J, Zhou S, Hubbs JL, Foltz RJ, Hollis DR, Light KL, Wong TZ, Kelsey CR, Marks LB. Association Between RT-Induced Changes in Lung Tissue Density and Global Lung Function. *International Journal of Radiation Oncology Biology Physics* 2009;74:781-789.
64. Vinogradskiy Y, Castillo R, Castillo E, Chandler A, Martel MK, Guerrero T. Use of weekly 4DCT-based ventilation maps to quantify changes in lung function for patients undergoing radiation therapy. *Med. Phys.* (Manuscript Submitted)
65. Guerrero T, Sanders K, Castillo E, Zhang Y, Bidaut L, Pan T, Komaki R. Dynamic ventilation imaging from four-dimensional computed tomography. *Phys. Med. Biol.* 2006;51:777-791.
66. Rietzel E, Pan T, Chen GTY. Four-dimensional computed tomography: Image formation and clinical protocol. *Med. Phys.* 2005;32:874-889.
67. Vedam SS, Keall PJ, Kini VR, Mostafavi H, Shukla HP, Mohan R. Acquiring a four-dimensional computed tomography dataset using an external respiratory signal. *Phys. Med. Biol.* 2003;48:45-62.
68. Reinhardt JM, Ding K, Cao K, Christensen GE, Hoffman EA, Bodas SV. Registration-based estimates of local lung tissue expansion compared to xenon CT measures of specific ventilation. *Med. Image Anal.* 2008;12:752-763.
69. Yamamoto T, Kabus S, Klinder T, Lorenz C, Von Berg J, Blaffert T, Loo Jr BW, Keall PJ. Investigation of four-dimensional computed tomography-based pulmonary ventilation imaging in patients with emphysematous lung regions. *Phys. Med. Biol.*;56:2279-2298.

70. Yamamoto T, Kabus S, Klinder T, Von Berg J, Lorenz C, Loo Jr BW, Keall PJ. Four-dimensional computed tomography pulmonary ventilation images vary with deformable image registration algorithms and metrics. *Med. Phys.*;38:1348-1358.
71. Yamamoto T, Kabus S, Von Berg J, Lorenz C, Keall PJ. Impact of four-dimensional computed tomography pulmonary ventilation imaging-based functional avoidance for lung cancer radiotherapy. *International Journal of Radiation Oncology Biology Physics*;79:279-288.
72. Ding K, Bayouth JE, Buatti JM, Christensen GE, Reinhardt JM. 4DCT-based measurement of changes in pulmonary function following a course of radiation therapy. *Med. Phys.*;37:1261-1272.
73. Castillo R, Castillo E, Martinez J, Guerrero T. Ventilation from four-dimensional computed tomography: Density versus Jacobian methods. *Phys. Med. Biol.*;55:4661-4685.
74. Castillo E, Castillo R, Martinez J, Shenoy M, Guerrero T. Four-dimensional deformable image registration using trajectory modeling. *Phys. Med. Biol.*;55:305-327.
75. Simon BA. Non-invasive imaging of regional lung function using X-ray computed tomography. *J. Clin. Monit. Comput.* 2000;16:433-442.
76. Britton KR, Starkschall G, Liu H, Chang JY, Bilton S, Ezhil M, John-Baptiste S, Kantor M, Cox JD, Komaki R, Mohan R. Consequences of Anatomic Changes and Respiratory Motion on Radiation Dose Distributions in Conformal Radiotherapy for Locally Advanced Non-Small-Cell Lung Cancer. *International Journal of Radiation Oncology Biology Physics* 2009;73:94-102.

77. Hartkens T. *Algorithm System Anwendungen*.
78. Fan M, Marks LB, Hollis D, Bentel GG, Anscher MS, Sibley G, Coleman RE, Jaszczak RJ, Munley MT. Can we predict radiation-induced changes in pulmonary function based on the sum of predicted regional dysfunction? *J. Clin. Oncol.* 2001;19:543-550.
79. Lind PA, Marks LB, Hollis D, Fan M, Zhou SM, Munley MT, Shafman TD, Jaszczak RJ, Coleman RE. Receiver operating characteristic curves to assess predictors of radiation-induced symptomatic lung injury. *International Journal of Radiation Oncology Biology Physics* 2002;54:340-347.
80. Fuld MK, Easley RB, Saba OI, Chon D, Reinhardt JM, Hoffman EA, Simon BA. CT-measured regional specific volume change reflects regional ventilation in supine sheep. *J. Appl. Physiol.* 2008;104:1177-1184.
81. Anscher MS, Kong FM, Andrews K, Clough R, Marks LB, Bentel G, Jirtle RL. Plasma transforming growth factor $\hat{P}1$ as a predictor of radiation pneumonitis. *International Journal of Radiation Oncology Biology Physics* 1998;41:1029-1035.
82. De Jaeger K, Seppenwoolde Y, Kampinga HH, Boersma LJ, Belderbos JSA, Lebesque JV. Significance of plasma transforming growth factor- $\hat{P}2$ levels in radiotherapy for non-small-cell lung cancer. *International Journal of Radiation Oncology Biology Physics* 2004;58:1378-1387.
83. Fogarty GB, Muddle R, Sprung CN, Chen W, Duffy D, Sturm RA, McKay MJ. Unexpectedly severe acute radiotherapy side effects are associated with single nucleotide polymorphisms of the melanocortin-1 receptor. *International Journal of Radiation Oncology Biology Physics*;77:1486-1492.

84. Liao Z, Wei Q, Martel MK, Gomez D, Liu Z, Guam X, Lu C, Komaki R, Tucker SL. Incorporating SNPs as Biomarkers to Improve the Fit of the Lyman Model for Radiation Pneumonitis. *Int. J. Radiat. Oncol. Biol. Phys.* 2008.
85. Vinogradskiy YY, Balter P, Followill DS, Alvarez PE, White RA, Starkschall G. Verification of four-dimensional photon dose calculations. *Med. Phys.* 2009;36:3438-3447.
86. Starkschall G, Britton K, McAleer MF, Jeter MD, Kaus MR, Bzdusek K, Mohan R, Cox JD. Potential Dosimetric Benefits of Four-Dimensional Radiation Treatment Planning. *International Journal of Radiation Oncology Biology Physics* 2009;73:1560-1565.

Vita

Yevgeney Vinogradskiy was born in Cishinau, Moldova on June 1st, 1984, the Son of Luda Vinogradskiy and Yakov Vinogradskiy. After completing his work at The Roeper School, Birmingham, Michigan in 2002, he entered the University of Michigan in Ann Arbor, Michigan. He received the degree of Bachelor of Science and Engineering in Nuclear Engineering from the University of Michigan in May, 2006. In September of 2006 he entered The University of Texas Health Science Center at Houston Graduate School of Biomedical Sciences.

Permanent Address:
116 Palm springs way
Simpsonville, SC, 29681